

# **ATOMIC METAL/POLYANILINE COMPOSITES**

A Thesis  
Presented to  
The Academic Faculty

by

**Alex P. Jonke**

In Partial Fulfillment  
of the Requirements for the Degree  
Doctor of Philosophy in the  
School of Chemistry and Biochemistry

Georgia Institute of Technology  
August 2013

**COPYRIGHT 2013 BY ALEX P. JONKE**

# ATOMIC METAL/POLYANILINE COMPOSITES

Approved by:

Dr. Jiří Janata, Advisor  
School of Chemistry and Biochemistry  
*Georgia Institute of Technology*

Dr. Lawrence Bottomley  
School of Chemistry and Biochemistry  
*Georgia Institute of Technology*

Dr. Facundo Fernandez  
School of Chemistry and Biochemistry  
*Georgia Institute of Technology*

Dr. Mira Josowicz  
School of Chemistry and Biochemistry  
*Georgia Institute of Technology*

Dr. Dennis W. Hess  
School of Chemical & Biomolecular  
Engineering  
*Georgia Institute of Technology*

Date Approved: June 13, 2013

To my wife, daughter, mother, sister, and brother, I love you guys.

## ACKNOWLEDGEMENTS

After six years of graduate studies at the Georgia Institute of Technology, I have worked hard and many people have helped me along the way. There are so many people to thank for all the support and encouragement to get me to this point. Life is short, but precious. I want everyone to know how truly thankful and blessed I feel to have been given this chance.

First, I have to thank Prof. Art Janata and Dr. Mira Josowicz for giving me the gift of opportunity by accepting me into their research group. I can't say enough about them. Being part of their group has been like being a part of their family. They have given advice and encouragement, invited me into their home on occasion, and has always been there to guide and mentor me in my research.

I would like to thank my family who has been there for me throughout my graduate studies. My wife, Michelle Jonke, has always stood by me and has encouraged me to continue when I had doubts. She has believed in me from the start, and I am thankful for it. I love you! I would like to thank my daughter Samantha for being my constant motivation and distraction. I definitely need to thank my mother Christina Haskew. She has taught me about hard work and perseverance by being an example. She has always been there for me which has been such a blessing in my life. I hope I make you proud. I thank the rest of my family for being special people that I could not imagine my life without, especially Erica Bruno, Jeff Haskew, Darby Burke, and Gitti Crispino.

I also need to thank all people that have helped me academically. I would have pulled my hair out at the bench if it were not for Ryan West, Jennifer Steeb, George

Yu, and Ryan Cantor. I would like to thank the members of my committee for taking the time out of their busy schedules to evaluate my work. I would also like to thank the lab coordinator, David Jenson, during my time as a teaching assistant for his advice and support. For answering constant emails about anything and everything so quickly, I also want to thank Cam Tyson for his dedication to the students in this program.

# TABLE OF CONTENTS

	Page
ACKNOWLEDGEMENTS	iv
LIST OF TABLES	ix
LIST OF FIGURES	x
SUMMARY	xvi
 <u>CHAPTER</u>	
1 Introduction	1
1.1 Objective	1
1.2 Polyaniline	1
1.3 Polyaniline as a Support Matrix	3
1.4 Gold and Palladium as Catalysts	6
2 Atomic Gold Deposition on Polyaniline	9
2.1 Atomic Gold Deposition Cycle	9
2.2 Electrochemical Polymerization of Polyaniline Films	12
2.3 Deposition of Atomic Gold in PANI	12
3 Optimization of Atomic Gold Deposition Cycle	21
3.1 The Need for Optimization	21
3.2 Optimization of the Film Degradation Prior to Gold Deposition	21
3.3 Fourier Transform Infrared Spectroscopy (FTIR) Evaluation of the Stable PANI Matrix	24
3.4 Minimizing PANI Degradation During Gold Deposition	26
3.5 Gold Deposition Using Optimized Conditions	28
3.6 Effect of Deposited Gold on the Electrochemistry of PANI	29
3.7 Work Function of PANI/Au <sub>N</sub> Films	31

3.8 X-Ray Photoelectron Spectroscopy (XPS)	34
4 Odd-Even Pattern Observed in Polyaniline/(Au <sub>0</sub> – Au <sub>8</sub> ) Composites	37
4.1 Electrochemical Preparation of Polyaniline Gold Composite Films	37
4.2 Odd-Even Pattern in the Electro-oxidation of n-Propanol	38
4.3 Odd-Even Pattern in the FTIR	45
5 Effect of Atomic Gold on Electrooxidation of Alcohols in Alkaline Medium	49
5.1 Introduction	49
5.2 Preparation of Modified Electrodes	50
5.3 Oxidation of Linear Alcohols	51
5.4 Oxidation of Butanols	55
5.5 Oxidation of Branched Isomers	57
5.6 Proposed Oxidation Mechanisms	58
6 Atomic Clusters of Pd and Au <sub>N</sub> Pd <sub>M</sub> in Polyaniline	64
6.1 Introduction	64
6.2 Preparation of Pd <sub>N</sub> and Au <sub>N</sub> Pd <sub>M</sub> Composites	64
6.3 PANI/Pd <sub>1-6</sub> Oxidation of n-PrOH	67
6.4 FTIR of PANI/Pd <sub>1-6</sub>	73
6.5 Bimetallic Alloys of Au and Pd in PANI	75
6.6 Oxidation of n-PrOH with PANI/Au <sub>N</sub> Pd <sub>M</sub> Electrodes	78
7 Oxidation of Methanol and Ethanol on PANI/Au <sub>n</sub> Pd <sub>1</sub> Electrodes	85
7.1 Introduction	85
7.2 Experimental	85
7.3 Catalytic Activity for Oxidation of Methanol, Ethanol, and iso-Propanol	86
7.4 Comparison to the HOMO-LUMO Gap Energies	91
7.5 Scan Rate and Concentration Effects	92

8	Future Work	95
8.1	Different Metals	95
8.2	Different Deposition Sequences	95
8.3	Catalytic Activity for Additional Reactions	96
8.4	Carbon Substrate and Scaling Up	97
APPENDIX A:	Polyaniline Supported Atomic Gold Electrodes: Comparison with Macro Electrodes	99
A.1	Introduction	99
A.2	Experimental	101
A.3	Results	102
APPENDIX B:	Gel Hybrid Material as the Sensing Gate of CHEMFET	114
B.1	Introduction	114
B.2	Experimental	115
B.3	Results and Discussion	117
REFERENCES		127
VITA		137

## LIST OF TABLES

	Page
Table 5.1: Survey of cyclic voltammogram parameters for AGE-5 and AGE-6. Pt/PANI and Pt/PANI/Au <sub>macro</sub> are shown for reference	52
Table B.1: Changes in $V_{th}$ of CHEMFETs determined as a function of the added mole fraction of IL, $\chi$ , relative to the PANI-CSA with no IL in the gate material	119
Table B.2: Ratio of band transitions for different mole fractions ( $\chi$ ) of PANI-CSA/IL	120
Table B.3: Film thickness normalized results for 90% response times corresponding to Figure B.5	125

## LIST OF FIGURES

	Page
Figure 1.1: (A) PANI base general composition and oxidation states: (B) pernigraniline base (C) emeraldine base (D) leucoemeraldine base	2
Figure 1.2: Salt forms of PANI. leucoemeraldine salt (top), emeraldine salt (middle), and pernigraniline salt (bottom)	3
Figure 1.3: Calculated HOMO-LUMO gap energies for atomic clusters of gold with the lowest energy structures	7
Figure 2.1: Cyclic pathway for the deposition of atomic gold in PANI	9
Figure 2.2: Timing diagram for the atomic gold deposition cycle on PANI	11
Figure 2.3: Electrochemical Flow Cell	13
Figure 2.4: Schematic of the Experimental Setup	13
Figure 2.5: Ag/AgCl in 0.1M KCl reference electrode with double junction of 0.1M KNO <sub>3</sub> in agar	14
Figure 2.6: Cyclic voltammogram of a 2.5mM solution of hexamine ruthenium (III) redox couple in 1M KNO <sub>3</sub>	15
Figure 2.7: Overlaid CVs of PANI/Au <sub>0</sub> recorded in 0.1M HCl normalized to the moles of PANI for the first deposition cycle (A), for all 8 cycles (B), and CVs of PANI/Au <sub>8</sub> for all 8 cycles (C)	16
Figure 2.8: Overlaid reduction peaks of AuCl <sub>4</sub> <sup>-</sup> after the subtraction of PANI/Au <sub>0</sub> from PANI/Au <sub>8</sub> for cycles 1-8	18
Figure 2.9: The calculated number of moles expected of AuCl <sub>4</sub> <sup>-</sup> that can be reduced per cycle based on a 2Au:1PANI repeat unit stoichiometry	19
Figure 3.1: Cyclic voltammograms of PANI before (---) and after (—) holding at +0.8V for 300s in (A) 0.1M HCl, (B) 0.1M HBF <sub>4</sub> and (C) 0.1M HClO <sub>4</sub>	22
Figure 3.2: Cyclic voltammograms of PANI in 0.1M HCl (A) initially before overoxidation, (B) after 30 minutes at +0.8V, (C) after 60 minutes at +0.8V, and (D) after 90 minutes at +0.8V	23

Figure 3.3: FTIR spectra of (a) PANI and (b) PANI after 1hr oxidative degradation at +0.8V in 0.1M HCl	25
Figure 3.4: Cyclic voltammograms of PANI in 0.1M HClO <sub>4</sub> before (---) and after (—) 300s of holding the potential at (A) +0.8V, (B) +0.7V, and (C) +0.65V	27
Figure 3.5: Optimized timing diagram for the atomic deposition of gold into PANI	29
Figure 3.6: Cyclic voltammograms for (A) PANI/Au <sub>0</sub> and (B) PANI/Au <sub>8</sub> taken before the first gold deposition cycle and after each deposition cycle for 1 through 8 cycles	30
Figure 3.7: Depiction of the charge transfer complex formed between gold and PANI	32
Figure 3.8: Relative changes in work function of PANI/Au <sub>N</sub> films for N = 0 - 9 measured versus a vibrating gold grid reference electrode	32
Figure 3.8: Relative changes in work function of PANI/Au <sub>N</sub> films (for N = 0 - 9) versus the natural log of N+1	33
Figure 3.10: XPS spectra of PANI/Au <sub>N</sub> , N=5, 6, 7, and 8	36
Figure 4.1: CVs of bare Pt (---) and PANI on Pt (—) in (A) 1M NaOH and in (B) 0.5M n-propanol in 1M NaOH at 20mV/s	39
Figure 4.2: Effect of added 0 to 8 Au atoms to PANI on oxidation of 0.5M n-propanol in 1M NaOH (—) taken at 20 mV/s	41
Figure 4.3: Peak current densities from the oxidation of n-PrOH versus the number of inserted gold atoms for (I) the first oxidation peak and (II) the second oxidation peak	42
Figure 4.4: Linear dependence of peak current on n-PrOH concentration for PANI/Au <sub>6</sub> for (■) the first oxidation peak and (▲) second oxidation peak	43
Figure 4.5: Peak current densities of peak I and peak II for PANI/Au <sub>2</sub> for different concentrations of the chloroaurate solution	44
Figure 4.6: FTIR of PANI indicating the location of the N-H, N=Q=N, and N-B-N peaks	46
Figure 4.7: Peak shift of N-H stretch at 3300cm <sup>-1</sup> for PANI/Au <sub>N</sub> (N=0-8) plotted versus the number of Au cycles (solid line) showing an odd-even pattern	47

Figure 4.8: Plot of $1/R$ for PANI/Au <sub>N</sub> (N=0-8) versus the number of Au cycles showing an odd-even pattern	47
Figure 5.1: Survey of cyclic voltammograms recorded in a series of 0.5M linear alcohols in 1M KOH on the following electrodes: (A) Au BAS, (B) Pt/PANI, (C) Pt/PANI/Au <sub>macro</sub> , (D) AGE-2, (E) AGE-4, (F) AGE-6, (G) AGE-3, (H) AGE-5 and (I) AGE-7	52
Figure 5.2: Cyclic voltammograms recorded in the series of 0.5M linear alcohols in 1M KOH on (A) Pt/PANI, (B) Pt/PANI/Au <sub>macro</sub> , (C) AGE-5 and (D) AGE-6	54
Figure 5.3: Survey of cyclic voltammograms recorded in a series of 0.5M butanols in 1M KOH on the following electrodes: (A) Au BAS, (B) Pt/PANI, (C) Pt/PANI/Au <sub>macro</sub> , (D) AGE-2, (E) AGE-4, (F) AGE-6, (G) AGE-3, (H) AGE-5 and (I) AGE-7	56
Figure 5.4: Cyclic voltammograms recorded in the series of 0.5M butanols in 1M KOH on (A) Pt/PANI, (B) Pt/PANI/Au <sub>macro</sub> , (C) AGE-5 and (D) AGE-6	57
Figure 5.5: Cyclic voltammograms recorded in 0.5M branched alcohols in 1M KOH on the following electrodes: (A) Au BAS, (B) Pt/PANI, (C) Pt/PANI/Au <sub>macro</sub> , (D) AGE-2, (E) AGE-4, (F) AGE-6, (G) AGE-3, (H) AGE-5 and (I) AGE-7	58
Figure 5.6: Cyclic voltammograms of Pt/PANI in 1M n-PrOH in 1M NaOH with oxygen (dashed line) and without oxygen (solid line)	59
Figure 5.7: Cyclic voltammograms of a glassy carbon electrode in (A) 1M NaOH and (B) 0.5M n-PrOH in 1M NaOH	60
Figure 5.8: Cyclic voltammograms of PANI deposited on a glassy carbon electrode in (A) 1M NaOH and (B) 1M n-PrOH in 1M NaOH	61
Figure 5.9: CVs of PANI/Au <sub>6</sub> in 0.5M n-PrOH in 1M NaOH before bubbling with N <sub>2</sub> for 1hr (dashed line) and after bubbling with N <sub>2</sub> for 1hr (solid line)	62
Figure 6.1: CV of 0.1M HClO <sub>4</sub> (dashed line) and 1mM K <sub>2</sub> PdCl <sub>6</sub> in 0.1M HClO <sub>4</sub> (solid line) from -0.2V to +1.5V at a scan rate of 20mV/s	65
Figure 6.2: Stripping voltammograms of Pd in (A) 0.1M HCl and in (B) 0.1M HClO <sub>4</sub>	66

Figure 6.3: CV of (A) PANI coated Pt and (B) Pd coated Pt BAS in 1M NaOH from -0.8V to +0.45V	68
Figure 6.4: CVs of PANI/Pd <sub>N</sub> for N=1-6 in 1M NaOH from -0.8V to +0.45V at a scan rate of 20mV/s	69
Figure 6.5: Cyclic voltammograms of 0.5M n-PrOH in 1M NaOH recorded (A) with Pt electrode (dashed line) and PANI deposited on Pt (solid line), and (B) with Pd coated BAS electrode	70
Figure 6.6: CVs of PANI/Pd <sub>N</sub> for N=1-6 from -0.8V to +0.45V in 0.5M n-PrOH in 1M NaOH	72
Figure 6.7: Peak current at +0.34V versus the number of Pd cycles	73
Figure 6.8: FTIR peak shift for the N-H stretching at 3300cm <sup>-1</sup> for PANI/Pd <sub>N</sub> for N=0-6	74
Figure 6.9: Plot of 1/R from FTIR versus N for PANI/Pd <sub>N</sub> (N=1-6) showing the oxidation level of the PANI changes as inserted Pd acts as a dopant	75
Figure 6.10: The molar ratios of Au:Pd for Au <sub>1.5</sub> Pd <sub>1</sub> (top) and Au <sub>1.4</sub> Pd <sub>2</sub> (bottom)	77
Figure 6.11: CVs of PANI/Au <sub>N</sub> Pd <sub>1</sub> for N=1-5 from -0.8V to +0.45V in 0.5M n-PrOH in 1M NaOH	79
Figure 6.12: CVs of PANI/Au <sub>N</sub> Pd <sub>2</sub> for N=1-4 from -0.8V to +0.45V in 0.5M n-PrOH in 1M NaOH	80
Figure 6.13: Peak currents (solid lines) of n-PrOH oxidation (at approximately -0.04V) versus the number of inserted Au atoms in Au <sub>N</sub> Pd <sub>1</sub> (top) and for Au <sub>N</sub> Pd <sub>2</sub> (bottom)	81
Figure 6.14: Comparison of CVs for the oxidation of 0.5M n-PrOH in 1M NaOH for atomic clusters consisting of a total of 3 metal atoms	82
Figure 6.15: CVs of Au <sub>2</sub> Pd <sub>1</sub> in 0.5M n-PrOH in 1M NaOH when (A) Pd is deposited first and (B) Au is deposited first	83
Figure 7.1: Cyclic voltammograms recorded in 0.5M MeOH in 1M KOH on (a) Pt/PANI-Au <sub>n=2 to 7</sub> and (b) Pt/PANI-Pd <sub>n=2 to 6</sub>	86
Figure 7.2: Voltammograms recorded in (a) 1M KOH with (b) 0.5M MeOH, (c) 0.5M EtOH and (d) 0.5M i-PrOH on Pt/PANI-Au <sub>n=1 to 5</sub> Pd <sub>1</sub>	88

Figure 7.3: Oxidation peak currents densities for $Au_n$ (dashed lines) and $Au_{n-1}Pd$ (solid lines) versus the total number of atoms in the cluster for (a) MeOH and (b) EtOH	90
Figure 7.4: Current densities of the oxidation peak in the forward scan (shown in red) for (a) 0.5 M MeOH and (b) 0.5M EtOH in 1.0M KOH at Pt/PANI- $Au_nPd_1$ electrode ( $n = 1-5$ ) are compared with the calculated HOMO-LUMO gaps of the ground states of $Au_nPd_1$ clusters for $n=1-5$	92
Figure 7.5: Scan rate dependence of cyclic voltammograms recorded in (a) 0.5M MeOH and (b) 0.5M EtOH in 1.0M KOH solution on Pt/PANI- $Au_3Pd_1$ electrode	93
Figure 7.6: Concentration dependence of cyclic voltammograms recorded on Pt /PANI- $Au_4Pd_1$ in 1.0 M KOH solution with increasing concentrations of (a) MeOH and of (b) EtOH	94
Figure A.1: Steady-state cyclic voltammograms for (1) Pt/PANI, (2) Pt/PANI/ $Au_4$ and (3) Pt/PANI/ $Au_5$	103
Figure A.2: Oxidation of 0.5 M n-PrOH, in 1 M KOH recorded at polycrystalline Au electrode (BAS)	104
Figure A.3: Survey of the steady-state CVs for oxidation of (a) n-PrOH and (b) i-PrOH for Pt/PANI/ $Au_N$ ( $2 < N < 7$ ) electrodes	105
Figure A.4: Dependence of peak current on square root of scan rate for Pt/PANI/ $Au_6$ for both alcohols	107
Figure A.5: The activation pattern of polycrystalline Au electrode (BAS)	108
Figure A.6: The survey presentation of the activation pattern for the AGEs ( $2 < N < 7$ ) for n-PrOH	110
Figure A.7: Comparison of the activation pattern for (rows) Pt/PANI/ $Au_4$ and Pt/PANI/ $Au_5$ and for n-PrOH and i-PROH (columns)	111
Figure B.1: Comparison of $I_D-V_G$ curves recorded for CHEMFET's with cast PANI-CSA and PANI-CSA/IL gel-hybrid gate material, respectively	118
Figure B.2: Comparison between electronic properties of PANI-CSA films cast on quartz glass (a) without and with (b) 0.51 $\chi$ , (c) 0.68 $\chi$ and (d) 0.76 $\chi$ of ionic liquid	121

Figure B.3: Gate voltage change of CHEMFET with gate layer cast from PANI-CSA with [THA][Tf <sub>2</sub> N] ( $\chi = 0.76$ ) to stepwise changes to ammonia	122
Figure B.4: Comparison between averaged sensitivities to ammonia of CHEMFET's as a function of mole fraction of IL in the PANI-CSA matrix	123
Figure B.5: Responses for step up (35 to 55ppm) and step down (55 to 35ppm) in ammonia concentration for PANI films with and without ILs	124

## SUMMARY

It is ideal to theoretically predict the activity of a catalyst. It has been recognized that not only the type of metal, but also its atomic size plays an important role in catalysis. In the past, atomic clusters have been created by sputtering from a sacrificial metal plate and then using a mass selector to choose cluster sizes from 1-233 atoms of gold. This approach has practical limitations. In this thesis, I describe a procedure by which atomic clusters of gold containing 1-8 atoms are deposited in polyaniline as an isolation matrix. My atomic deposition follows a cyclic pathway. Atomic clusters of palladium and atomic alloys of gold and palladium are also deposited in polyaniline using the same process. It is to show that this method will also work for other metals. These composite materials are characterized, and the catalytic activity for alcohol oxidation is evaluated.

This thesis is divided into seven chapters. The first chapter discusses the chemistry of polyaniline for using gold and palladium as catalysts. The technique developed to deposit the atomic clusters is discussed in the second chapter. This technique deposits one atom of metal per imine site on polyaniline, per cycle. The cycle is repeated n-times until a cluster of specified size,  $M_n$ , and composition has been synthesized. It is known that polyaniline plays an important role in stabilization of the formed clusters which prevents their aggregation. The optimization of this technique is the topic of the third chapter along with the description of how these composite films are produced. To end this chapter, the composite films are

characterized by cyclic voltammetry, Kelvin probe, and X-ray photoelectron spectroscopy.

In chapters 4 and 5, the catalytic activity of the polyaniline/gold composites for the oxidation of alcohols in alkaline media using cyclic voltammetry is evaluated. In chapter 4, the correlation of the electrochemical activity for the oxidation of n-PrOH with the odd-even pattern from the calculated HOMO-LUMO gap energies for the same size clusters is shown. It is shown that the infrared spectrum of polyaniline with different sizes of atomic gold clusters also follows the odd-even pattern. Chapter 5 expands on the discussion of the catalytic oxidation of alcohols. The oxidation of methanol, ethanol, propanol, and butanol is surveyed. The peak currents are again dominated by the odd-even pattern.

In chapter 6, the versatility of the atomic deposition cycle is shown by depositing atomic palladium clusters. The peak currents for the oxidation of n-PrOH by these palladium composite films again follows the predicted pattern of the calculated HOMO-LUMO gap energies for atomic palladium clusters. This chapter also explores bimetallic atomic clusters of gold and palladium. The results indicate that the catalytic activity depends on the orientation of the cluster in the polyaniline matrix. Chapter 7 discusses the oxidation of methanol, ethanol, and isopropanol on  $Au_nPd_1$  bimetallic atomic clusters. The addition of palladium in the cluster increases the peak current densities for the oxidation of both alcohols except for the most stable of the atomic gold clusters, while it inactivated the electrodes for isopropanol. The possible future work for this project is discussed in chapter 8.

Overall, this thesis has developed a novel and unique technique for depositing atomic metal clusters into a polyaniline matrix. The technique is versatile enough to

deposit atomic metal clusters other than gold, as shown by creating atomic palladium clusters and atomic bimetallic clusters of gold and palladium. This is extremely useful, since this single technique can produce many different types of atomic catalysts. The composite materials have been shown to be catalytically active for the oxidation of alcohols in alkaline media. This indicates a significant improvement to conserve precious metals while still retaining a high catalytic activity.

# CHAPTER 1

## INTRODUCTION

### 1.1 Objective

The main objective of this thesis is to deposit gold into a polyaniline matrix one atom at a time to form atomic clusters of gold. The atoms are deposited in a cyclic pathway that is repeated until the desired number of atoms is reached. The catalytic activities of the clusters are unique for each cluster size. Using the same cyclic pathway of atomic deposition of gold, other pure metals or a mixture of metals can be deposited in a similar way. An efficient catalyst containing only a few atoms will greatly reduce the cost to produce the catalyst.

### 1.2 Polyaniline

Polyaniline (PANI) is an electroactive polymer of aniline. PANI has been of great interest due to its environmental stability<sup>1-3</sup>, conductivity<sup>4,5</sup>, and for its redox properties<sup>6,7</sup>. PANI is made up of repeat benzenoid and quinoid units. The general formula for PANI is shown in Figure 1.1A. PANI has three oxidation states. The pernigraniline state is the fully oxidized form (Figure 1.1B). The emeraldine state is the partially oxidized state (Figure 1.1C), and the leucoemeraldine state is the fully reduced form (Figure 1.1D)<sup>8</sup>.

Polyaniline is formed from the monomer aniline in a radical polymerization. The cation radical of aniline reacts with the cation radical of p-aminodiphenylamine to form the trimer. Continuation of these reactions forms oligomers and eventually the polymer<sup>9</sup>.

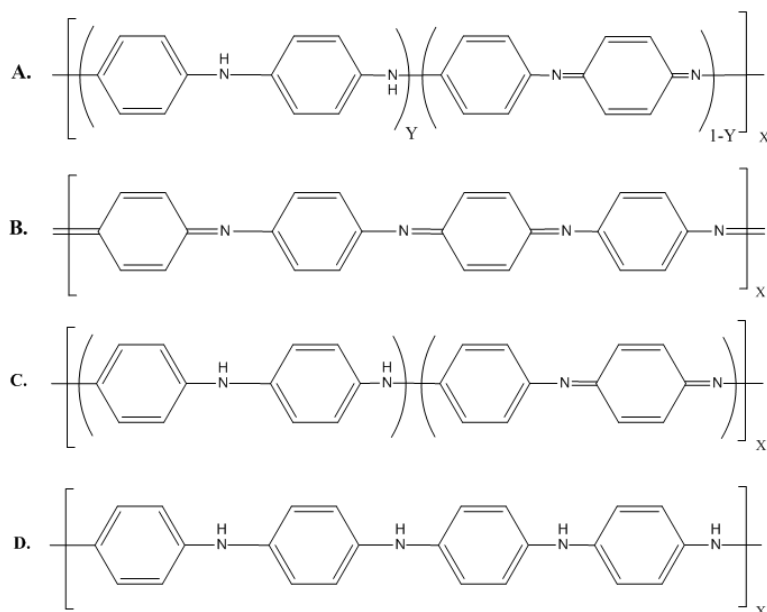


**Figure 1.1.** (A) PANI base general composition and oxidation states: (B) pernigraniline base (C) emeraldine base (D) leucoemeraldine base.

The insulating emeraldine base can be rendered conducting by protonation with a protonic acid to yield the emeraldine salt<sup>10</sup>. Only the emeraldine salt form of PANI is conducting. The salt forms are shown in Figure 1.2. The salt form will be important when inserting metal atoms in the polymer.

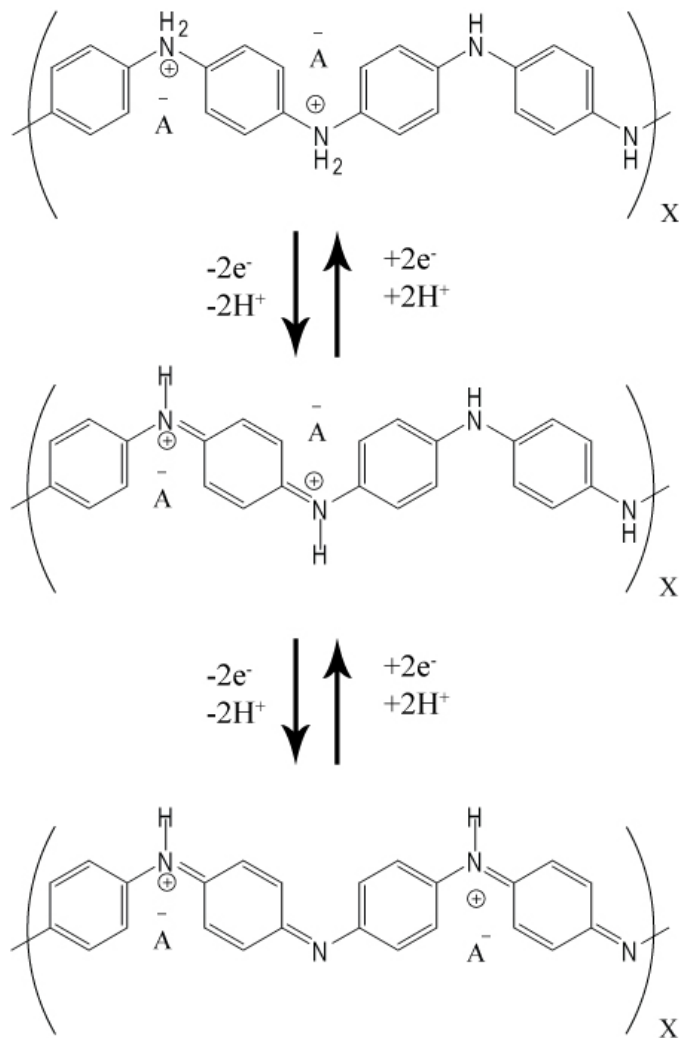


**Figure 1.2.** Salt forms of PANI. leucoemeraldine salt (top), emeraldine salt (middle), and pernigraniline salt (bottom).

### 1.3 Polyaniline as a Support Matrix

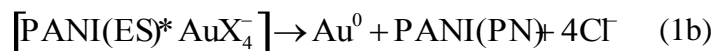
The interest of this study is in atomic gold clusters supported in a polyaniline matrix. The chemical properties of gold change as the size approaches the nanometer size. Where bulk gold is inert, nanoclusters of gold have been found to have interesting new properties such as optical properties, as displayed by the surface plasmon<sup>11</sup>, and catalytic properties for such reactions as carbon monoxide oxidation<sup>12</sup>.

These emerging properties are size dependent, and the high surface to volume ratio of these nanoclusters results in a large number of binding sites for catalysis and chemical sensing. A combination of these nanoclusters with a conducting polymer can give a material with new properties. The nanoclusters may impart magnetic, catalytic, or sensing properties to the polymer matrix.

The catalytic effect of gold nanoclusters is not only size dependent, but also depends on the substrate. Although oxygen can absorb onto the gold, it is believed that the role of the substrate in the catalysis is to increase the activity of molecular oxygen<sup>13</sup>. The most common substrates to date have been metal oxides such as oxides of titanium, iron, cobalt, nickel, zinc, and zirconium<sup>14-17</sup>.

Conducting polymers have also proven to be a suitable host matrix for dispersing metallic nanoparticles. Polyaniline with Pd<sup>18</sup> and with Pt<sup>19</sup> nanoclusters have shown catalytic activity. Gold nanoclusters in polyaniline with multiwalled carbon nanotubes have also shown catalytic activity for methanol oxidation<sup>20</sup>, however, their study failed to include results for PANI/Au without the carbon nanotubes.

The metal anions of AuX<sub>4</sub><sup>-</sup> have a high affinity for the protonated imine repeating units in PANI<sup>21</sup>. For example, the chloroaurate anion has a K<sub>eq</sub>=10<sup>10</sup> with the protonated imine nitrogen<sup>22</sup>. It has been shown that these anions can spontaneously reduce from AuX<sub>4</sub><sup>-</sup> to Au<sup>0</sup> on polyaniline in the emeraldine salt form, PANI(ES)<sup>21,23</sup>. This reaction is shown in equation 1 where PANI(ES) is the reducing agent in the three electron reduction of AuX<sub>4</sub><sup>-</sup>, where PANI(PN) stands for the pernigraniline form of PANI.



One obstacle to nanocluster growth is controlling the size of the final cluster. This has typically been done by adding capping agents such as thiols or surfactants<sup>24,25</sup>. In the case of the reduction of gold occurring at the imine nitrogen of polyaniline, the PANI chain should act as a barrier against aggregation. Therefore, Au clusters formed in PANI matrix are uncapped. For this reason their catalytic properties are expected to be different from those of the capped Au clusters. However, it has been found that by simply dipping a platinum plug coated with PANI into an aqueous solution of  $\text{KAuBr}_4$  that the gold clusters that were formed were much larger than expected<sup>22</sup>. In fact, the size of the gold clusters formed was more than what could have been formed from the electrons supplied by the PANI corresponding to the stoichiometry in equation 1. In aqueous media, this reaction will proceed until the imine sites have been completely blocked or the anion is exhausted.

In order to control the deposition of gold, a ‘bottom up’ approach has been suggested<sup>26</sup>. In this approach, it is proposed that one atom is deposited at a time on the imine sites of polyaniline. Each deposition cycle starts with dipping the PANI into a solution of  $\text{Ce}(\text{SO}_4)_2$  to fully oxidize the film. The film is then removed and dipped into a dilute solution of  $\text{KAuCl}_4$  to bind the chloraurate anion per imine site. The excess solution is rinsed off, and the chloraurate is reduced by exposure to a solution of hydrazine. However, with this approach, each time the film is removed from solution, the PANI can revert back to the previous oxidation state by relaxation of the polymer and spontaneous reduction of the gold can occur. To achieve an atom by atom deposition on

PANI, precise control of the potential of the film and solution flow to the film must be maintained.

#### **1.4 Gold and Palladium as Catalysts**

Nano-sized gold has been extensively investigated because physical and chemical properties of gold clusters are known to change with their size<sup>27-29</sup>. Both bulk gold and gold nanoclusters have catalytic properties for oxidation of alcohols in alkaline medium,<sup>30-36</sup> and for carbon monoxide<sup>37,38</sup>. There are several reports of gold clusters containing only a few atoms being catalytically active<sup>39,40</sup>. The stability of atomic gold clusters of Au<sub>N</sub> where N = 1-10 depends on binding energy, dissociation energy, second order difference in total energy, and HOMO-LUMO energy gap (Figure 1.3)<sup>41-43</sup>. These theoretical studies show that neutral (ground state) gold clusters exhibit an odd-even oscillation due to electron-pairing effect for the second order difference in total energy and in the HOMO-LUMO energy gap where the even numbered gold clusters are more stable than the odd numbered clusters. Gold clusters made of 2 and 6 atoms have the largest HOMO-LUMO gap and dissociation energy, while the second order difference in total energy is the lowest for these two, which confirms their high stability<sup>41-43</sup>. The Au<sub>2</sub> and Au<sub>6</sub> clusters have two dimensional structures<sup>44,45</sup>.

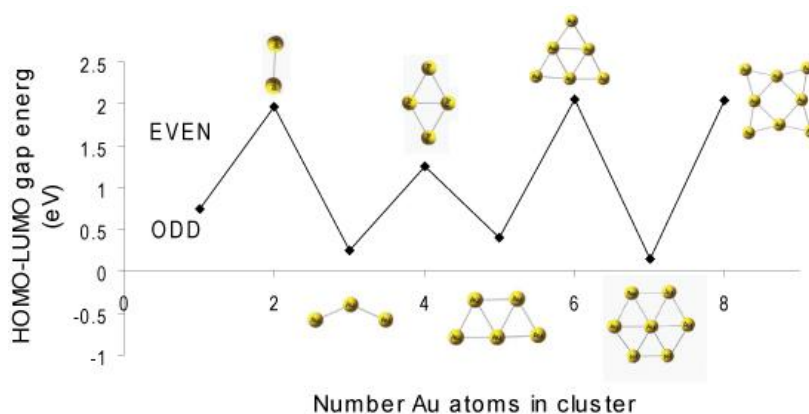


**Figure 1.3.** Calculated HOMO-LUMO gap energies for atomic clusters of gold with the lowest energy structures<sup>41,42</sup>.

It is known that catalytic performances of gold clusters depend on their preparation methods, support matrix, and their size<sup>39,46-50</sup>. In this study we use as the support matrix a polyaniline (PANI) film electrochemically deposited on a Pt electrode. It has been demonstrated that both, PANI containing metal precipitates and PANI modified electrodes, show electrocatalytic oxidation of primary alcohols in alkaline and acidic medium,<sup>51-55</sup> but the catalytic effect is higher in the alkaline medium.

Palladium deposited into a PANI matrix has shown catalytic activity for formic acid oxidation<sup>56</sup>, Suzuki coupling reactions<sup>57,58</sup>, hydrogenation reactions<sup>59,60</sup> as well as the oxidation of alcohols such as methanol and ethanol<sup>18,54,61-63</sup>. Bimetallic or trimetallic clusters containing more than one type of metal can have chemical and physical properties that change with the size, composition, or atomic ordering. The influence of the neighboring atoms in bimetallic clusters can lead to different or sometimes better catalytic activities than those of the monometallic clusters. In the case of gold and palladium, the different activity mainly arises from differences in their electron

configuration and their electronegativities. Gold has a 5d electron configuration, which leads to a stable metal-metal bond. On the other hand, Pd has a closed 4d shell, and requires the promotion of one electron to the 5s shell in order to form a stable metal-metal bond. Atomic gold clusters with less than 10 atoms have a 2D planar geometric configuration<sup>42</sup>, while atomic Pd clusters favor a 3D geometry. When introducing a single atom of Au or Pd into a pure cluster of the other metal, those shapes do not change, but when the composition consists of an equal amount of the two, then the most stable configuration lies somewhere in between the two<sup>64</sup>. Bimetallic clusters of Au and Pd have shown activity for the oxidation of alcohols<sup>65,66</sup> including selective oxidation of glycerol<sup>67</sup> and has also been used for the direct synthesis of hydrogen peroxide<sup>68</sup>. Therefore, the electrooxidation of n-propanol in alkaline medium has been chosen as the indicator of size defined catalytic activity. The main reaction for the oxidation of alcohols is the dehydrogenation of the alcohol to form the corresponding carboxylic acid, in this case, propionic acid.

## CHAPTER 2

### ATOMIC GOLD DEPOSITION ON POLYANILINE

#### 2.1 Atomic Gold Deposition Cycle

The controlled method of deposition of one gold atom per imine site of PANI without interrupting the electrochemical contact to the film follows a “cyclic deposition” approach, as shown in Figure 2.1.

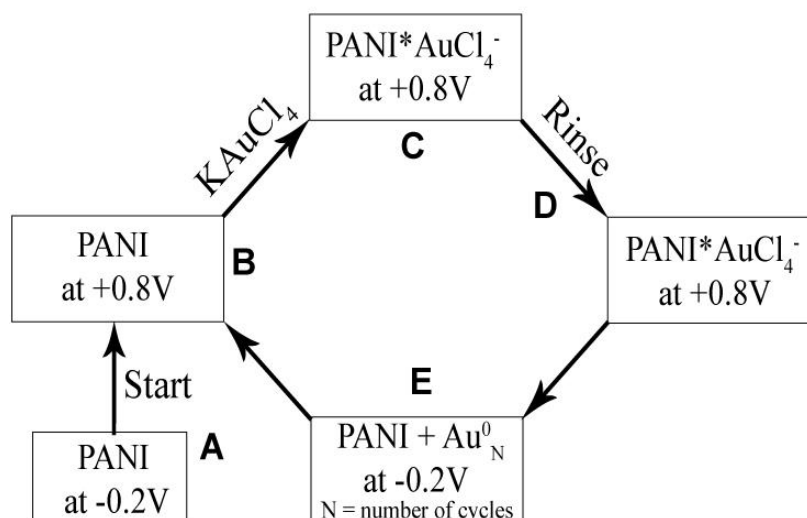


**Figure 2.1.** Cyclic pathway for the deposition of atomic gold in PANI.

The process begins with sweeping the potential from -0.2V (A) to +0.8V (B). When holding the potential at +0.8V, the PANI(ES) is oxidized to the PANI(PN) form. The PANI(PN) complexes with AuCl<sub>4</sub><sup>-</sup>, but it cannot spontaneously reduce AuCl<sub>4</sub><sup>-</sup> to atomic gold. While the potential is held at +0.8V, the film is exposed to a solution of KAuCl<sub>4</sub> to form a stoichiometric PANI(PN)\*AuCl<sub>4</sub><sup>-</sup> complex (C) according to reaction 1a. The

excess  $\text{AuCl}_4^-$  anions that are not attached to PANI(PN) are then thoroughly rinsed away with a 0.1M HCl solution (D). The potential is then scanned in the negative direction to -0.2V which reduces the  $\text{PANI(PN)}^*\text{AuCl}_4^-$  complex to atomic gold and PANI in reduced form (E). Once the  $\text{AuCl}_4^-$  is reduced, the imine sites on PANI become free and are available again for the accommodation of  $\text{AuCl}_4^-$  anions in the next cycle. If the amount of PANI remains the same for each cycle, then we can assume that the amount of gold reduced in each cycle should also be the same. Unfortunately, there is an oxidative degradation resulting in the loss of PANI occurring in parallel with the Au deposition. Therefore, the number of available imine sites in PANI decreases slightly.

The steps from A to E in Figure 2.1 are also shown in the timing diagram for the atomic gold deposition cycle in PANI (Figure 2.2). A total of nine samples were prepared that include PANI with 0 to 8 gold deposition sequences, which will be referred to as  $\text{PANI/Au}_N$  where  $N=0\dots 8$ . The sample  $\text{PANI/Au}_0$  underwent eight consecutive cycles where the use of the  $\text{KAuCl}_4$  solution was always substituted with a 0.1M HCl solution. This was done in order to determine the extent of PANI degradation during our procedure.

As mentioned above, the potential of the PANI film and the introduction of the  $\text{KAuCl}_4$  solution must be carefully controlled in order to avoid spontaneous reduction. This was accomplished using the timing diagram shown in Figure 2.2.

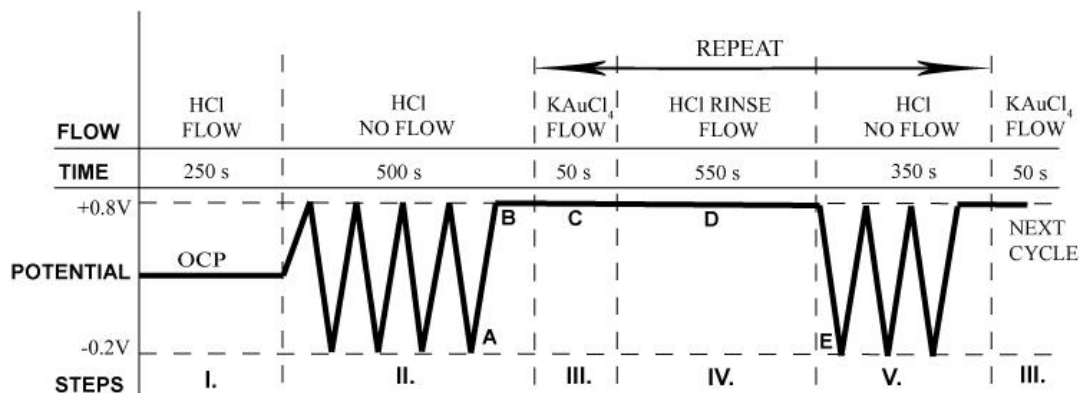


**Figure 2.2.** Timing diagram for the atomic gold deposition cycle on PANI. The letters A-E are assigned to the same processes as in Figure 2.1.

The PANI film is held at open cell potential ( $E_{oc}$ ) while the cell is rinsed with 0.1M HCl for a period of 250 seconds (step I). The flow of HCl is stopped and four cyclic voltammograms (CV) are recorded with a scan rate of 20mV/s from +0.8V to -0.2V (step II). Before the solution of  $AuCl_4^-$  is introduced, the potential is held at +0.8V at the end of this step for 50s to make sure that the entire film is oxidized to the PANI(PN) form (step II). As the potential of the electrode is held for another 50s at +0.8V, the PANI(PN) film is exposed to  $10^{-5}$ M  $KAuCl_4$  in 0.1M HCl by flowing the solution through the cell (step III). Excess  $AuCl_4^-$  anions that are not attached to the PANI film are rinsed away with 0.1M HCl for 550 s while the potential is still held at +0.8V (step IV). This step is crucial because it ensures that only the anions stoichiometrically attached to the PANI are reduced. The flow of HCl is stopped, and the potential of the film is swept at a rate of 20mV/s from +0.8V to -0.2V to reduce the attached  $AuCl_4^-$  ( $Au^{3+}$ ) to atomic gold ( $Au^0$ ). This reduction will free up the imine sites for the next gold deposition cycle. The subsequent CVs are then recorded to characterize the film. After recording the CVs, the potential is held at +0.8V to oxidize the film completely without re-oxidizing the atomic

gold (step V). The film is now ready for the next cycle. Steps III, IV, and V are repeated until the desired number of gold atoms ( $N=1 \dots 8$ ) are deposited. The film is then brought back to the open cell potential to end the sequence.

## **2.2 Electrochemical Polymerization of Polyaniline Films**

The polymerization of PANI was performed in a three electrode electrochemical cell. The polymerization was carried out on one side of a Pt (1000Å) coated on Ti (100Å) 10MHz polished quartz crystal microbalance (QCM) (International Crystal Manufacturing OKC, OK, USA) from a 0.1 M aniline/2 M HBF<sub>4</sub> aqueous solution at a constant potential of +0.9V for 200 seconds. The reference electrode was a Ag/AgCl in 1 M KCl, and the counter electrode was a Pt foil. The film was then cycled from -0.2V to +0.8V at a scan rate of 20mV/s in 0.1M HCl until stable. Data was collected using a Solartron SI1287 electrochemical interface.

## **2.3 Deposition of Atomic Gold in PANI**

This procedure requires that the potential of PANI and the exposure time to a AuCl<sub>4</sub><sup>-</sup> solution must be precisely controlled. In order to fulfill the requirements, a flow through cell was used as shown in Figure 2.3.

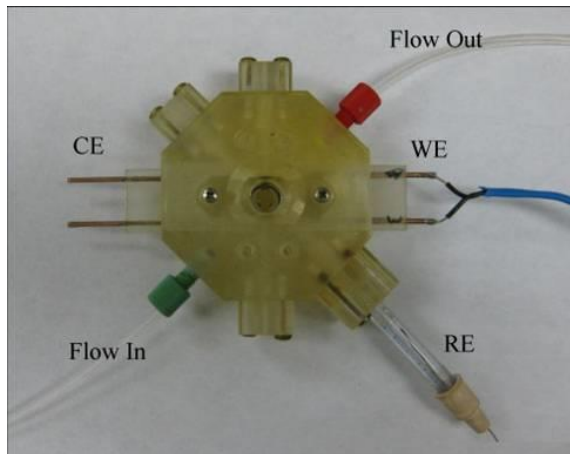


**Figure 2.3.** Electrochemical Flow Cell

The experimental setup is shown in Figure 2.4. By using this arrangement, the electrochemical contact to the PANI film is never interrupted while the PANI is in contact with  $\text{AuCl}_4^-$  solution.

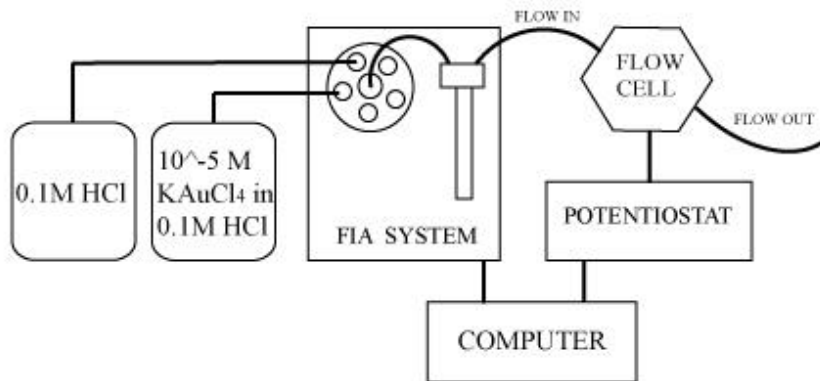


**Figure 2.4.** Schematic of the Experimental Setup

The PANI coated QCM is the working electrode. It is placed on one side of the flow cell. A bare Pt QCM placed on the other side of the flow cell is the counter electrode. Both QCMs are sealed in place using Viton o-rings. The QCMs are mounted in the center of the flow cell so they are above and below the solution flow, respectively.

Contacts to the counter and working electrodes are made from the sides of the crystals. A special reference electrode was constructed in order to fit the flow cell and to accommodate the orientation in the flow cell. The reference electrode is a Ag/AgCl in 0.1M KCl with a double junction of 0.1M KNO<sub>3</sub> in agar as shown in Figure 2.5. All the potentials are reported versus this reference electrode. It is mounted through another side port of the flow cell. The flow cell also contains separate inlet/outlet side-ports.

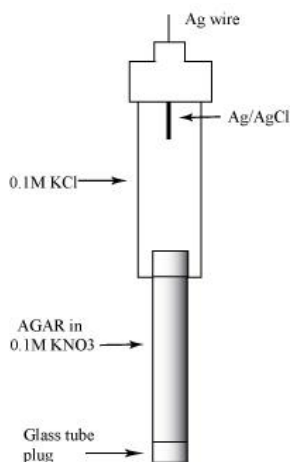


**Figure 2.5.** Ag/AgCl in 0.1M KCl reference electrode with double junction of 0.1M KNO<sub>3</sub> in agar.

The potential of the reference electrode was determined by cyclic voltammetry in a 2.5mM solution of hexamine ruthenium (III) redox couple in 1M KNO<sub>3</sub>. The standard potential of the hexamine ruthenium (III) redox couple is 0.100V vs NHE. From the oxidation and reduction peak potentials in the voltammogram, the standard potential of the redox couple was determined to be -0.228V vs the constructed reference electrode as shown in Figure 2.6, therefore the potential of the reference electrode was determined to be 0.328V vs NHE.

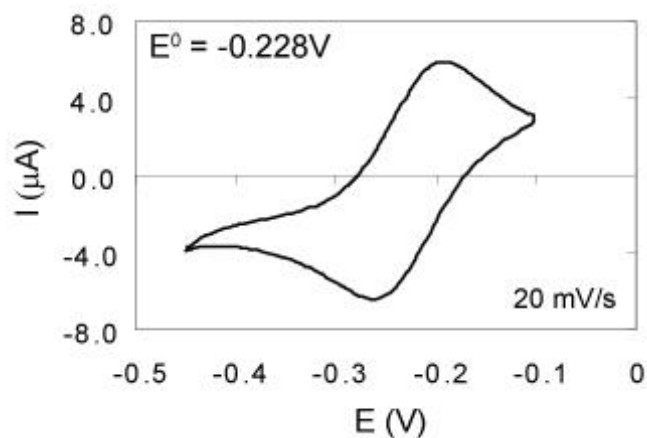


**Figure 2.6.** Cyclic voltammogram of a 2.5mM solution of hexamine ruthenium (III) redox couple in 1M  $\text{KNO}_3$ .

The applied potential to the film is controlled by an OMNI 90 potentiostat (Cypress Systems, Lawrence, KS. USA). The rotating selector valve and syringe pump on a FIAlab flow injection system (Alitea Instruments, Medina, WA. USA) controls the flow of the solution through the cell. The solutions of 0.1M HCl and  $10^{-5}\text{M}$   $\text{KAuCl}_4$  in 0.1M HCl were degassed prior to use in order to eliminate the formation of air bubbles inside the flow cell. Operations of the potentiostat and the flow injection system were controlled simultaneously using a Labview program.

It is well known that PANI undergoes oxidative damage. Therefore, we first tested our method of sequential gold insertion into PANI by looking at the stability and behavior of PANI as it goes through consecutive deposition cycles, according to our timing diagram in Figure 2.2, but exposed to 0.1M HCl instead of the  $\text{AuCl}_4^-$  solution. Cyclic voltammograms for PANI/ $\text{Au}_0$  normalized to the number of moles of PANI present at the electrode are shown in Figure 2.7A.

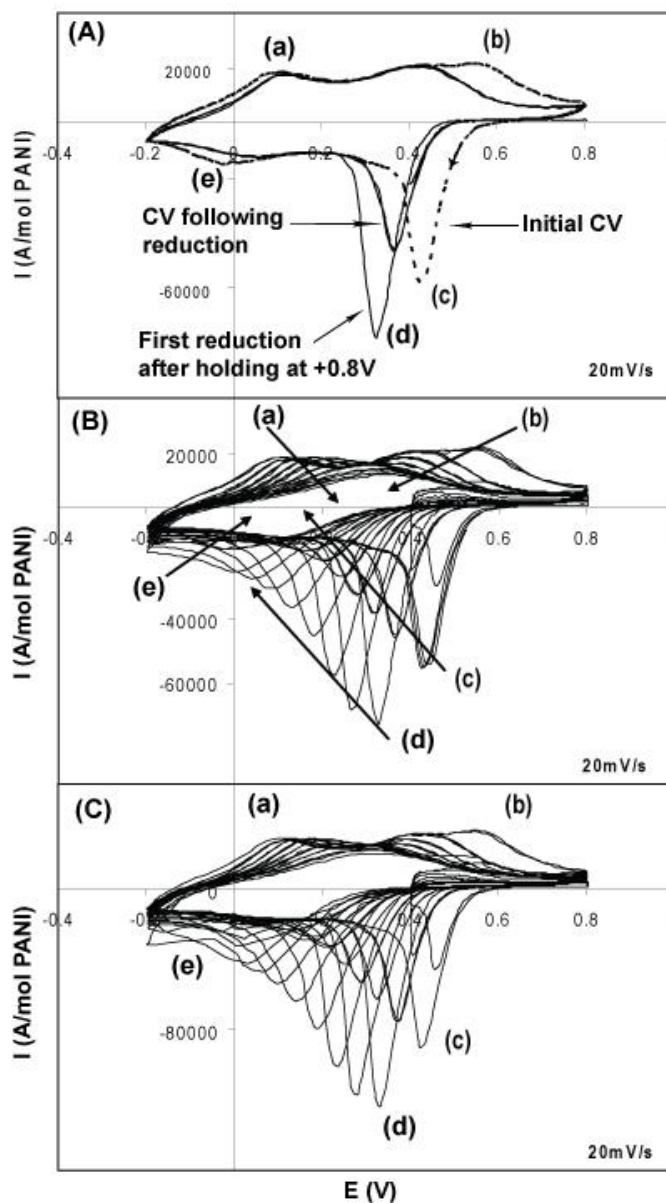


**Figure 2.7.** Overlaid CVs of PANI/Au<sub>0</sub> recorded in 0.1M HCl normalized to the moles of PANI for the first deposition cycle (A), for all 8 cycles (B), and CVs of PANI/Au<sub>8</sub> for all 8 cycles (C) following the timing diagram in fig. 2.2. Peaks (a) and (b) are the oxidation peaks, and peaks (c) and (e) are the reduction peaks of PANI. Peak (d) is the first reduction peak after holding at +0.8V for 650s.

According to the timing diagram in Figure 2.2, the initial CV of the PANI film was recorded in step II. The first reduction sweep following the holding of the potential at

+0.8V and the next two CVs recorded immediately following this reduction (step V) are also included. Figure 2.7B shows the CVs for PANI/Au<sub>0</sub> for all eight cycles. The peaks labeled (a) and (b) correspond to the oxidation and (c) and (e) to the reduction of PANI. The peaks also correspond to ion migration in and out of the film in order to maintain charge neutrality<sup>69,70</sup>. Peak (a) has been attributed to the exit of a proton from the film as the first oxidation occurs around +0.10V. That peak is used for normalization as the measure of electroactive PANI available at the electrode. As the film is further oxidized, anions enter the film at peak (b) around +0.56V. On the negative scan at +0.43V, peak (c) is the exit of the anions, and peak (e) at -0.03V is the reentry of the protons. Solvent migration, which is scan rate independent, in and out of the film also occurs with the ion migration making the characterization with electrochemical quartz microbalance (EQCM) problematic<sup>71</sup>. Peak (d) which appears (+0.33V) in the first reduction scan towards the potential of -0.2V after holding at +0.8V, can be assigned to the reduction and release of the degradation products from the film<sup>72,73</sup>. However, this peak also corresponds to the reduction of the AuCl<sub>4</sub><sup>-</sup> anions of the formed [PANI(PN)\*AuCl<sub>4</sub><sup>-</sup>] complex ( $E_{\text{AuCl}_4^-/\text{Au}_0} = +0.44\text{V}$  in 1M HCl). The forward peaks and reverse peaks all shrink and shift with each deposition cycle. Peaks (b), (c), and (d) shift to more negative potentials, while (a) and (e) are shifting to more positive potentials. This behavior corresponds to the oxidative degradation of PANI when being held at +0.8V for prolonged time as reported by others<sup>72,73</sup>. Figure 2.7C shows the consecutive normalized CVs for all eight gold deposition cycles for PANI/Au<sub>8</sub>.

As can be seen, qualitatively there are the same peaks with similar shifts and shrinkages as in PANI without gold (see Figure 2.7B). To determine the net amount of

$\text{AuCl}_4^-$  reduced to  $\text{Au}^0$  in each reduction step, we needed to look at peak (d) for each cycle individually. To account for the oxidative loss of PANI in each cycle, the reduction peak (d) for PANI/Au<sub>8</sub> and PANI/Au<sub>0</sub> was normalized to the number of moles of PANI (determined from the QCM frequencies using the Sauerbray equation,  $-\Delta f/f = C_f m_{\text{PANI}}$ ). In order to determine the charge due to the reduction of  $\text{AuCl}_4^-$ , we subtracted the area of the normalized reduction peaks (d) for PANI/Au<sub>0</sub> from PANI/Au<sub>8</sub>. This subtracted charge is then the result of the reduction of the  $\text{AuCl}_4^-$  anion to atomic gold alone. The peaks from this normalization procedure (i.e. PANI/Au<sub>8</sub> - PANI/Au<sub>0</sub>) for all eight cycles are shown in Figure 2.8.

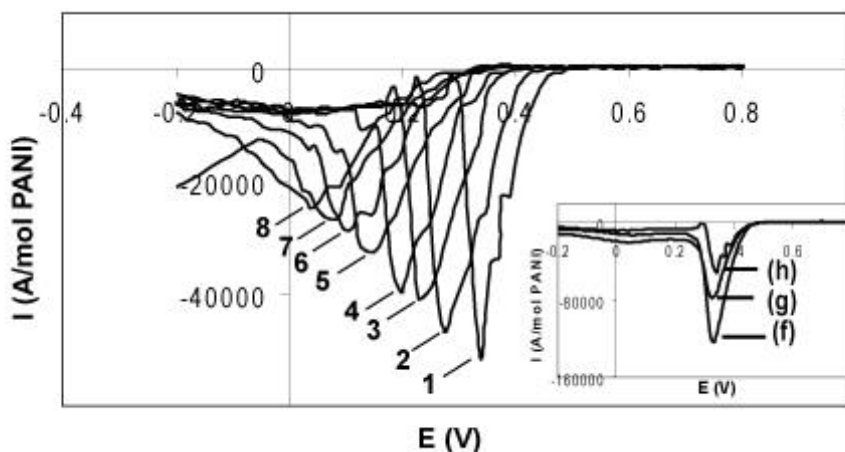


**Figure 2.8.** Overlaid reduction peaks of  $\text{AuCl}_4^-$  after the subtraction of PANI/Au<sub>0</sub> from PANI/Au<sub>8</sub> for cycles 1-8. An example of this subtraction is shown in the inset for the first cycle from Fig 2.7B and Fig 2.7C, where PANI/Au<sub>0</sub> (g) is subtracted from PANI/Au<sub>8</sub> (f) to obtain the reduction peak of  $\text{AuCl}_4^-$  (h).

The inset shows an example of the subtraction, where (f) is the normalized reduction peak from the first cycle of PANI/Au<sub>8</sub>, (g) is the normalized reduction peak from the first cycle of PANI/Au<sub>0</sub>, and (h) is the subtracted result.

From the peak areas in Figure 2.8, the number of moles of gold reduced in each cycle was determined by using Faraday's law. Figure 2.9 shows the number of moles of  $\text{AuCl}_4^-$  reduced for each cycle (1- 8) in PANI/Au<sub>8</sub>.

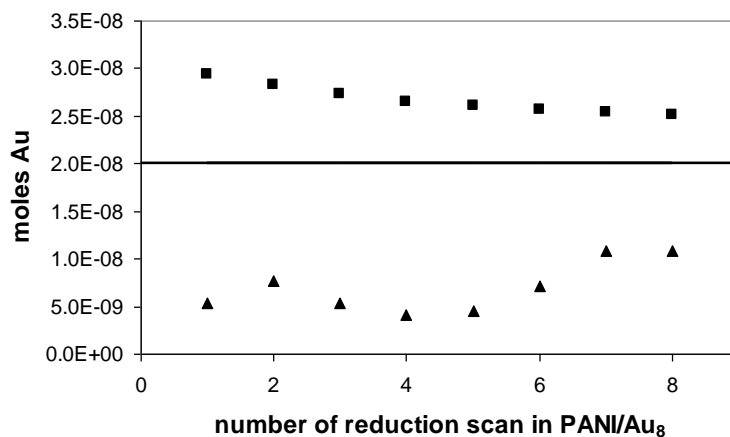


**Figure 2.9.** The calculated number of moles expected of  $\text{AuCl}_4^-$  that can be reduced per cycle based on a 2Au:1PANI repeat unit stoichiometry (■), and the actual number of moles of  $\text{AuCl}_4^-$  reduced for each reduction step in sample PANI/Au<sub>8</sub> (▲). The solid line indicates the total number of moles of  $\text{AuCl}_4^-$  in solution per cycle.

Taking into account the decrease in PANI due to degradation, the theoretical number of moles that could be reduced using a stoichiometric ratio of 2Au:1PANI was also calculated. For comparison, the total number of moles of  $\text{AuCl}_4^-$  in the solution is also shown (solid line).

For a constant amount of PANI, we would expect a constant amount of gold to be deposited for each cycle. As seen in Figure 2.9, there is a consistent amount of gold being deposited with a slight increase for the last few cycles. A possible explanation is that the amount of PANI in the later cycles decreases but the concentration of  $\text{AuCl}_4^-$

solution that it is exposed to remains the same. In order to satisfy the stoichiometric ratio of 2Au:1PANI, we would need to increase the concentration of our  $\text{AuCl}_4^-$  solution.

## CHAPTER 3

### OPTIMIZATION OF ATOMIC GOLD DEPOSITION CYCLE

#### 3.1 The need for optimization

In the original process, the atomic gold deposition and the oxidative degradation of PANI at +0.8V were occurring simultaneously making it difficult to gain clear information on the impact of the deposited gold on the electrochemical behavior of PANI. The degradation process is caused by breaking of the polymer chains due to formation of quinones or quinone imines resulting in the loss of the material<sup>74</sup>. The rate of the degradation depends on several factors including the type of the anion in the acidic media<sup>75-77</sup>, the length of time the film is held at the overoxidation potential<sup>73</sup>, the magnitude of the applied potential<sup>72</sup>, and the thickness of the film<sup>78</sup>. The degradation of PANI follows a first order kinetics<sup>79</sup>, so most of the damage will occur early, reaching a stable material. Herein, we separated the two steps. First we prepare the matrix in stable state by performing the preconditioning degradation of PANI, and then use this optimized material under the optimized experimental conditions to minimize further degradation of the matrix.

#### 3.2 Optimization of the Film Degradation Prior to Gold Deposition

The PANI film was deposited on one side of the QCM crystal (working electrode) from a 0.1M aniline/2M HBF<sub>4</sub> aqueous solution at a constant potential of +0.9V for 200 seconds. Figure 3.1 compares how the initial CV of PANI from -0.2V to +0.8V is changing after holding PANI at +0.8V for 300s in 0.1M HCl (Figure 3.1A), in 0.1M

HBF<sub>4</sub> (Figure 3.1B), and in 0.1M HClO<sub>4</sub> (Figure 3.1C) under the same conditions as the 0.1M HCl.

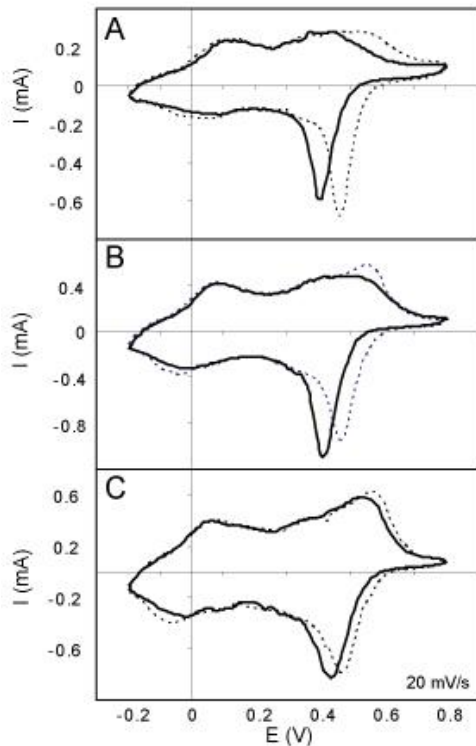


**Figure 3.1.** Cyclic voltammograms of PANI before (---) and after (—) holding at +0.8V for 300s in (A) 0.1M HCl, (B) 0.1M HBF<sub>4</sub> and (C) 0.1M HClO<sub>4</sub>.

PANI has two oxidation peaks in the initial CVs around +0.10V and +0.55V. The position of the oxidation peak around +0.55V is clearly affected by the anion of the acid. As the overoxidation of PANI occurs, these peaks tend to shift toward each other until they merge<sup>72</sup>.

To determine the degree of degradation, the negative shift of the second oxidation peak of PANI was measured. It was observed that there was a shift of 87mV in 0.1M HCl, 46mV in HBF<sub>4</sub>, and 32mV in 0.1M HClO<sub>4</sub>. Therefore, the rate of degradation

follows the order of  $\text{HCl} > \text{HBF}_4 > \text{HClO}_4$  in agreement with previous findings<sup>76</sup>. From this, the initial overoxidation of PANI was performed in 0.1M HCl.

Since the overoxidation of PANI follows first order kinetics,<sup>79</sup> very little degradation occurs beyond a certain point. To determine the holding time to reach this point, we held a PANI film at +0.8V for 0, 30, 60, and 90 minutes as shown in Figure 3.2.

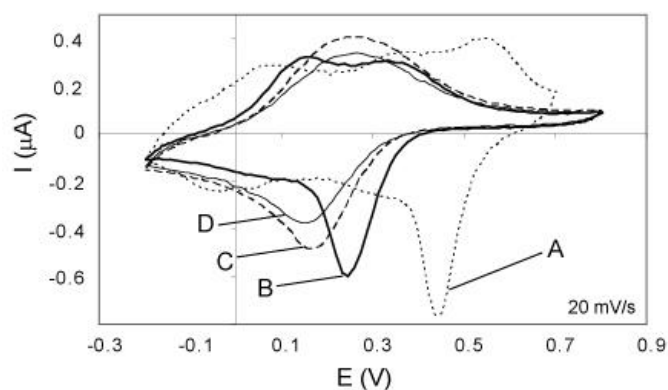


**Figure 3.2.** Cyclic voltammograms of PANI in 0.1M HCl (A) initially before overoxidation, (B) after 30 minutes at +0.8V, (C) after 60 minutes at +0.8V, and (D) after 90 minutes at +0.8V.

The shift in the second oxidation peak is again used to determine the extent of overoxidation. There is a peak shift of 212mV between the initial CV and after 30 minutes, and a peak shift of 70mV between 30 and 60 minutes. However, there is only a slight shift of 3mV between the CV after 60 minutes and the CV after 90 minutes. From this, it was concluded that a holding time of 1hr in 0.1M HCl would be sufficient to obtain a stable matrix for the gold deposition.

### **3.3 Fourier Transform Infrared Spectroscopy (FTIR) Evaluation of the Stable PANI Matrix**

FTIR measurements were performed using a BIO-RAD FTS-6000 with a BIO-RAD UMA-500 IR microscope attachment in the range of 700-3800 wavenumbers. IR reflectance spectra were obtained using the rapid scan mode at a mirror modulation frequency of 20 kHz, with the aperture open, a filter setting of 5, and a resolution setting of 4  $\text{cm}^{-1}$ . An average of 32 scans was used to produce each spectrum. The PANI samples were analyzed while still on the Pt QCM. Background spectra were obtained using the bare Pt surface on the QCM under the same spectroscopic conditions as the samples. The background was subtracted from the sample spectra using BIO-RAD WIN-IR PRO software. Areas and peak assignments were obtained using the same software.

The FTIR spectra obtained for a freshly prepared PANI film after cycling in 0.1M HCl and for the same film after a 1 hour overoxidation period at +0.8V are shown in Figure 3.3.

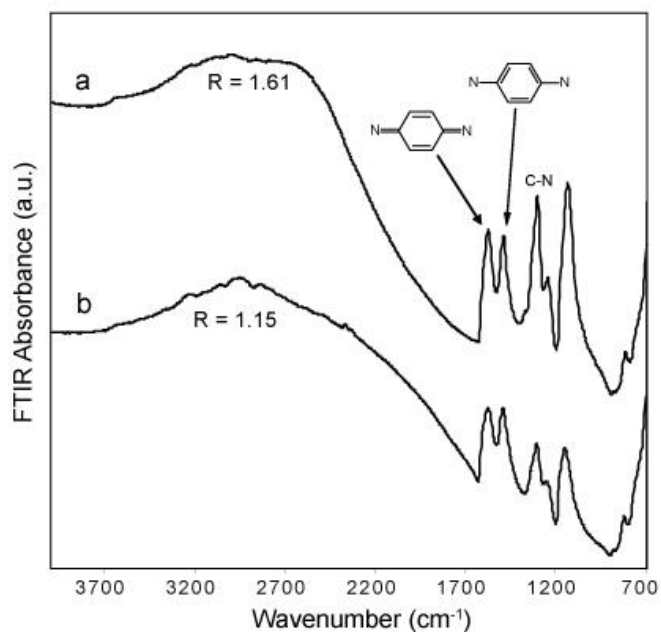
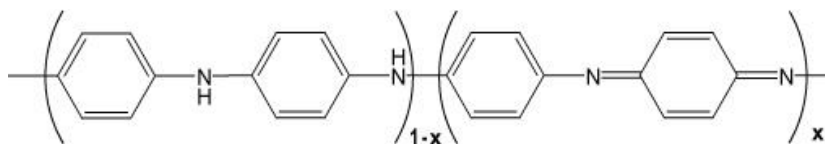


**Figure 3.3.** FTIR spectra of (a) PANI and (b) PANI after 1hr oxidative degradation at +0.8V in 0.1M HCl. The ratio (R) of quinoid to benzenoid units are labeled for each film.

The spectrum shows a small decrease in peak area as expected with mass loss due to overoxidation. The characteristic bands for the benzenoid and quinoid rings of PANI are located at 1495 and 1579 $\text{cm}^{-1}$  respectively<sup>80</sup> and only slightly shift to 1492 and 1576 $\text{cm}^{-1}$  in the overoxidized PANI. The oxidation level of the polymer can be determined from the ratio (R) of these units.



$$R = \frac{\text{Area}_{\text{quinoid}}}{\text{Area}_{\text{benzenoid}}}$$

The determined R values for PANI before and after overoxidation at +0.8V for 1 hour were 1.61 and 1.15, respectively. The composition of the PANI matrix changes slightly

in the overoxidized film indicating that the number of quinoid units decreases. The change of shape of the CV shown in Figure 3.2 indicates that the overoxidation affects the ion exchange properties of the PANI film. However, the imine sites needed for gold reduction are still present in the overoxidized film.

### **3.4 Minimizing PANI Degradation During Gold Deposition**

Further degradation of the films was minimized by optimizing the deposition conditions. The three parameters that have been changed were the holding time, the type of acid and the holding potential. The changes are elaborated below:

(i) Exposure to the chloraurate solution and subsequent rinsing while held at a potential of +0.8V in our previous method was 550s. This time was reduced to 300s while maintaining the same amount of time for chloraurate exposure as well as using the same volume of solution for the subsequent rinsing step.

(ii) The solution during the gold deposition was changed from 0.1M HCl to 0.1M HClO<sub>4</sub> which showed the least amount of degradation in Figure 3.1.

(iii) PANI was held at three different overoxidation potentials in 0.1M HClO<sub>4</sub> for 300s. Figure 3.4A, 3.4B, and 3.4C shows the initial and final CVs after holding a PANI film at a potential of +0.80V, +0.70V, and +0.65V respectively.

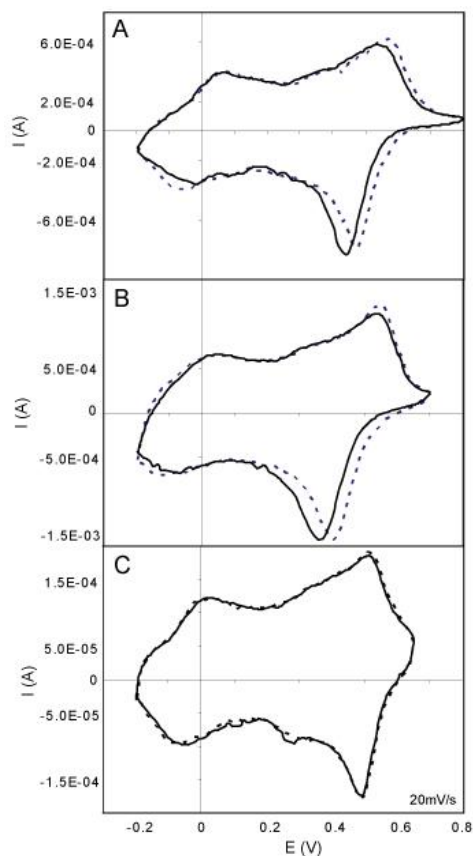


**Figure 3.4.** Cyclic voltammograms of PANI in 0.1M HClO<sub>4</sub> before (---) and after (—) 300s of holding the potential at (A) +0.8V, (B) +0.7V, and (C) +0.65V. The CVs were recorded from -0.2V to the holding potential, respectively.

The initial and final CVs were obtained from -0.2V to the overoxidation potential. Once again, the negative shift of the second oxidation peak from the initial CV to the final CV was used to determine the extent of overoxidation. It was found that there was a shift of 32mV after holding the film at +0.80V, 17mV at +0.70V, and 0mV at +0.65V. The most favorable result was for the overoxidation potential of +0.65V. However, the final oxidation peak in the CV was not completed before the potential scan switched to the negative direction as seen in Figure 3.4C. If any part of the film is not fully oxidized, there could be uncontrolled spontaneous reduction of the chloraurate anion. Therefore, the optimal holding potential was determined to be +0.7V for the gold deposition cycles.

### 3.5 Gold Deposition Using Optimized Conditions

Under the optimized conditions, polyaniline was deposited in the flow cell from 0.1M aniline in 2M HBF<sub>4</sub> at +0.9V for 200s. The solution was exchanged with 0.1M HClO<sub>4</sub> and ten cyclic voltammograms were performed for the exchange of anions. The potential was then held for one hour at +0.8V to oxidatively degrade and stabilize the polyaniline. After the preparative degradation step, the flow cell was rinsed with a solution of 0.1M HClO<sub>4</sub>, and a total of 5 CVs were performed from -0.2V to +0.7V. The film was then held at +0.7V to keep the PANI in a fully oxidized state and was exposed to a solution of 10<sup>-4</sup>M KAuCl<sub>4</sub> in 0.1M HClO<sub>4</sub> for 50 seconds to form a PANI\*AuCl<sub>4</sub><sup>-</sup> complex. All excess AuCl<sub>4</sub><sup>-</sup> anions were thoroughly rinsed away with 0.1M HClO<sub>4</sub>, and the potential was swept to -0.2V to reduce the complexed AuCl<sub>4</sub><sup>-</sup> to atomic gold. The holding time at +0.7V during the exposure to the chloroaurate solution and subsequent rinsing was 300 seconds to ensure diffusion of AuCl<sub>4</sub><sup>-</sup> to the bulk of the film. The final step was to perform 5 CVs from -0.2V to +0.7V. At this point, the film is ready to begin the next gold deposition cycle by holding the potential at +0.7V, so that it can be exposed to the chloroaurate solution. The updated timing diagram for the gold deposition cycles is shown in Figure 3.5.

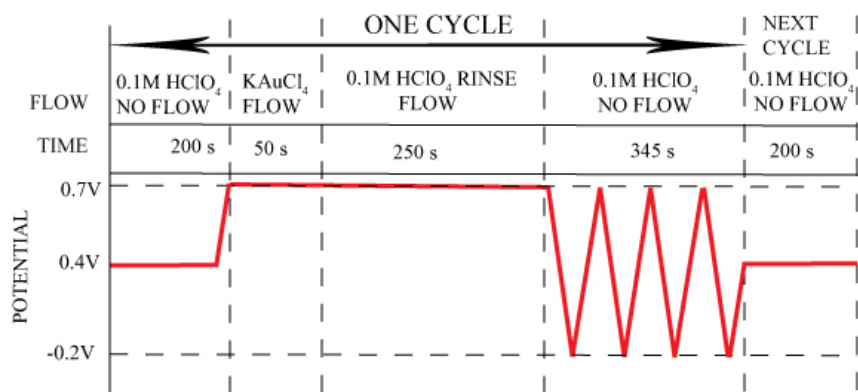


**Figure 3.5.** Optimized timing diagram for the atomic deposition of gold into PANI.

### 3.6 Effect of Deposited Gold on the Electrochemistry of PANI

Composite electrodes containing PANI/Au<sub>0.9</sub> were prepared following the optimized conditions. The electrode with no gold was prepared by undergoing eight gold deposition cycles using 0.1M HClO<sub>4</sub> without chloroaurate present. This was done to determine the extent of oxidative degradation of the PANI throughout the complete set of cycles. The cyclic voltammograms of the films were monitored throughout the process of atomic gold deposition as shown in Figure 3.6.

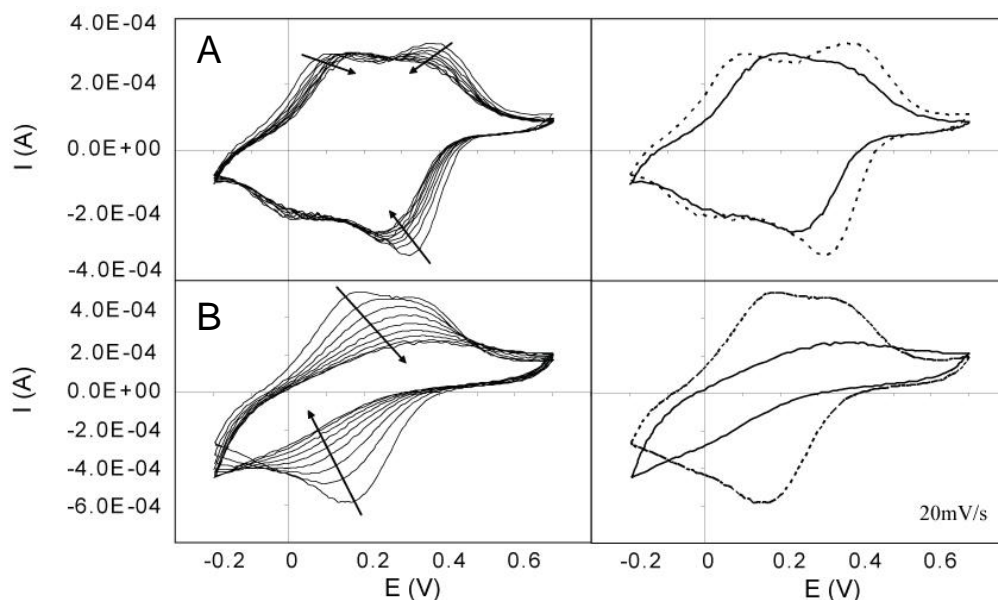


**Figure 3.6.** Cyclic voltammograms for (A) PANI/Au<sub>0</sub> and (B) PANI/Au<sub>8</sub> taken before the first gold deposition cycle and after each deposition cycle for 1 through 8 cycles. The arrows show the progression of the peaks through the 8 cycles. The CVs were recorded from -0.2 to +0.7V in 0.1M HClO<sub>4</sub>. Figures on the right show the first and last CV only.

The first CV was recorded after the degradation step, but before the gold deposition cycles begin. The subsequent CVs shown were taken just after the reduction of the AuCl<sub>4</sub><sup>-</sup> to atomic gold in each of the deposition cycles for a total of 9 CVs. The arrows in Figure 3.6A for PANI/Au<sub>0</sub> indicate that the peaks shift slightly from the initial CV through the 8 cycles which is typical of a small amount of overoxidation. Overall, there was nothing remarkable happening to this film through 8 atomic gold deposition cycles. Figure 3.6B shows the CVs for the PANI/Au<sub>8</sub> sample taken at the same time periods as in the PANI/Au<sub>0</sub> sample. Again, the arrows indicate the shift of the peaks from the CV before the gold deposition cycles begin to the CV taken after the eighth cycle. There is a clear gradual progression from the initial CV to the final CV as more gold is deposited on the film. The final CV is now featureless and flat. It is clear that the number of

deposited gold atoms has a major effect on the electrochemical properties of the film. At this point, it is not clear to us what is causing this effect, but the decrease of conductivity of the films would be consistent with the flattening of the CV. We believe that the gold atoms deposited at the imine sites along the PANI chain will interrupt the electron flow along the chain and possibly between two adjacent chains. Our attempts to measure conductivity of the free standing film by four-point-probe technique failed due to the fragility of the film.

### 3.7 Work Function of PANI/Au<sub>N</sub> Films

The work function (WF) measurement of each film was obtained using a Besocke Delta-Phi-Electronik type S Kelvin Probe. It was measured in automatic balancing mode versus a vibrating gold grid reference electrode.<sup>81</sup> The setting for the offset potential was 6.0V. A free-standing PANI/Au<sub>N</sub> film was obtained from the QCM by applying a -5.0V pulse for 1s in 1M NaOH. To remove NaOH from the film, it was placed into dialysis tubing and dialysed against DI water overnight. The films were then mounted onto a metal Kelvin probe holder and dried. All WF measurements were run in triplicate.

The difference in the work function values of PANI and the deposited Au atoms will lead to the formation of a charge transfer complex within the film (Figure 3.7).



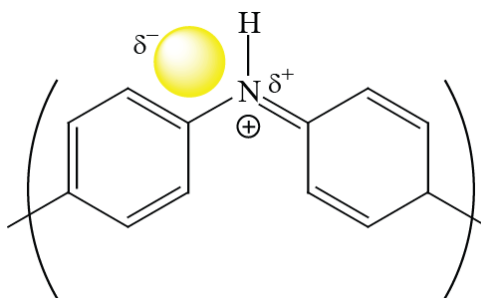


**Figure 3.7.** Depiction of the charge transfer complex formed between gold and PANI.

The relative changes of the work function of the films prepared at neutral pH were determined versus the PANI film without gold, as shown in Figure 3.8.

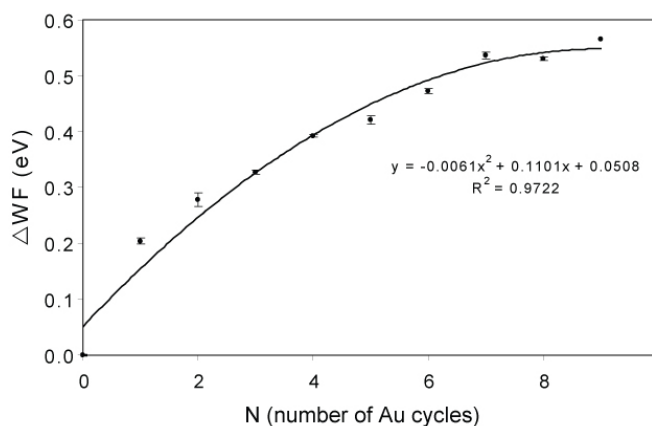


**Figure 3.8.** Relative changes in work function of PANI/Au<sub>N</sub> films for N = 0 - 9 measured versus a vibrating gold grid reference electrode.

The work function of the films increased with the number of cycles of atomic gold deposition. The WF of the PANI/Au<sub>1</sub> film is 204mV higher than PANI/Au<sub>0</sub> and increases to 565mV higher for PANI/Au<sub>9</sub>. In order to determine the charge transfer between PANI and the neutral gold atoms, an equation to calculate the charge transfer between neutral gas molecules and PANI was used<sup>82</sup>,

$$\Delta V_{WF} = \frac{kT}{2\delta e} \ln(Au_N + 1)$$

where  $\Delta V_{WF}$  is the measured changes in work function from PANI/Au<sub>0</sub>,  $k$  is the Boltzmann constant,  $T$  is the temperature,  $\delta$  is the fraction of charge shared between Au and PANI, and  $e$  is the charge. The equation was originally derived for charge-transfer doping with electrically neutral gas molecules<sup>83</sup>. It is shown here that this relationship applies also to electrically neutral gold atoms which act as charge transfer dopant for the PANI. To apply this equation, the change in work function was plotted versus the natural log of N+1 as seen in Figure 3.9.

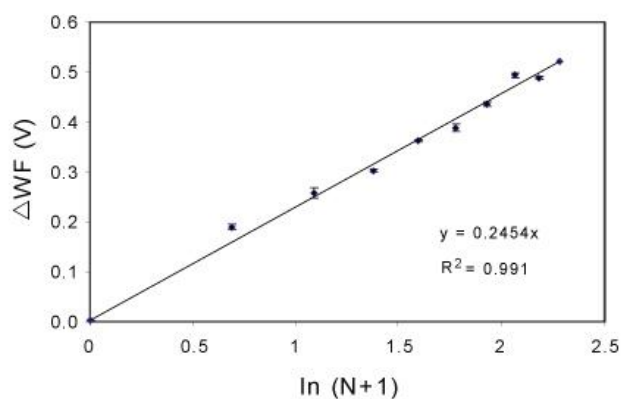


**Figure 3.9.** Relative changes in work function of PANI/Au<sub>N</sub> films (for N = 0 – 9) versus the natural log of N+1.

In this type of measurement, it is assumed that the surface dipole component of the work function remains constant. There was a linear relationship with good correlation between the relative changes in WF and the natural logarithm of N+1 where N is the number of gold atoms deposited per imine site per cycle. From the slope of the line, the partial charge transfer between the gold and stable matrix leads to the formation of a local

contact potential difference of 52.2mV. The linearity also suggests that the PANI matrix was stable, and that a consistent amount of gold was added during each cycle.

Pyrolytic microgravimetry was another method attempted to further characterize the films. Since the films were deposited on a QCM, the films were pyrolyzed in microwave oxygen plasma. It was hoped that the deposited gold would remain on the QCM while the organic matrix would be burned off, hence the mass of the deposited gold/cycle would be obtained. Although all films containing gold for  $N > 6$  showed increase of mass after the pyrolysis the correlation between the number of gold cycles  $N$  and residual mass was not reproducible and was statistically inconsistent. This experimental failure could be due to the fact that the kinetic energy of the plasma is too high and small gold clusters could have been dislodged and lost during the ashing step.

### **3.8 X-Ray photoelectron spectroscopy (XPS)**

The gold content in the PANI films deposited was determined using XPS. The XPS measurements were performed using a Physical Electronics Quantum 2000 Scanning ESCA Microprobe. This system uses a focused monochromatic Al  $K\alpha$  X-rays (1486.7 eV) source and a spherical section analyzer. The instrument has a 16 element multichannel detector. The X-ray beam used was a 100 W, 100  $\mu\text{m}$  diameter beam that was rastered over a 1.3 mm by 0.2 mm rectangle on the sample. The X-ray beam is incident normal to the sample and the photoelectron detector was at  $45^\circ$  off-normal. Wide scan data was collected using a pass energy of 117.4 eV. For the Ag $3d_{5/2}$  line, these conditions produce FWHM (width at half peak maximum) of better than 1.6 eV. The high energy resolution photoemission spectra were collected using a pass energy of

46.95eV. For the Ag3d<sub>5/2</sub> line, these conditions produced FWHM of better than 0.98 eV. The binding energy (BE) scale is calibrated using the Cu2p<sub>3/2</sub> feature at 932.62 ± 0.05 eV and Au 4f at 83.96 ± 0.05 eV for known standards. The sample experienced variable degrees of charging. Low energy electrons at ~1 eV, 20μA and low energy Ar<sup>+</sup> ions were used to minimize this charging. The Au 4f<sub>5/2</sub> and 4f<sub>7/2</sub> peaks were referenced to the C1s line at 284.8 eV.

High resolution XPS analysis was performed to confirm the presence of gold in the PANI films. Gold peaks (Au 4f<sub>5/2</sub> and 4f<sub>7/2</sub>) were identified at 84.1eV only for the samples that had N=6, 7, and 8 deposition cycles, Figure 3.10a. The N:C ratios correspond to the expected ratio of 0.166, Figure 3.10b. The Au:N atomic ratios plotted versus the number of gold deposition cycles increases for the samples with N=6, 7, and 8. Taking into consideration that XPS is a surface technique, samples with N<6 contain gold, but may not be accounted for by this technique.

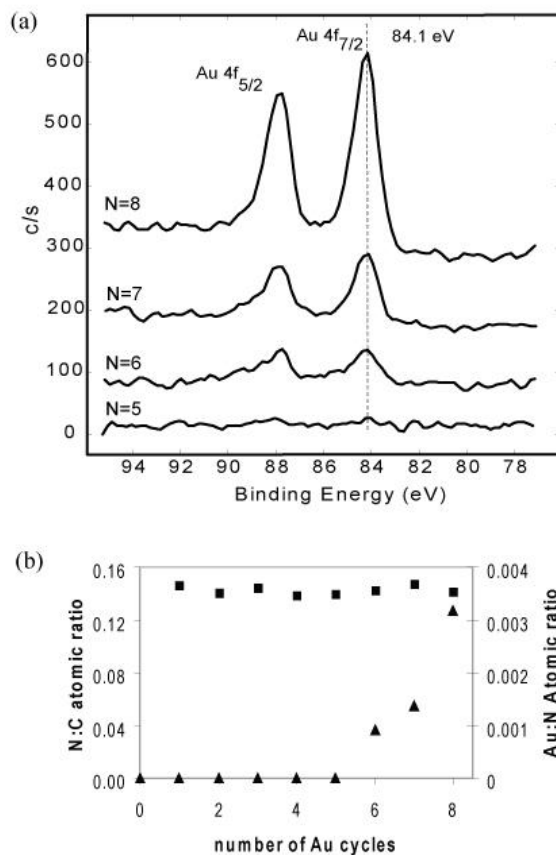


**Figure 3.10.** (a) XPS spectra of PANI/Au<sub>N</sub>, N=5, 6, 7, and 8 (b) Atomic ratios of N:C (■) and Au:N atomic ratios (▲) plotted against N=0....8 cycles using the XPS data.

These results are quite different from the previously reported results for a “top down” approach at controlled gold deposition on PANI<sup>26</sup>. In the previous approach, XPS showed a Au:N ratio around 0.001 after the second cycle and over 0.008 after the seventh cycle. However, we only see a ratio of just over 0.001 after the seventh cycle. Clearly, this method of deposition is much more controlled than previous attempts.

## CHAPTER 4

### Odd-Even Pattern Observed in Polyaniline/(Au<sub>0</sub> – Au<sub>8</sub>) Composites

#### 4.1 Electrochemical Preparation of Polyaniline Gold Composite Films

The preparation of the PANI/Au<sub>N</sub> films, where N equals the number of gold deposition cycles, was described previously. Briefly, the PANI was deposited on one side of a Pt (1000Å) coated on Ti (100Å) 10 MHz polished quartz crystal (QC) (International Crystal Manufacturing OKC, OK, USA) from a 0.1M aniline/2M HBF<sub>4</sub> aqueous solution at a constant potential of +0.9V for 200 seconds in a flow through cell. The flow through cell housing the Electrochemical Quartz Crystal Microbalance (EQCM) arranged in a flow injection analysis (FIA) format allows exchange of solutions while maintaining the electrical contact to the PANI film throughout the preparation steps of a deposition cycle. All potentials are referenced to the Ag/AgCl in 0.1 M KCl. The counter electrode was bare Pt deposited on quartz crystal. The electrochemically active area ( $A = 0.236 \text{ cm}^2$ ) on the crystal was defined by the o-ring. Cyclic voltammograms (CV) were recorded with an Omni 90 potentiostat (Cypress Systems Lawrence, KS) and the changes of mass were obtained from the Sauerbrey equation, using a PLO-10i phase lock oscillator (Maxtrek, Inc. Cypress, CA) and a model 53131A Universal Counter (Hewlett Packard Loveland, Co). All CVs were recorded with 20 mV/s scan rate. After coating the Pt electrode with PANI, the cell was rinsed with 0.1M HClO<sub>4</sub>, and the electrode was conditioned first by applying 10 CVs from -0.2V to +0.7V and then holding the potential at +0.8V for 1 hour in this electrolyte. The average thickness of the

PANI film prepared in this way was 4 $\mu$ m, as determined by the contact profilometry, and the average mass of the deposited PANI was 43 nmoles. After the conditioning step the flow cell was rinsed with a 0.1M HClO<sub>4</sub>, and total of 10 CVs were completed from -0.2V to +0.7V. The Au-cycle was initiated by holding the PANI at +0.7V while exposing it to solution of 10<sup>-4</sup>M KAuCl<sub>4</sub> in 0.1M HClO<sub>4</sub> for 50 seconds. Maintaining this high potential, keeps PANI in a fully oxidized state and leads to formation of the PANI\*AuCl<sub>4</sub><sup>-</sup> complex. The film was then rinsed of the excess of AuCl<sub>4</sub><sup>-</sup> with 0.1M HClO<sub>4</sub>, and the potential was scanned to -0.2V in order to reduce AuCl<sub>4</sub><sup>-</sup> to atomic gold. The total holding time at +0.7V during the exposure to the chloroaurate solution and subsequent rinsing was 300 seconds. The final step was to perform 5 more CVs from -0.2V to +0.7V in order to bring the film to its defined final state. At this point, the material was ready for the next gold deposition cycle. The cycle was repeated N-times in order to form the PANI/Au<sub>N</sub> of the desired composition. The N deposition cycles were varied from N=0 to 8.

#### **4.2 Odd-Even Pattern in the Electro-oxidation of n-Propanol**

CVs for the electro-oxidation of n-PrOH were recorded in 1M NaOH at a scan rate of 20mV/s from -0.6V to +0.45V using a Solartron SI1287 electrochemical interface. The reference electrode was a Ag/AgCl in 1M KCl, and the counter electrode was a platinum foil.

Before conducting the oxidation of n-propanol using the PANI/Au<sub>N</sub> composites, the CVs of the bare Pt electrode as well as of the PANI film deposited on Pt electrode (PANI/Au<sub>N=0</sub>) was examined in 1M NaOH, Figure 4.1A.

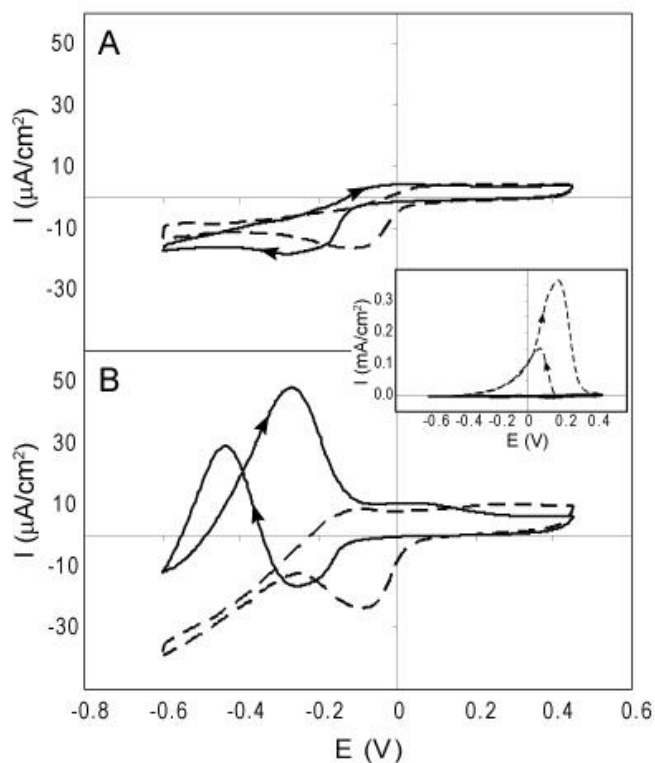


**Figure 4.1.** CVs of bare Pt (---) and PANI on Pt (—) in (A) 1M NaOH and in (B) 0.5M n-propanol in 1M NaOH at 20mV/s. Ten CVs were performed in the absence of n-propanol and five CVs were performed with n-propanol. Only the last CV for each is shown.

It can be seen that during the anodic sweep, the platinum surface is oxidized that gives rise to a cathodic reduction peak on the reverse scan. The surface oxide formation is shifting to more negative potential for the PANI coated Pt electrode when compared to the bare Pt electrode. Upon addition of 0.5 M n-PrOH to the 1M NaOH, the cyclic voltammograms at the bare Pt-electrode and at the PANI-coated Pt electrode are changing, Figure 4.1B. At the Pt electrode a small oxidation peak at -0.10V is seen causing a slight enhancement of the reduction peak when compared with voltammogram shown in Figure 4.1A. A similar result was reported by others.<sup>61</sup>

The voltammogram taken on the Pt/PANI shows two distinct oxidation peaks, on

the forward scan at -0.27V and on the reverse scan at -0.44V. The enhanced magnitude of the peak current on Pt/PANI indicates much higher catalytic activity to n-PrOH than at the bare Pt electrode. The inset in Figure 4.1 shows the CV of the catalytic oxidation of 0.5M n-PrOH in 1M NaOH on a bare polycrystalline gold electrode. The oxidation peak in the forward scan occurs at +0.18V, and on the reverse scan at +0.08V. The reduction current corresponds to the reduction of surface gold oxide, and it increases with the increasing the positive potential limit.<sup>31</sup>

An overview of the effect of atomic gold in PANI on electrochemical oxidation of n-PrOH in alkaline medium is given in Figure 4.2.

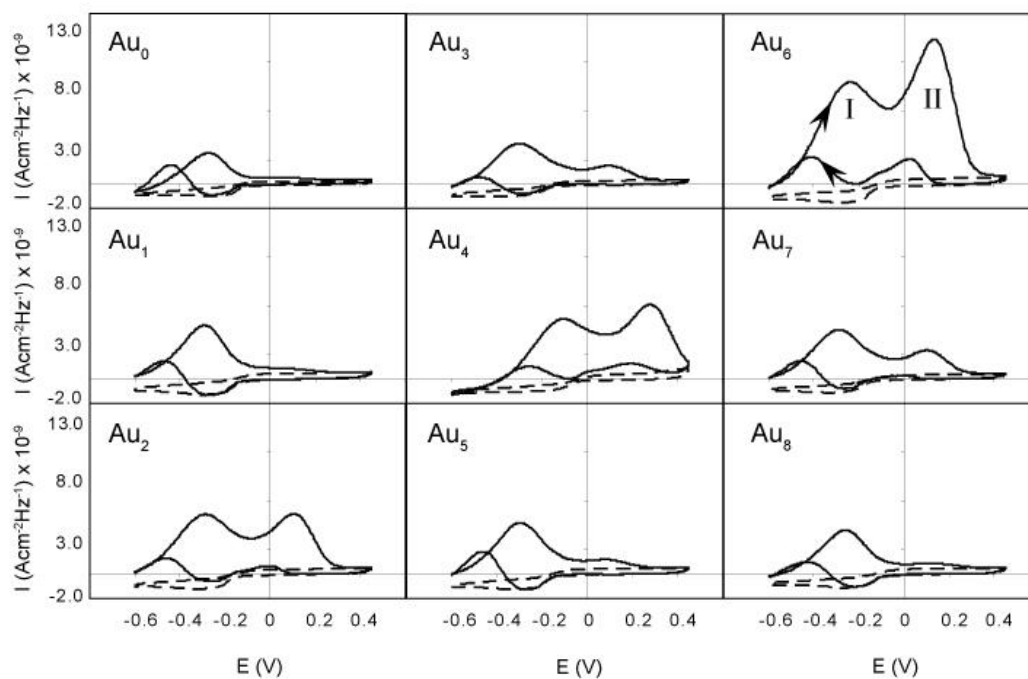


**Figure 4.2.** Effect of added 0 to 8 Au atoms to PANI on oxidation of 0.5M n-propanol in 1M NaOH (—) taken at 20 mV/s. The CVs in 1M NaOH (---) are also shown. The CVs are normalized to the mass of PANI from the frequency changes during the deposition on Pt. Only the last CV of ten is shown in the absence of n-propanol, and only the last CV of five with n-propanol is shown for simplicity. The peaks (I) and (II) shown in PANI/Au<sub>6</sub> panel are discussed in the text.

In this figure the CVs have been normalized to the mass of PANI deposited on the electrode in order to aid the visual comparison. The mass information is again obtained from the change of frequency of the EQCM during the deposition of the PANI, assuming the validity of the Sauerbrey equation in solution. For PANI/Au<sub>0</sub>, there is an oxidation peak in the forward scan around -0.27V (peak I) and an oxidation peak in the reverse scan at -0.44V, as seen previously in Figure 4.1B, while voltammograms in the potential region above 0V are featureless. On the other hand, in the PANI/Au<sub>N>0</sub> composites, a second oxidation peak (peak II) in the forward scan begins to emerge around +0.12V, which is due to the oxidation of n-PrOH on the atomic gold clusters. It provides a strong

indication that gold clusters are present in the films and that the presence of PANI provides a conducting network which facilitates the electrooxidation.

The peak II is shifted by -50 mV when compared with the oxidation peak potential on a polycrystalline gold electrode (see Figure 4.1, insert). It is important to point out that oxidation potential of peak (II) does not vary much with the number of Au atoms in the gold clusters; only the peak current is strongly affected. It suggests that the changes in peak current mirror the changes in the catalytic activity for n-PrOH oxidation.

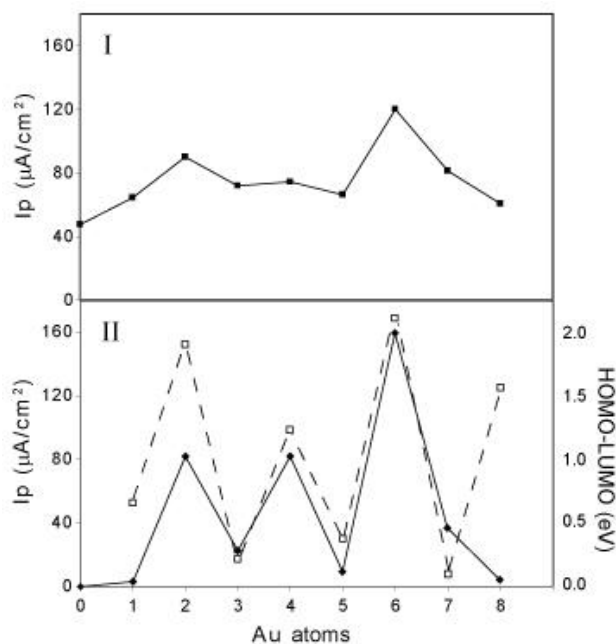


**Figure 4.3.** Peak current densities (evaluated from Figure 4.2) from the oxidation of n-PrOH versus the number of inserted gold atoms for (I) the first oxidation peak and (II) the second oxidation peak. Peaks I and II are labeled for Au<sub>6</sub> in Figure 4.2. The concentration of n-PrOH was 0.5M in 1M NaOH. The dashed line represents calculated variation of the HOMO-LUMO gap energy<sup>41,42</sup>.

It is observed, that by adding gold to the PANI films, the peak (I) also shows some oscillatory changes of the PANI activity in the presence of the alcohol, although less so than the peak (II) (Figure 4.3). The highest catalytic activity is noticeable at 2 and 6 gold

deposition cycles. The peak currents for the peak (II) in the forward scan are shown at the bottom of Figure 4.3. There is a substantial increase in peak current for PANI/Au<sub>N</sub> where N=2, 4, and 6, with N=6 having the highest value. The fluctuation of the peak current density displays an odd-even pattern with the even numbered clusters showing the highest peak currents, with the exception of N=8.

Since catalysis only speeds up the rate of the reaction, the peak currents should increase linearly with of concentration of the n-PrOH. The current densities for peaks (I) and peak (II) are plotted versus the concentration of n-propanol for PANI/Au<sub>6</sub> in Figure 4.4. The slopes of the concentration dependence lines for peak (I) and peak (II) are  $5.4 \times 10^{-8} \text{mAcm}^{-2}\text{M}^{-1}$ , and  $2.5 \times 10^{-7} \text{mAcm}^{-2}\text{M}^{-1}$ , respectively.

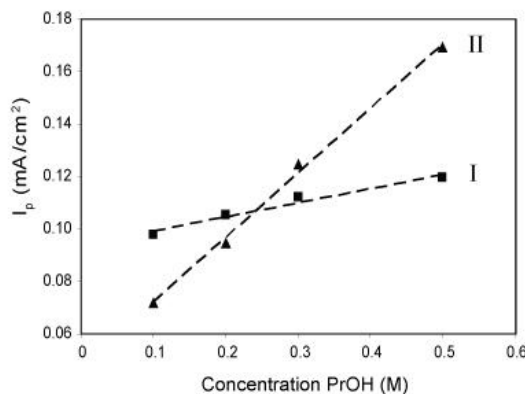


**Figure 4.4.** Linear dependence of peak current on n-PrOH concentration for PANI/Au<sub>6</sub> for (■) the first oxidation peak and (▲) second oxidation peak.

It would be optimal if all the imine sites on PANI were occupied by chloroaurate in order to create the most clusters possible. The number of imine sites on PANI can be calculated at a specific potential if the amount of PANI is known. From this, the concentration of chloroaurate can be calculated so that all the sites are occupied. However, many of these imine sites are lost after the oxidative degradation of PANI

occurs, and there is just no way to know how many are left. Therefore, the concentration of the chloraurate solution was optimized. If the concentration is high, then it would take a large amount of rinsing to make sure all excess  $\text{AuCl}_4^-$  anions have been removed after complexation. If the concentration is too low, then not all the imine sites in PANI would be occupied. The concentration of the chloraurate solution was increased to observe the effects on the peak current densities of the oxidation peaks in the cyclic voltammogram for PANI/Au<sub>2</sub> (Figure 4.5).

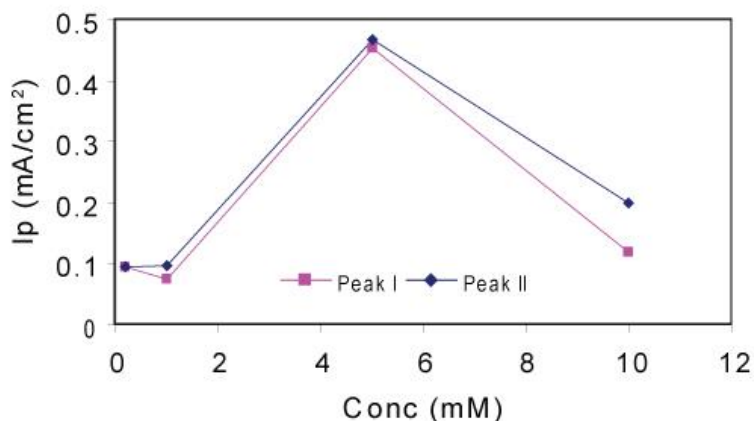


**Figure 4.5.** Peak current densities of peak I and peak II for PANI/Au<sub>2</sub> for different concentrations of the chloraurate solution.

As can be seen, there is very little difference in the peak current densities for peak I and peak II of PANI/Au<sub>2</sub> for the oxidation of 0.5M n-PrOH in 1M NaOH when 0.2mM or 1mM is used. Since there is little difference, it is assumed that all the imine sites on PANI have been occupied by  $\text{AuCl}_4^-$  in the complexation step. As the concentration of the chloraurate solution is increased to 5mM, the peak current densities increase dramatically. This could be due to large amounts of gold present from the reduction of excess anions not rinsed away. At even higher concentrations, the peak current densities

now decrease. At this point, it is speculated that there is an even larger amount of gold present from the reduction of excess anions not rinsed away. This large amount of gold is losing the catalytic activity defined by the atomic sizes of the clusters. In order for this process to work at high concentrations of a chloroaurate solution, the rinsing time of the deposition procedure must be increased as well as using larger volumes to ensure complete rinsing. Here, the concentration was kept at 0.2mM to ensure that all excess anions are removed using the current rinsing step in the optimized timing diagram. Using a lower concentration will also reduce the amount of waste.

### **4.3 Odd-Even Pattern in the FTIR**

FTIR measurements of PANI/Au<sub>N</sub> were performed under the same conditions as previously described. It is expected that Au atoms will remain close to or at the nitrogen sites of PANI as they are formed in the polymer matrix. The close proximity should effect the N-H stretching vibration in the region around 3300cm<sup>-1</sup>. Also, if gold is acting as a dopant for PANI, then the oxidation level of the film should change. This change can be reflected in the ratio (R) of quinoid (~ 1590cm<sup>-1</sup>) to benzoid (~ 1510cm<sup>-1</sup>) units. Figure 4.6 shows the location of these peaks.

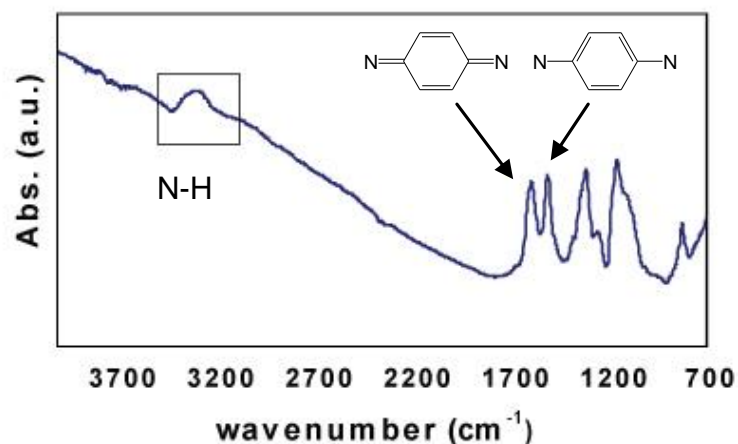


**Figure 4.6.** FTIR of PANI indicating the location of the N-H ( $3300\text{cm}^{-1}$ ), N=Q=N ( $\sim 1590\text{cm}^{-1}$ ), and N-B-N ( $\sim 1510\text{cm}^{-1}$ ) peaks.

The FTIR spectra for PANI/Au<sub>N</sub> after N=0 to 8 atomic gold cycles were recorded after cycling in 0.1M HClO<sub>4</sub> and stopping the cycles at +0.4V. Figure 4.7 shows the peak shifts of the N-H stretch for the composite films. This shift follows the same odd-even pattern as the HOMO-LUMO gap energies for Au clusters containing 0-8 clusters. The HOMO-LUMO gap energies are calculated for planar clusters as shown in Figure 1.3. The similarity in pattern breaks down at eight atoms. It is believed that at this point, the substrate influence on the cluster containing eight atoms is sufficient enough to induce a three dimensional structure which will also change the properties of the clusters. It is also possible that at this point, the clusters are large enough to overcome spatial separation and aggregate.

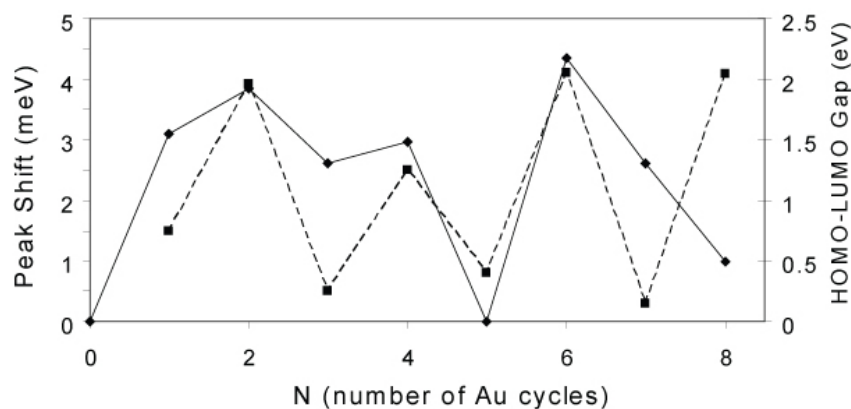


**Figure 4.7.** Peak shift of N-H stretch at  $3300\text{cm}^{-1}$  for PANI/Au<sub>N</sub> (N=0-8) plotted versus the number of Au cycles (solid line) showing an odd-even pattern. The calculated HOMO-LUMO gaps for atomic clusters are plotted as a dashed line.

These shifts are all to lower energy. When polyaniline is doped with an electron withdrawing group, the N-H bond is weakened and is shifted to a lower energy. Also, an electron withdrawing dopant can withdraw an electron to oxidize the amine group to an imine group. This effect can be seen in Figure 4.8 where  $1/R$  is plotted versus the number of Au atoms in the cluster.

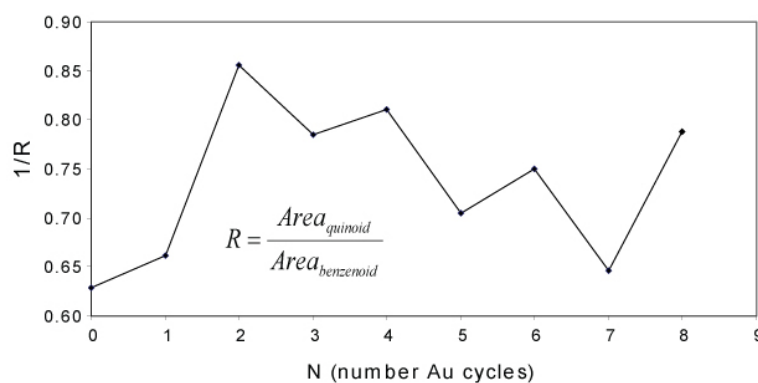


**Figure 4.8.** Plot of  $1/R$  for PANI/Au<sub>N</sub> (N=0-8) versus the number of Au cycles showing an odd-even pattern.

Again, the odd-even pattern is observed, where the PANI containing odd numbered clusters has more quinoid groups than the next even numbered cluster resulting from this oxidation.

## CHAPTER 5

### Effect of Atomic Gold on Electrooxidation of Alcohols in Alkaline Medium

#### 5.1 Introduction

This chapter is dedicated to the survey of electrochemical oxidation of lower aliphatic alcohols (C1 - C4) and of all their isomers in 1M KOH. The focus is on the effect of number of gold atoms on selectivity of the oxidation reaction. This aspect is important not only from the theoretical point of view, but may have an interesting implication on design of selective materials for amperometric sensors. The odd-even pattern of activity of the AGEs is again the dominating effect<sup>84</sup>. The even numbered AGEs, particularly AGE-6, show between 10 to 30 times higher activity than the odd numbered ones. The previously observed differences in electrooxidation behavior of n-propanol and isopropanol prompted us to examine the differences in the entire C1 to C4 alcohol series.

In order to highlight the benefits of the atomic structuring, it is necessary to compare the atomic gold electrodes with conventional electrodes containing PANI and some form of gold. The study has been divided into three sections: linear alcohols, branched alcohols, and the isomers of butanol. Although the odd-even pattern in peak current densities is consistent and visible throughout the entire series, AGEs containing Au<sub>5</sub> and Au<sub>6</sub> have been selected as representative members of the odd and even series, and their oxidation is examined in greater detail.

## 5.2 Preparation of Modified Electrodes

A standard three electrode cell and CHI660 potentiostat (CH Instrument, Inc) were used in all electrochemical experiments. The counter electrode was a platinum foil. For experiments with solid gold electrode, a 0.0113 cm<sup>2</sup> gold disk from Bioanalytical Systems Inc. (BAS) was used. The AGEs were based on platinum quartz crystal microbalance (QCM) disks and were modified accordingly with PANI and atomic gold clusters containing Au<sub>N</sub> for N = 2-7<sup>84,85</sup> as described previously using the optimized conditions. The AGEs will be referred to by the number of gold atoms in the cluster, i.e. AGE-N. Their geometrical surface area was 0.244 cm<sup>2</sup>. The reported responses are shown as current densities and potentials are referred to Ag/AgCl in 1M KCl//1M KNO<sub>3</sub> double-junction reference electrode (E= 236 mV vs SHE). For each experiment, cyclic voltammograms were recorded with a scan rate of 50mV/s. Only the final stable CVs are shown and the reverse scans are presented as dashed lines.

The Pt/PANI/Au<sub>macro</sub> electrode was prepared as follows. First, PANI was deposited on the Pt QCM using the same parameters used for the AGEs. Ten cyclic voltammograms were recorded in 0.1M HClO<sub>4</sub> with a scan rate of 50mV/s from -0.2V to 0.8V followed by holding the potential of the electrode at open cell potential for 5 minutes. The electrode was then dipped in a solution of 0.2mM KAuCl<sub>4</sub> in 0.1M HClO<sub>4</sub> for 50 seconds and rinsed thoroughly with 0.1M HClO<sub>4</sub>. This process results in an uncontrolled amount of Au to be inserted into the PANI<sup>23</sup>. The dipping time of 50 s was selected in order to yield an electrode with the current density comparable to that obtained with atomic Au modified electrodes.

### 5.3 Oxidation of Linear Alcohols

The behavior of linear alcohols at the relevant electrodes is presented in Figure 5.1. The peak potentials and the peak currents for oxidation of all the alcohols are summarized in Table 5.1. There are three “conventional” gold electrodes that have been used for this study. They are in the top row of Figure 5.1, from the left: (A) solid disk Au electrode, (B) PANI deposited on platinum (Pt/PANI) and (C) platinum electrode coated with PANI, which was dipped in solution of  $\text{AuCl}_4^-$  (Pt/PANI/Au<sub>macro</sub>). These three types of electrodes were obtained without the cyclic procedure by which the atomic gold electrodes are formed. Therefore, their comparison with the “even atoms” electrodes (middle row, D-F) and the “odd atoms” electrodes (bottom row, G-I) in Figure 5.1 highlights the net effect of atomic structuring on the electrochemical behavior of gold. It should be noted that the current density scales, as shown, are different. In panels C, D, E, and F they are approximately five times larger than those shown in panels B, G, H, and I. Obviously, the solid Au electrode (Figure 5.1A) has a completely different pattern and a much higher current density than the rest. The purpose of this organization and the chosen format of presentation is to highlight the qualitative features of the different electrodes. The calculated stable geometrical configurations of atomic gold clusters<sup>41</sup> are shown as icons in the respective panels.

**Table 5.1.** Survey of cyclic voltammogram parameters for AGE-5 and AGE-6. Pt/PANI and Pt/PANI/Au<sub>macro</sub> are shown for reference.

Electrode	Au <sub>0</sub>				Au <sub>Macro</sub>				AGE-5				AGE-6			
	Peak I		Peak II		Peak I		Peak II		Peak I		Peak II		Peak I		Peak II	
Alcohol	E <sub>p</sub> (V)	i <sub>p</sub> (mA/cm <sup>2</sup> )	E <sub>p</sub> (V)	i <sub>p</sub> (mA/cm <sup>2</sup> )	E <sub>p</sub> (V)	i <sub>p</sub> (mA/cm <sup>2</sup> )	E <sub>p</sub> (V)	i <sub>p</sub> (mA/cm <sup>2</sup> )	E <sub>p</sub> (V)	i <sub>p</sub> (mA/cm <sup>2</sup> )	E <sub>p</sub> (V)	i <sub>p</sub> (mA/cm <sup>2</sup> )	E <sub>p</sub> (V)	i <sub>p</sub> (mA/cm <sup>2</sup> )	E <sub>p</sub> (V)	i <sub>p</sub> (mA/cm <sup>2</sup> )
MeOH	-0.226	0.44			-0.196	2.9			-0.317	0.41	-0.025	0.45	-0.240	2.7		
EtOH	-0.281	0.28			-0.149	2.4			-0.275	0.28	0.264	0.26	-0.200	5.2	0.137	0.78
n-PrOH	-0.095	0.18			-0.102	0.58	0.188	0.32	-0.101	0.18			-0.050	5.5	0.283	2.1
i-PrOH	-0.122	0.18	0.080	0.10	-0.159	0.75	0.223	1.5	-0.162	0.18			-0.125	1.6	0.260	3.0
n-BuOH	-0.238	0.47	0.070	0.12	-0.117	0.34	0.154	0.38	-0.183	0.40	0.107	0.29	-0.176	4.5	0.178	3.2
i-BuOH	-0.278	0.13	0.050	0.10	-0.113	1.0	0.193	1.1	-0.191	0.45	0.135	0.29	-0.210	2.6	0.157	2.1
2-BuOH	-0.232	0.022	0.015	0.068	-0.120	0.36	0.250	2.3	-0.206	0.18	0.162	0.53	-0.195	0.77	0.166	4.6

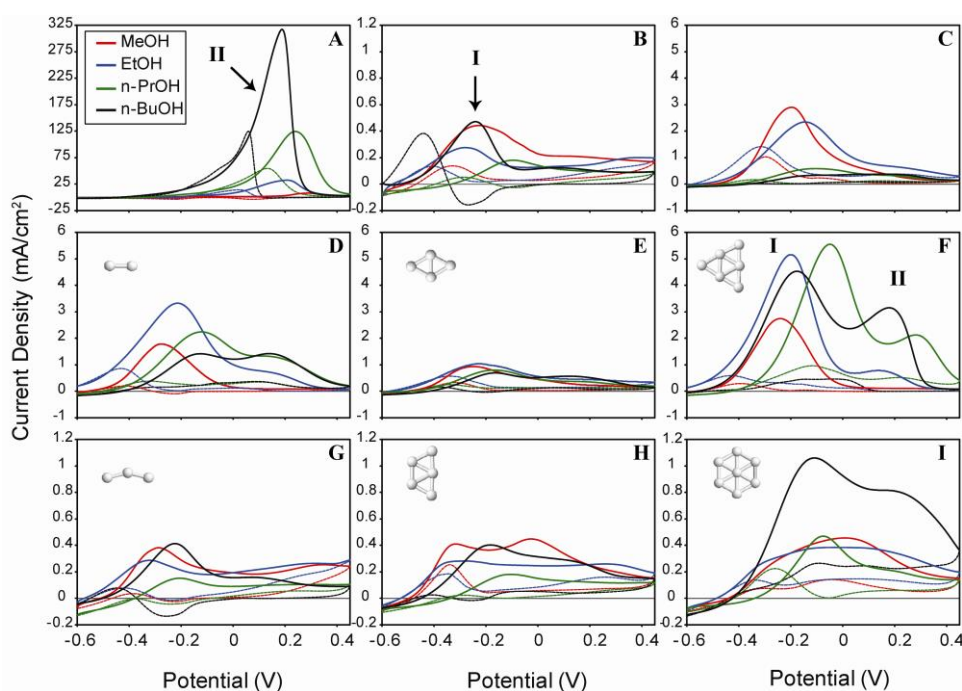


**Figure 5.1.** Survey of cyclic voltammograms recorded in a series of 0.5M linear alcohols in 1M KOH on the following electrodes: (A) Au BAS, (B) Pt/PANI, (C) Pt/PANI/Au<sub>macro</sub>, (D) AGE-2, (E) AGE-4, (F) AGE-6, (G) AGE-3, (H) AGE-5 and (I) AGE-7.

In the absence of gold, the cyclic voltammogram of Pt/PANI shows a characteristic oxidation peak in the range -230 to -280 mV on the forward scan for MeOH, EtOH and n-BuOH (Figure 5.1B). The forward oxidation peak for n-PrOH is almost 200 mV more positive (-0.095 mV). The cathodic oxidation peaks (shown as dashed lines) are

correspondingly more negative by approximately 110 mV than the forward oxidation peaks for all the alcohols and is attributed to the regeneration of active sites on the platinum. During the oxidation, the Pt surface is progressively blocked by the intermediates and products, which are desorbed on reverse scan, resulting in a more negative oxidation peak. This seemingly paradoxical oxidation which appears on solid platinum has been studied and described in detail<sup>86-91</sup>. The potential region between 0 and +450 mV is featureless. Similar adsorption-desorption pattern is observed also on solid polycrystalline gold electrode where the oxidation pattern is shifted to more positive potentials by more than 500 mV (Figure 5.1A).

The unstructured gold electrode (Pt/PANI/Au<sub>macro</sub>) is used as the most relevant reference for the structured atomic gold electrodes (Figure 5.1 D through I). The peak in the CV obtained on this electrode (Figure 5.1C) is approximately 450 mV more negative than the peak obtained at a solid Au electrode (Figure 5.1A), and is attributed to the synergistic effect of Pt and PANI<sup>92</sup>. The additional lowering of the oxidation potential by approximately 50mV is obtained by atomic structuring of gold in PANI. The differences between odd and even number AGEs for linear alcohols are highlighted in Figure 5.2 in which AGE-5 (Figure 5.2C) and AGE-6 (Figure 5.2D) are shown as the representative members of the odd-even groups. The current density scale for AGE-5 is five times larger than for AGE-6 in order to emphasize the differences between the two patterns. The CVs of Pt/PANI (Figure 5.2A) and Pt/PANI/Au<sub>macro</sub> (Figure 5.2B) are again shown for reference. Peaks I and II, which are discussed further are labeled in Figure 5.1A, Figure 5.1B and Figure 5.2D.

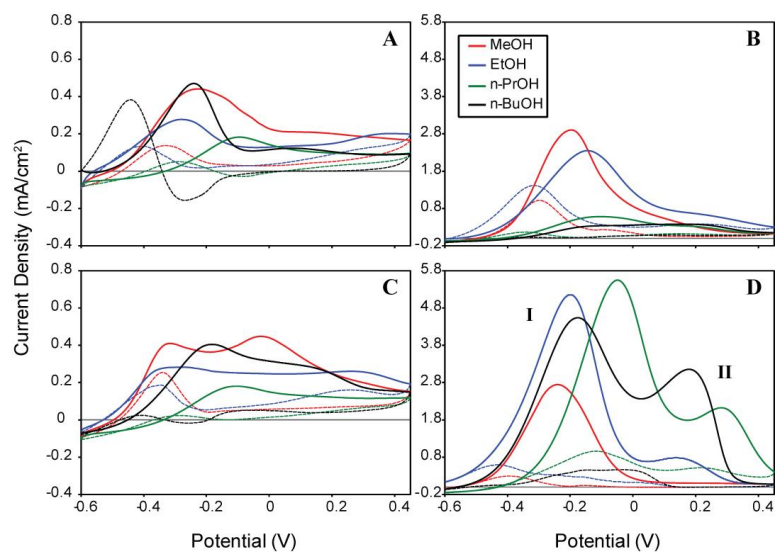


**Figure 5.2.** Cyclic voltammograms recorded in the series of 0.5M linear alcohols in 1M KOH on (A) Pt/PANI, (B) Pt/PANI/Au<sub>macro</sub>, (C) AGE-5 and (D) AGE-6

The CVs obtained at AGE-6 (and to some extent also at AGE-2) resemble the pattern of the CV for MeOH on unstructured Pt/PANI/Au<sub>macro</sub> (Figure 5.1C), albeit at lower potentials, indicating more facile oxidation. There are other notable differences, namely the amount of gold in AGEs is much smaller than in unstructured Pt/PANI/Au<sub>macro</sub><sup>23</sup>.

A significant and well-defined oxidation pattern develops at AGE-6. There is a minor second oxidation peak present for EtOH but two prominent and well-separated oxidation peaks for n-PrOH and n-BuOH. The current densities at AGE-6 are ten times higher than for AGE-5 (Figure 5.2C). The reverse scan features related to oxidation of adsorbed products on Pt are relatively small, suggesting that the pattern is dominated by the atomic gold dispersed in the PANI matrix.

## 5.4 Oxidation of Butanols

The BuOH series is surveyed in Figure 5.3. Again, the three “conventional” gold electrodes are shown in the top row as a contrast to the AGEs. The current density scale of the even AGEs and Pt/PANI/Au<sub>macro</sub> (Figure 5.3C, D, E, and F) is five times larger than that of the odd AGEs and Pt/PANI (Figure 5.3B, D, H, and I) to allow for better visualization of the features in the CVs. The peak potentials as well as the current densities of the oxidation peaks in the forward scan provide justification of the origin of the two peaks identified in Figure 5.2D. There is a single oxidation peak in the forward scan in the potential range of 151mV to 217mV (Figure 5.3A). The cyclic voltammograms recorded on the AGEs show an oxidation peak in this potential region suggesting that this peak, Peak II, corresponds to oxidation of the alcohol involving the atomic gold. The analysis of current densities of this peak further supports this suggestion. The highest current density on the solid Au disk electrode is seen for 2-BuOH followed by n-BuOH then i-BuOH. This same trend in current densities for Peak II is observed for the majority of the AGEs.

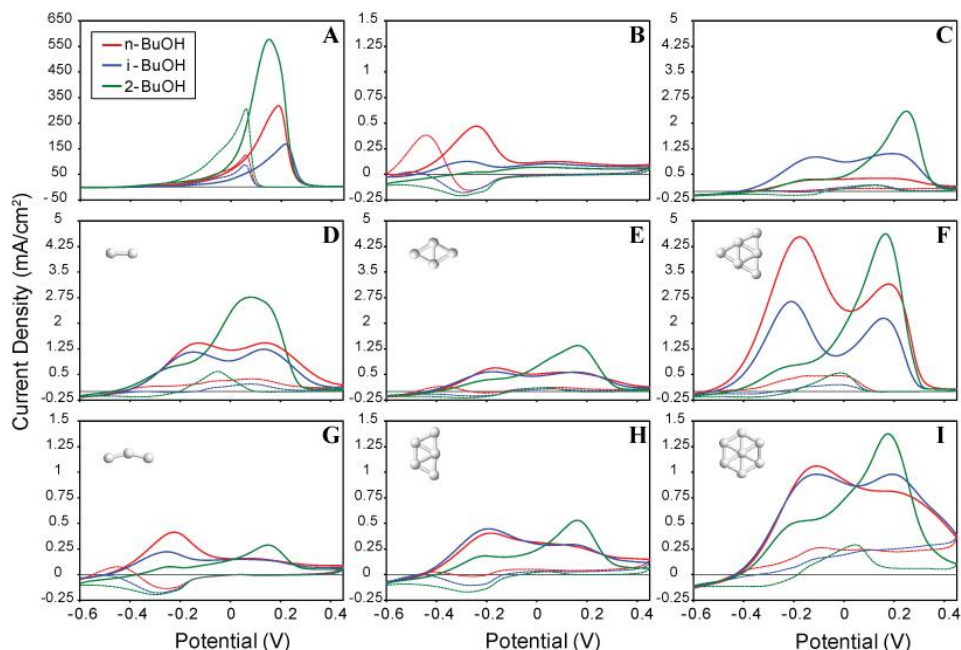


**Figure 5.3.** Survey of cyclic voltammograms recorded in a series of 0.5M butanols in 1M KOH on the following electrodes: (A) Au BAS, (B) Pt/PANI, (C) Pt/PANI/Au<sub>macro</sub>, (D) AGE-2, (E) AGE-4, (F) AGE-6, (G) AGE-3, (H) AGE-5 and (I) AGE-7.

Voltammograms recorded on Pt/PANI, also show only a single oxidation peak in the forward scan, but this peak occurs in the potential range of -278 mV to -232 mV (Figure 5.3B). This suggests that Peak I, which occurs in a similar potential range for the AGEs, is likely due to the oxidation of the alcohol at Pt/PANI. Once more, the trend of the current densities for the oxidation peak on Pt/PANI is similar to that of Peak I of the CVs recorded on the AGEs with the highest oxidation current density occurring for n-BuOH followed by i-BuOH then 2-BuOH. However, the number of gold atoms in the PANI does have an effect on Peak I. In the presence of even numbered gold, the current density of Peak I is enhanced. For AGE-6, the current density of Peak I is almost ten times larger than that of Pt/PANI for n-BuOH indicating that the presence of even number of atomic

gold enhances the oxidation at Pt/PANI electrode. The details of AGE-5 and AGE-6 for the butanol series are shown in Figure 5.4.

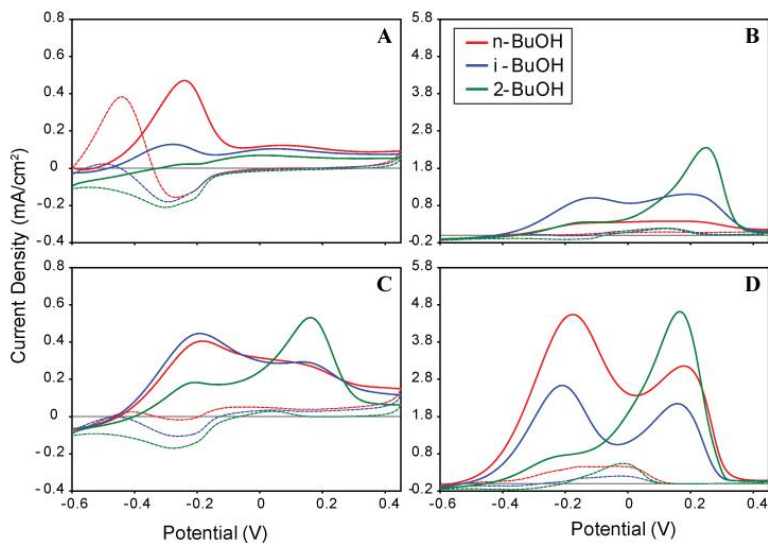


**Figure 5.4.** Cyclic voltammograms recorded in the series of 0.5M butanols in 1M KOH on (A) Pt/PANI, (B) Pt/PANI/Au<sub>macro</sub>, (C) AGE-5 and (D) AGE-6.

### 5.5 Oxidation of Branched Isomers

The overview of oxidation of branched alcohols is shown in Figure 5.5. The activities of Pt/PANI and Pt/PANI/Au<sub>macro</sub> are shown here as reference. The even AGEs have again significantly higher activity than the odd ones. The most notable feature is the strong response from 2-BuOH at all electrodes. Both the i-PrOH and i-BuOH show two oxidation peaks at AGE-6 while i-BuOH is more easily oxidized (by 80-100 mV) than i-PrOH.

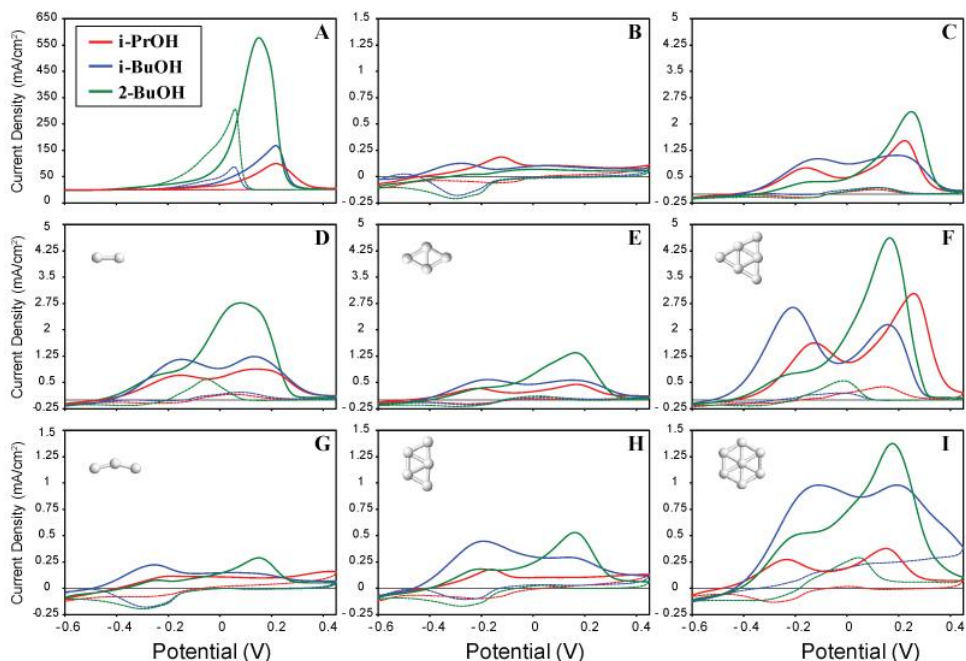


**Figure 5.5.** Cyclic voltammograms recorded in 0.5M branched alcohols in 1M KOH on the following electrodes: (A) Au BAS, (B) Pt/PANI, (C) Pt/PANI/Au<sub>macro</sub>, (D) AGE-2, (E) AGE-4, (F) AGE-6, (G) AGE-3, (H) AGE-5 and (I) AGE-7.

## 5.6 Proposed Oxidation Mechanisms

Interpretation of the effect of atomic gold revolves around the origin of Peak I and Peak II. Their magnitude and position are strongly influenced by the structure of the modified electrode, the presence of oxygen, and the choice of electrolyte. Peak I is absent in the pure, solid Au electrode. It appears in the range -95 to 281 mV and only in the presence of oxygen at solid platinum (Figure 5.6) covered with PANI, with or without any gold. Naturally, it is present in all AGEs. Figure 5.6 shows the CV of Pt/PANI in 1M n-PrOH in 1M NaOH with oxygen present (dashed line) and after the NaOH was bubbled with nitrogen for 1hr to remove oxygen. Peak I is present when oxygen is in solution and is absent when the oxygen has been removed. The presence of oxygen is necessary for peak I to be present.

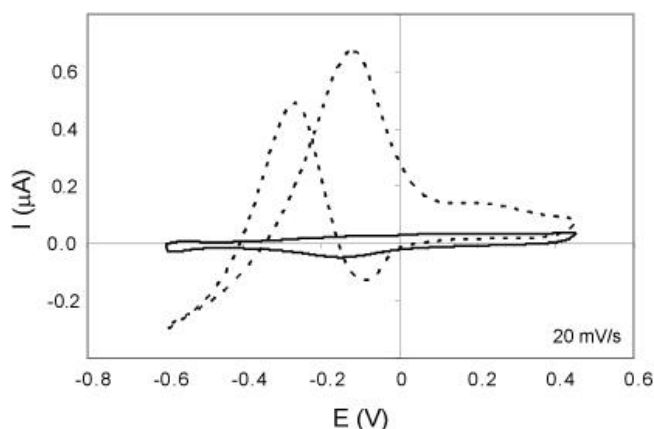


**Figure 5.6.** Cyclic voltammograms of Pt/PANI in 1M n-PrOH in 1M NaOH with oxygen (dashed line) and without oxygen (solid line).

As seen previously for n-PrOH, the bare platinum had very little catalytic activity, but there was significant activity when PANI was present on the platinum (Figure 4.1). To determine if the peak is due to the presence of the platinum or the PANI, the substrate was changed from platinum to a glassy carbon electrode. Figure 5.7 shows the CVs of a glassy carbon electrode in 1M NaOH and in 0.5M n-PrOH in 1M NaOH. The two CVs do not differ from each other and the glassy carbon electrode is not catalytically active for n-PrOH. PANI was deposited on the glassy carbon electrode and the experiment was repeated (Figure 5.8). Again, the two CVs are almost identical even when the potential range was widened and the concentration of n-PrOH was increased to 1M. The only difference is a slight bump around +0.05V that has a current that is extremely small compared to the currents seen for the Pt/PANI electrode in the same electrolyte.

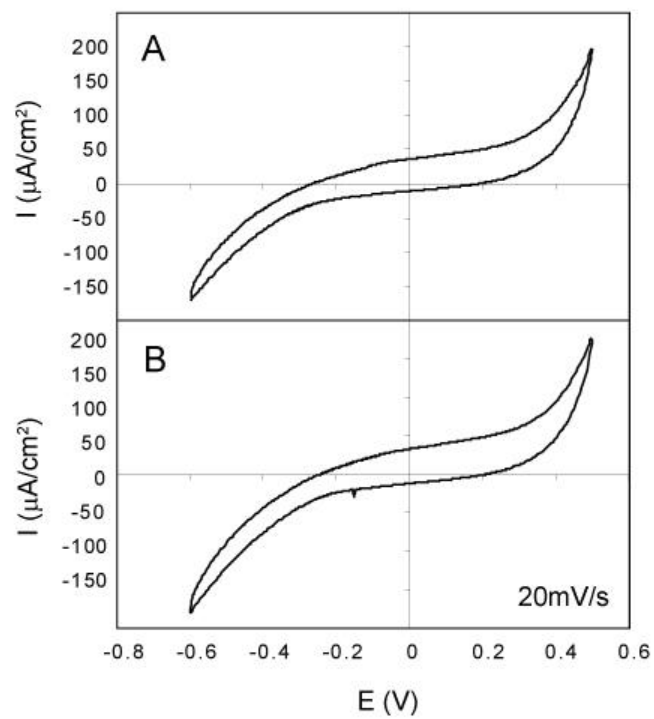


**Figure 5.7.** Cyclic voltammograms of a glassy carbon electrode in (A) 1M NaOH and (B) 0.5M n-PrOH in 1M NaOH.

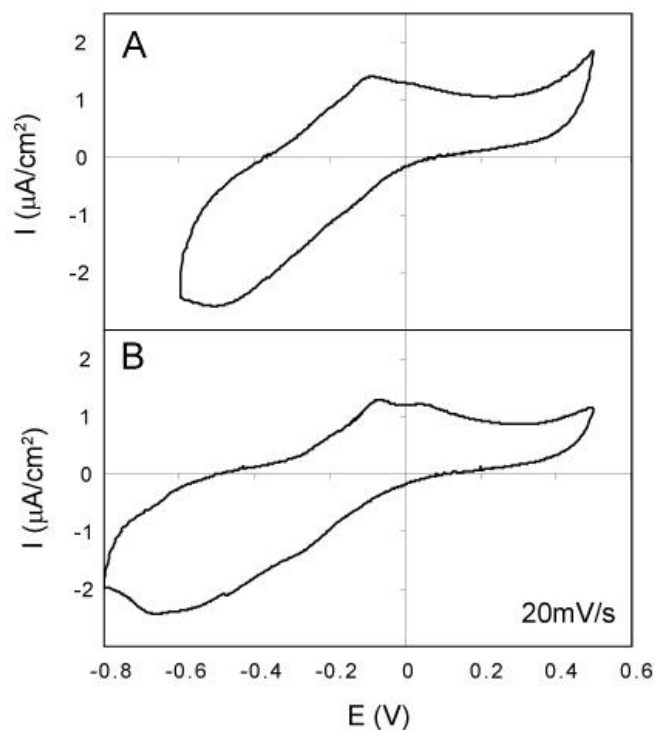


**Figure 5.8.** Cyclic voltammograms of PANI deposited on a glassy carbon electrode in (A) 1M NaOH and (B) 1M n-PrOH in 1M NaOH.

The relative sensitivity of peak I to individual alcohols can be seen in Figure 5.1B where the current density increases in the order MeOH < EtOH ~ n-PrOH < n-BuOH. That order is roughly maintained in AGE-6 for Peak I. Based on these observations we conclude that PANI facilitates adsorption of the alkoxy anion on the Pt surface followed by the oxidative removal of the alpha hydrogen from the alcohol<sup>92</sup>. The increasing acidity (pKa value) the alcohols in the above series further contributes to the higher oxidation rate.

Peak II at solid Au electrode is appearing at more positive potentials, in the range +200 to +250 mV. The order of peak current densities for individual alcohols is again EtOH < nPrOH < nBuOH, while MeOH is not showing any activity. That sequence is

repeated in AGE-6 with a wider spread in the peak oxidation potentials (+137 to +260 mV). In this sequence EtOH is most easily oxidized, but n-BuOH has the highest peak current activity. Also, the absence of oxygen makes little difference (Figure 5.9). In the absence of oxygen, peak II only slightly decreases, but interestingly, peak I is also present. There has been some evidence in the literature that reactive oxygen species can be generated on atomic gold clusters from water which would account for this<sup>93-95</sup>. The similarity of behavior of Peak II between activity at solid Au electrode (Figure 5.3A) and AGE-6 (Figure 5.3F) is even more striking for the butanol series. For the solid gold electrode, the order of peak current densities for individual butanols is i-BuOH < n-BuOH < 2-BuOH. This same order of peak current densities for the butanols is seen on AGE-6. Our observations are in line with the oxidation of alcohols in alkaline medium at Pt and Au electrodes, which has been subject of recent investigations<sup>30,34-36,96-102</sup>.

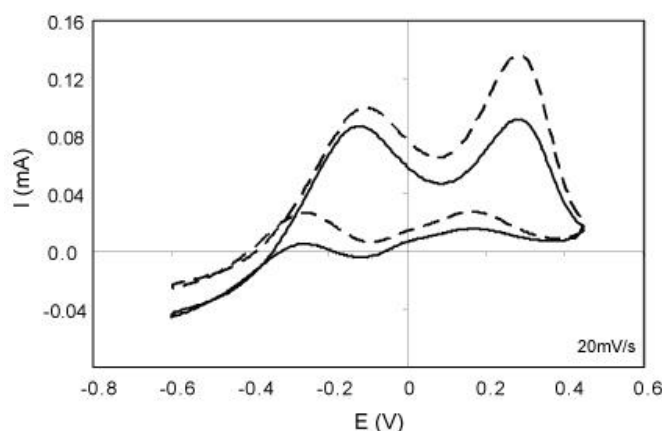
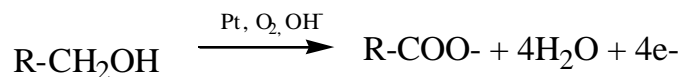


**Figure 5.9.** CVs of PANI/Au<sub>6</sub> in 0.5M n-PrOH in 1M NaOH before bubbling with N<sub>2</sub> for 1hr (dashed line) and after bubbling with N<sub>2</sub> for 1hr (solid line).

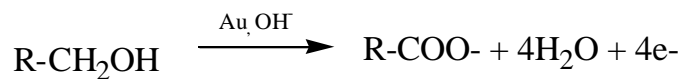
In conclusion, Peak I is due to oxidation of the alcohol on platinum. Peak I is not seen if we deposit PANI on a glassy carbon electrode, so the electrooxidation is not due to the

presence of PANI. The presence of oxygen is required, and PANI increases the electrooxidation by enhancing the adsorption of the alkoxy anion on the platinum. The presence of atomic gold acts as a dopant for PANI and changes its level of oxidation which further enhances the electrooxidation of the alcohol. Although intermediates were not identified, we can propose a mechanism based on our data and on findings in the literature that the overall electrooxidation of Peak I has the following equation.



The final product is the carboxylic acid, but it is neutralized in alkaline media to the carboxylate anion.

For Peak II, the electrooxidation of the alcohols occurs at the atomic gold clusters by the mechanism previously proposed where  $\text{OH}^-$  is adsorbed on the gold<sup>34</sup> and the overall reaction is:



In both mechanisms, the aldehyde is formed first which is then rapidly oxidized to the carboxylic acid in alkaline media.

## CHAPTER 6

### Atomic Clusters of Pd and Au<sub>N</sub>Pd<sub>M</sub> in Polyaniline

#### 6.1 Introduction

It is desirable to have a versatile method for the preparation of a wide range of metal catalysts with controlled atomic distribution. In order to show the versatility of this cyclic pathway method, we have chosen to deposit atomic clusters of palladium and bimetallic atomic clusters of palladium-gold in PANI. The influence of the atomic size of Pd<sub>1-6</sub>, and the stoichiometry of bimetallic Au<sub>1-5</sub>Pd<sub>1</sub>, and Au<sub>1-4</sub>Pd<sub>2</sub> on the electrochemical oxidation of n-propanol is demonstrated, and the obtained results are compared with the calculated HOMO-LUMO gap energies for clusters of the same size.

#### 6.2 Preparation of Pd<sub>N</sub> and Au<sub>N</sub>Pd<sub>M</sub> Composites

The same cyclic deposition of single atoms of gold may be applied to other metals as well. The cycle has to be adjusted to accommodate the reduction potentials of the metal that is to be deposited while still holding the PANI film in a fully oxidized state.

Using a Pt BAS working electrode, a Pt foil counter, and a Ag/AgCl in 1M KCl reference electrode, the cyclic voltammogram from -0.2V to +1.5V at a scan rate of 20mV/s of a 1mM solution of K<sub>2</sub>PdCl<sub>6</sub> in 0.1M HClO<sub>4</sub> is shown in Figure 6.1. The dashed line represents the CV of the background electrolyte. It shows a reduction peak at +0.399V that represents the reduction of platinum oxide on the electrode surface. The solid line represents the CV in 1mM K<sub>2</sub>PdCl<sub>6</sub> in 0.1M HClO<sub>4</sub> and displays several

oxidation and reduction peaks. The oxidation peaks in the forward direction at +0.666V and +1.317V represent the transitions from Pd<sup>0</sup> to Pd<sup>+2</sup> and then to Pd<sup>+4</sup>. The reduction peaks in the reverse scan at +1.179V, +0.480V, and 0.399V represent the transition of Pd<sup>+4</sup> to Pd<sup>+2</sup>, Pd<sup>+2</sup> to Pd<sup>0</sup>, and the reduction of the platinum oxide, respectively. The two reduction peaks for Pd are 0.699V apart which is in excellent agreement to the published value of 0.697V. The transition of Pd<sup>+2</sup> to Pd<sup>0</sup> that occurs at +0.480V is of interest for the atomic deposition cycles. Since the reduction to the atomic form is the only transition of interest for the atomic deposition cycles, a solution of K<sub>2</sub>PdCl<sub>4</sub> was used for further experiments.

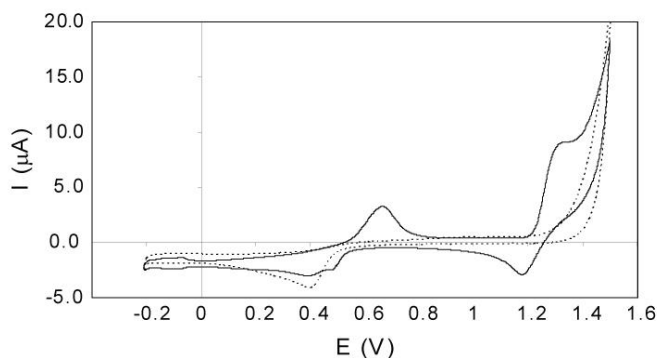


**Figure 6.1.** CV of 0.1M HClO<sub>4</sub> (dashed line) and 1mM K<sub>2</sub>PdCl<sub>6</sub> in 0.1M HClO<sub>4</sub> (solid line) from -0.2V to +1.5V at a scan rate of 20mV/s.

For multiple deposition cycles, it is important not to reoxidize the metal atoms that have been previously deposited. After electroplating Pd on a Pt BAS electrode, linear sweep voltammetry was performed to determine if the previously deposited Pd would be lost in the next cycle. Figure 6.2A shows the stripping voltammogram of Pd in 0.1M HCl. There are two oxidation peaks corresponding to the oxidation of Pd<sup>0</sup> to Pd<sup>+2</sup> and then finally to Pd<sup>+4</sup>. In Figure 6.2B, there are no oxidation peaks when stripping Pd

in 0.1M HClO<sub>4</sub>. Since HClO<sub>4</sub> is used in the atomic deposition cycles, there will be no loss of Pd in subsequent deposition cycles.

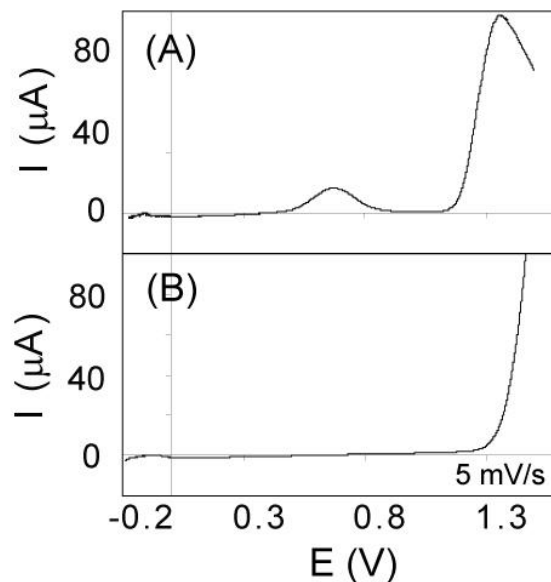


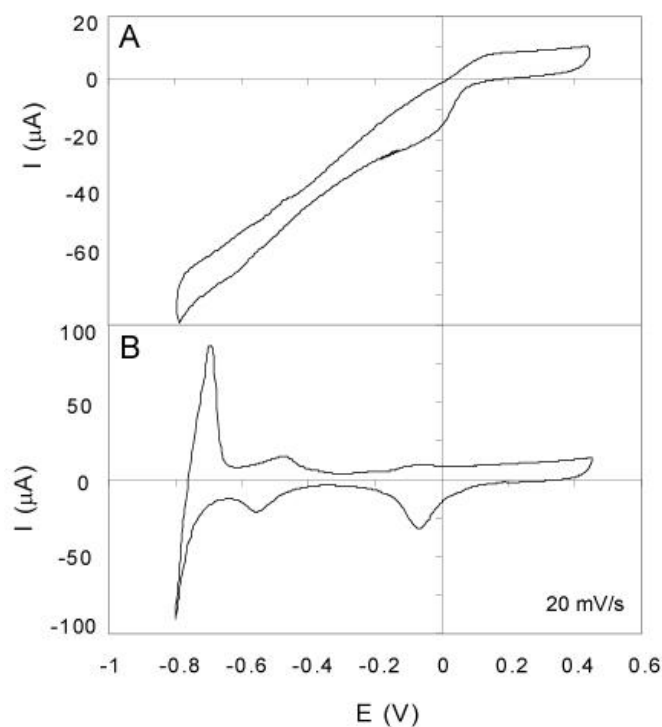
**Figure 6.2.** Stripping voltammograms of Pd in (A) 0.1M HCl and in (B) 0.1M HClO<sub>4</sub>.

The preparation of the PANI/Pd<sub>N</sub> films, where N equals the number of deposition cycles, was similar to the gold deposition sequence with only minor changes. The PANI deposition and conditioning steps were the same. The Pd cycle was initiated by holding the PANI at +0.8V while exposing it to solution of 0.2mM K<sub>2</sub>PdCl<sub>4</sub> in 0.1M HClO<sub>4</sub>. This leads to formation of the PANI\*PdCl<sub>4</sub><sup>-2</sup> complex. The film was then rinsed of the excess of PdCl<sub>4</sub><sup>-2</sup> with 0.1M HClO<sub>4</sub>, and the potential was scanned to -0.2V in order to reduce PdCl<sub>4</sub><sup>-2</sup> to atomic palladium. The final step was to perform 5 more CVs from -0.2V to +0.8V. At this point, the material was ready for the next deposition cycle. The cycle was repeated N-times in order to form the PANI/Pd<sub>1-6</sub> composite materials.

### 6.3 PANI/Pd<sub>1-6</sub> Oxidation of n-PrOH

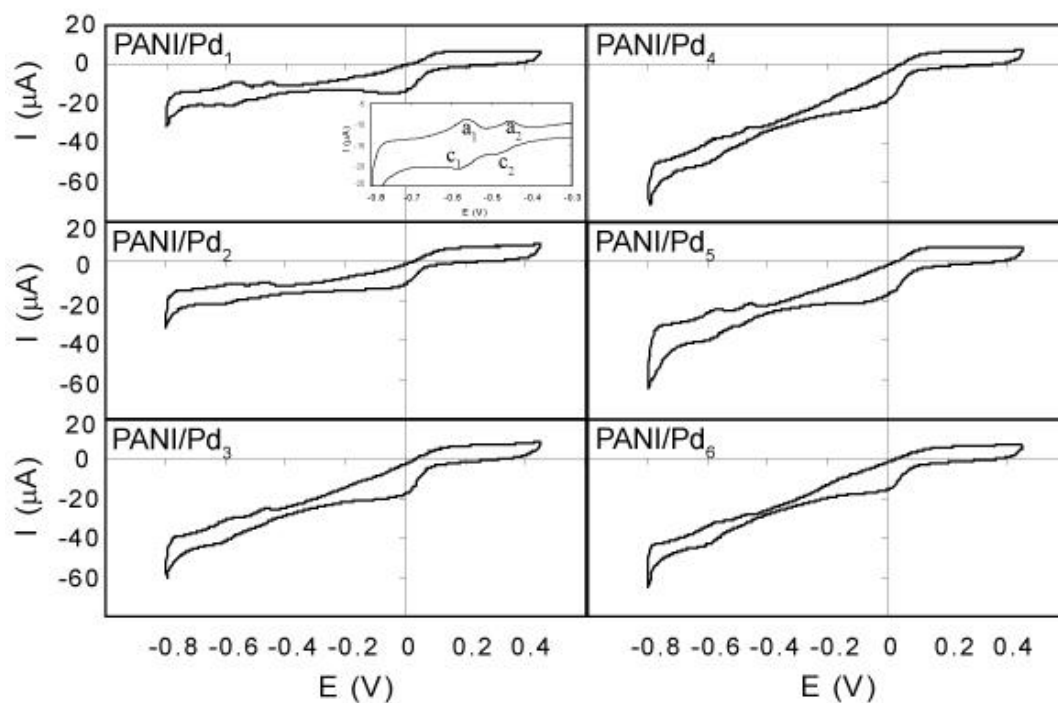
All cyclic voltammograms were recorded in 0.5M n-PrOH in 1M NaOH at a scan rate of 20mV/s from -0.8V to +0.45V using a Solartron SI1287 electrochemical interface. Platinum foil was used as the counter electrode. All potentials are versus a Ag/AgCl in 1M KCl//1M KNO<sub>3</sub> reference electrode. The CVs were recorded until a steady state was achieved. Only the last cycles are shown. A Pd coated BAS electrode was constructed by plating a Pt BAS electrode (Bioanalytical Systems, West Lafayette, Indiana, USA) with palladium by applying a potential of -0.2V for 500s in 1mM K<sub>2</sub>PdCl<sub>4</sub> in 0.1M HClO<sub>4</sub>.

In Figure 6.3A, the CV of PANI coated Pt in 1M NaOH is shown. The CV displays no remarkable peaks. However, in Figure 6.3B, the CV of a Pd plated Pt BAS electrode in 1M NaOH shows several remarkable features. The peak in the forward scan at -0.034V and the corresponding peak in the reverse scan at -0.078V correspond to the formation and reduction of surface palladium oxide on Pd, respectively. The peaks in the forward scan at -0.455V and at -0.554V in the reverse sweep correspond to hydrogen adsorption and desorption on the Pd surface, respectively, as it is well known that Pd is highly sensitive to the presence of hydrogen<sup>103,104</sup>. Finally, the peaks at -0.691V in the forward scan and -0.8V in the reverse scan correspond to the absorption of hydrogen into palladium and its reoxidation, respectively.



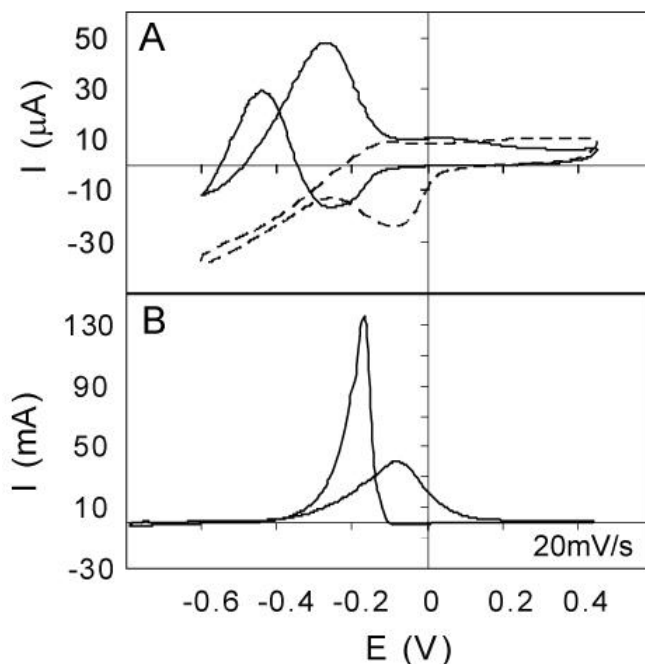
**Figure 6.3.** CV of (A) PANI coated Pt and (B) Pd coated Pt BAS in 1M NaOH from -0.8V to +0.45V.

Figure 6.4 shows the CVs of PANI/Pd<sub>N</sub> for N = 1 to 6 in 1M NaOH from -0.8V to +0.45V at a scan rate of 20mV/s. These CVs display a pair of peaks in the negative potential region. A close up of these peaks are shown in the inset. The peaks labeled a<sub>1</sub> and c<sub>1</sub> correspond to each other as well as a<sub>2</sub> and c<sub>2</sub>. The peak c<sub>1</sub> and c<sub>2</sub> correspond to hydrogen adsorption onto the Pd. In the bulk Pd, there is one peak that includes both of the peaks seen in the PANI/Pd<sub>N</sub> for this process, but on the PANI/Pd<sub>N</sub> electrodes, that single peak is now resolved into two separate peaks due to the small size of the Pd<sup>104</sup>.



**Figure 6.4.** CVs of PANI/Pd<sub>N</sub> for N=1-6 in 1M NaOH from -0.8V to +0.45V at a scan rate of 20mV/s. The insert shows a close up of the hydrogen adsorption peaks on Pd for PANI/Pd<sub>1</sub>.

The electrooxidation of n-PrOH was used as a marker for the characterization of the PANI films with atomic metal clusters prepared with the cyclic pathway method. Prior to the oxidation of n-PrOH by PANI/Pd<sub>1-6</sub>, the CVs were recorded for a Pt electrode (substrate), PANI coated Pt electrode (PANI/Pd<sub>N=0</sub>), and a Pd coated BAS electrode, Figure 6.5.



**Figure 6.5.** Cyclic voltammograms of 0.5M n-PrOH in 1M NaOH recorded (A) with Pt electrode (dashed line) and PANI deposited on Pt (solid line), and (B) with Pd coated BAS electrode.

The overlay of CVs recorded on the bare Pt electrode (dashed line) and on the PANI coated Pt electrode (solid line) is shown in Figure 6.5A. For the bare Pt electrode, there is no significant oxidation peak for n-PrOH in the anodic potential sweep, while the reduction of the surface oxide is seen in the cathodic sweep.

The CV acquired on the PANI coated Pt electrode displays two oxidation peaks; one on the forward scan at -0.27V and one on the reverse scan at -0.44V. The observed difference between CV's of those two electrodes indicates that Pt/PANI has higher catalytic activity to n-PrOH than the bare Pt electrode as described previously. The CV for the oxidation of n-PrOH in 1M NaOH on a bare palladium electrode is shown in Figure 6.5B. The oxidation peak of n-PrOH in the forward scan occurs at -0.06V, and the removal of species that were not oxidized in the forward scan occurs in the cathodic

sweep at the peak potential of -0.17V. These results have also been seen by others for the oxidation of n-PrOH on a Pd electrode in alkaline media<sup>62</sup>. The position of the oxidation peak in the forward direction of this CV will be useful later in identifying the oxidation peak in the composite films containing atomic Pd clusters.

The effect of the changes in the composition of the PANI/Pd<sub>N</sub> for N=1 to 6 on the oxidation of n-PrOH is shown in Figure 6.6. There is a prominent oxidation peak around -0.04V in the forward potential scan which corresponds to the oxidation of n-PrOH as seen on the bare Pd electrode (Figure 6.5B). Interestingly, for the PANI/Pd<sub>2</sub> electrode, there is a second very large peak seen around +0.34V. It is reasonable to assume, this second oxidation peak is due to further oxidation of the oxidation products of n-PrOH. Identification of the final oxidation product would need to be performed to confirm this assumption. However, the fact that this peak appears predominantly for PANI/Pd<sub>2</sub> electrode is significant by itself.

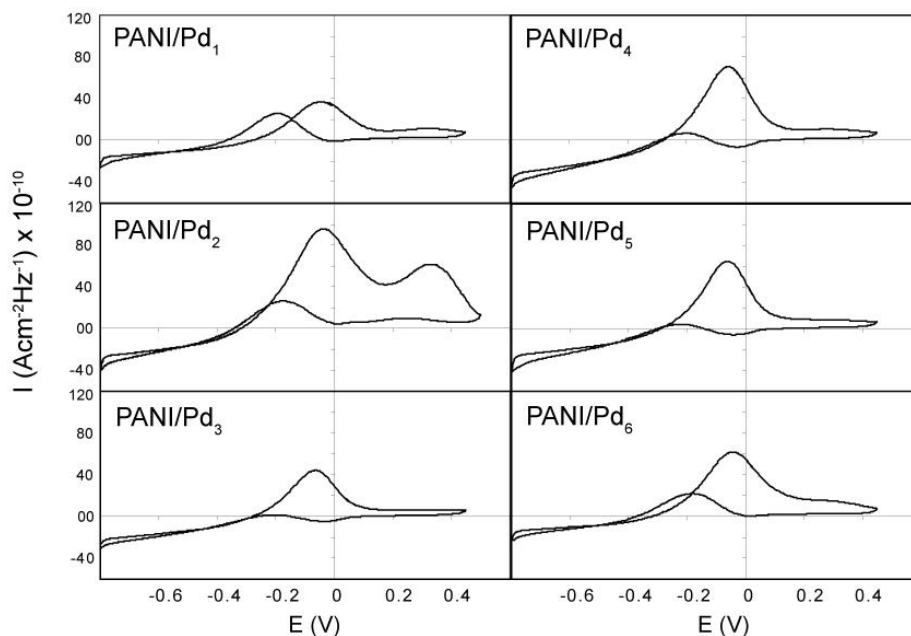


**Figure 6.6.** CVs of PANI/Pd<sub>N</sub> for N=1-6 from -0.8V to +0.45V in 0.5M n-PrOH in 1M NaOH. The CVs are normalized to the mass of PANI from the frequency changes during the deposition on Pt.

The magnitudes of the oxidation peak current densities obtained at +0.34V from Figure 6.6 are plotted in Figure 6.7 along with the theoretically predicted HOMO-LUMO gap energies for Pd clusters of the same size<sup>105</sup>. The pattern of the peak currents follows the same pattern as the predicted variation of the HOMO-LUMO gap energies for clusters containing the same number of Pd atoms. This is again a strong indication that our atomic number cluster corresponds to the number of deposition cycles performed, and that the atoms are deposited as atomic clusters and not just as single isolated atoms. The inset shows the oxidation peak currents of the first peak around -0.04V obtained from Figure 6.6. Again, these peak currents follow a similar trend as the predicted by HOMO-LUMO gap energies for Pd<sub>1-6</sub>. This fact apparently indicates that both of these peaks are influenced by the presence of the deposited Pd atoms in the PANI film.

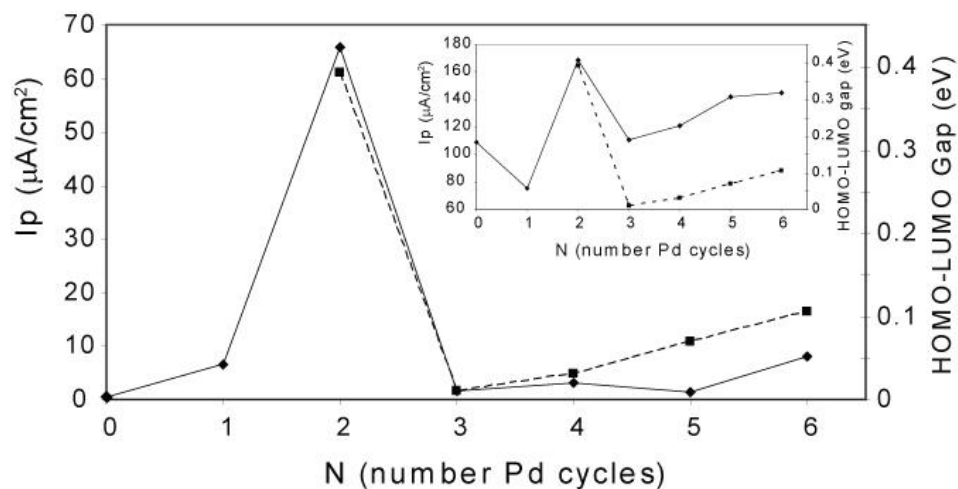


**Figure 6.7.** Peak current at +0.34V versus the number of Pd cycles (solid line). The dashed line represents calculated variation of the HOMO-LUMO gap energy<sup>102</sup>. The inset shows the  $I_p$  for peak I at -0.04V.

#### 6.4 FTIR of PANI/Pd<sub>1-6</sub>

Since these atomic metal clusters are believed to reside at the imine sites of PANI, the N-H stretching, located around  $3100\text{-}3500\text{cm}^{-1}$  in the FTIR spectra, should be affected by their presence. The FTIR data was collected under the same conditions as stated previously. Indeed, Figure 6.8 shows that the peak shifts of the N-H stretch for PANI/Pd<sub>N=1-6</sub> again follows the same pattern as the predicted changes of the HOMO-LUMO gap energies for the different sizes of atomic Pd clusters.

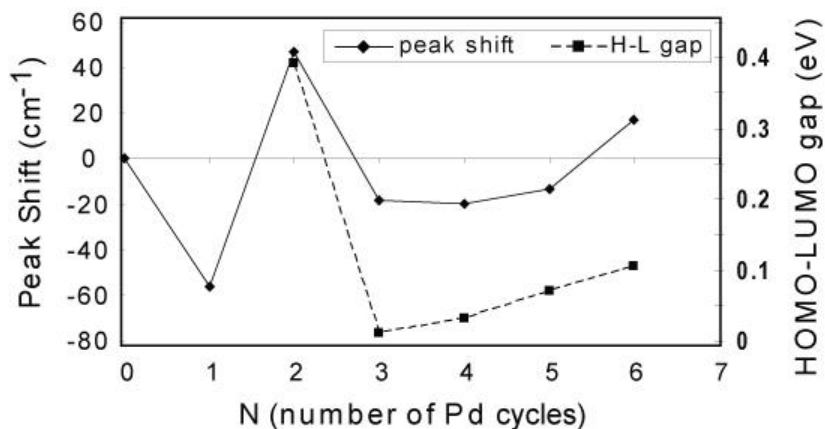


**Figure 6.8.** FTIR peak shift for the N-H stretching at  $3300\text{cm}^{-1}$  for PANI/Pd<sub>N</sub> for N=0-6. The dashed line represents calculated variation of the HOMO-LUMO gap energy<sup>102</sup>

The inserted Pd atomic clusters are apparently acting as a dopant for PANI. The R value, which is the ratio of the peak area of the quinoid units to the peak area of the benzenoid units, is a measure of the oxidation level of PANI and of the doping level. The FTIR data in Figure 6.9 shows that the  $1/R$  value follows the same pattern as the predicted HOMO-LUMO gap energies with the change of the size of the atomic Pd clusters. It is believed that upon doping some of the quinoid units are converted to benzenoid units by a spin unpairing mechanism<sup>80</sup>. This is due to the charge transfer complex that is formed between the metal atoms and the PANI matrix.

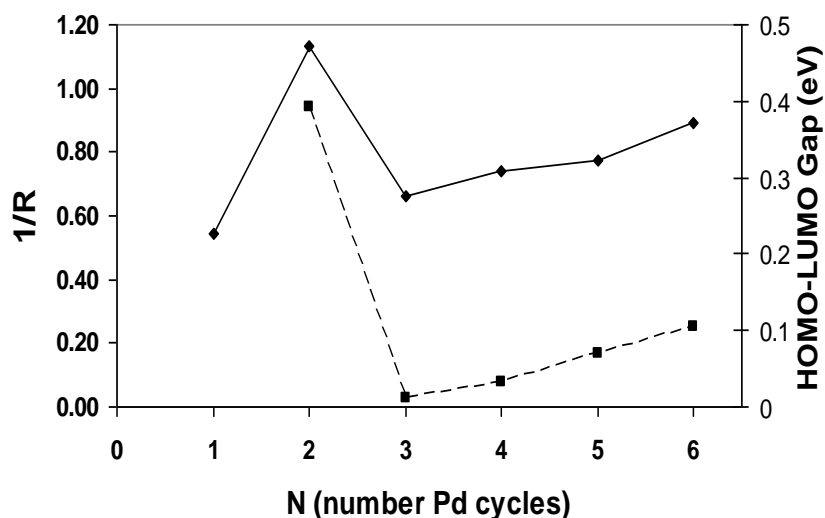


**Figure 6.9.** Plot of 1/R from FTIR versus N for PANI/Pd<sub>N</sub> (N=1-6) showing the oxidation level of the PANI changes as inserted Pd acts as a dopant. The predicted HOMO-LUMO gap energies are shown as a dashed line.

### 6.5 Bimetallic Alloys of Au and Pd in PANI

PANI films deposited with Au<sub>1.5</sub>Pd<sub>1</sub> and Au<sub>1.4</sub>Pd<sub>2</sub> were used for Ion Coupled Plasma Mass Spectrometry (ICP-MS) analysis to determine the molar ratios of Au:Pd. For elemental analysis, the PANI films with the atomic clusters were removed from the Pt-QCM by applying a potential pulse of -4V for 1s in 1M NaOH<sup>106</sup>. The films were then retrieved, washed and boiled down to dryness in 5ml of aqua regia. (CAUTION!!!) This step was repeated three times to completely dissolve the films. After this, the samples were boiled down three times to dryness with a solution of 8M HNO<sub>3</sub> with 1%HCl (v/v). The elemental analysis by ICP-MS on each dried sample was performed at

Argonne National Laboratory (ANL). All concentrations were prepared as wt./wt. measurements for higher precision and accuracy. The samples were brought back into solution with 5 mL of 3M HNO<sub>3</sub>/2% HCl for stabilization of Au and Pd within the solution matrix. Dilutions were made with 2% HNO<sub>3</sub> to a nominal concentration of 20ng/g for ICP-MS measurements. A multi-precious metal certified standard of 10mg/L of Au, Pt, and Pd in 2% HNO<sub>3</sub>/trace HCl was used in all calibration standards (High Purity Standards, SC) for elemental analyses. Calibration standards with nominal concentrations of 1 to 50 ng/g of Au, Pt, and Pd and 20 ng/g of In as the internal standard were prepared and matrix matched with the sample set.

Elemental analyses were performed using an ELAN DRC II ICP-MS (Perkin Elmer, CT). A SC-2-DX auto sampling system (ESI, Inc., Omaha, NE) introduced all samples into the ICP-MS. An all teflon sample introduction system, including a PC3 peltier cooled PFA cyclonic spray chamber and low-flow self-aspirating PFA nebulizer (ESI, Inc., Omaha, NE) was used to introduce samples into the plasma. All data was processed for concentration and amounts manually using macro-based calculation excel spreadsheets developed at ANL.

The theoretically and experimentally determined Au:Pd molar ratios for Au<sub>1.5</sub>Pd<sub>1</sub> and for Au<sub>1.4</sub>Pd<sub>2</sub> are shown in Figure 6.10. As can be seen, the pattern of the molar ratio of Au<sub>1.5</sub>Pd<sub>1</sub> determined experimentally is very close to the theoretically calculated values. The molar ratio pattern for Au<sub>1.4</sub>Pd<sub>2</sub> is not as similar if only the trend lines are compared. However, it can be noticed that the experimental values of the molar ratio for Au<sub>1</sub>Pd<sub>1</sub> and Au<sub>2</sub>Pd<sub>1</sub> are exactly the same as their theoretical values. The values only begin to diverge for the Au<sub>3</sub>Pd<sub>1</sub> and Au<sub>4</sub>Pd<sub>1</sub>.

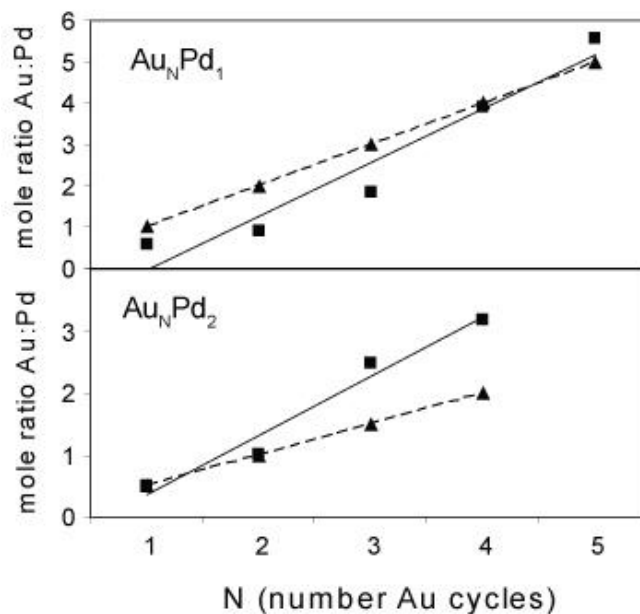


**Figure 6.10.** The molar ratios of Au:Pd for  $Au_{1-5}Pd_1$  (top) and  $Au_{1-4}Pd_2$  (bottom). The experimental values (■ connected with solid trend line) and the theoretical values (▲ connected with a solid trend line) are shown for comparison.

The similarity between the theoretical and experimental molar ratios of the two metals is further proof that these bimetallic clusters are not just individual atoms, but clusters made up of the same number of atoms as the number of cycles.

Based on these results, we can explain how the metal atoms preferentially deposit during the cyclic pathway. In the first cycle, the  $AuCl_4^-$  (or  $PdCl_4^{2-}$ ) is attaching to random imine sites of PANI. Once these anions are reduced to atomic gold, the next cycle can begin. In the next cycle, the Au or Pd is preferentially deposited at the sites that are already occupied by Au or Pd since a metal-metal bond will always be preferred. In addition to this, once the first atom of metal is deposited, a charge transfer complex is formed between the metal and the PANI arising from the differences in electron affinity.

The metal will have a slightly negative charge, while the imine site will become slightly more positive than it was before. Then in the next deposition cycle, the metal halide anions will have a higher affinity for the more positively charged imine sites over the other sites. However, deviations from the theoretical values may arise if some Au or Pd deposits at an unoccupied imine site. Since the metal-metal bond is preferred, the overall activity will be dictated by the clusters with the same number of atoms as the number of cycles.

From the data, we wanted to determine how many sites in the PANI film were occupied by the atomic clusters. The mass of the metal deposited was determined by ICP-MS and, the amount of PANI deposited was determined by a calibration curve constructed from the change in frequency of the QCM versus the amount of charge used to deposit the film. The number of moles of imine sites can be calculated for the PANI as deposited, however, many of these sites are lost in the conditioning step of PANI. There is no way to determine exactly how many of the original sites are lost. At this point, it can only be said that the amount of PANI is in molar excess.

### **6.6 Oxidation of n-PrOH with PANI/Au<sub>N</sub>Pd<sub>M</sub> Electrodes**

The oxidation of 0.5M n-PrOH was performed by cyclic voltammetry in 1M NaOH using the PANI/Au<sub>N</sub>Pd<sub>M</sub> electrodes using the same experimental parameters as for the PANI/Pd<sub>N</sub> electrodes. The CVs for the oxidation of n-PrOH on Au<sub>N</sub>Pd<sub>1</sub> for N = 1-5 are shown in Figure 6.11, and the CVs for the oxidation of n-PrOH on Au<sub>N</sub>Pd<sub>2</sub> for N = 1-4 are shown in Figure 6.12.

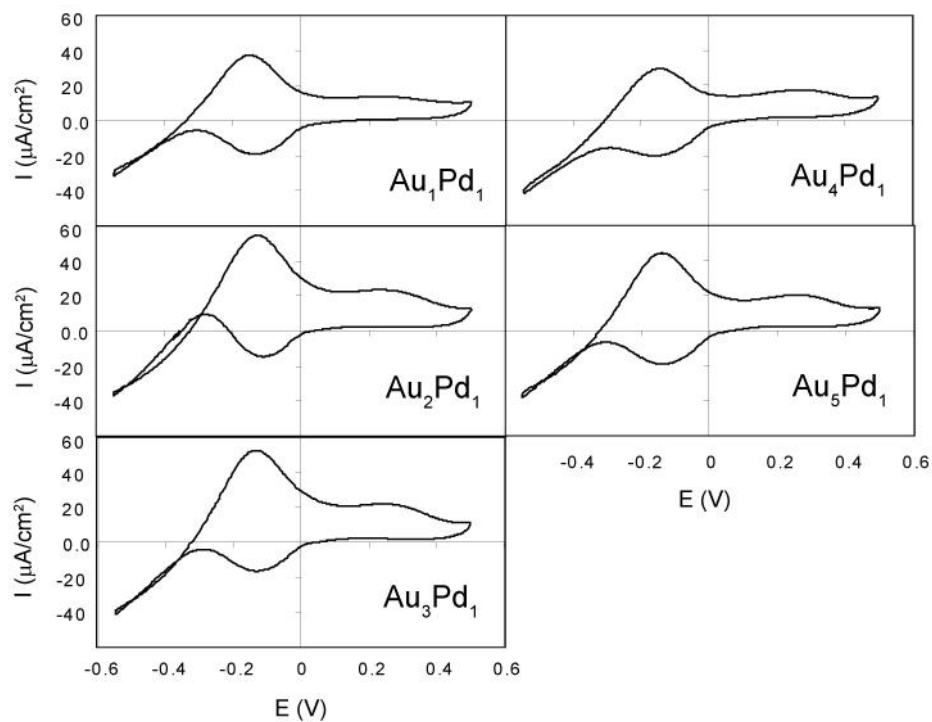


**Figure 6.11.** CVs of PANI/Au<sub>N</sub>Pd<sub>1</sub> for N=1-5 from -0.8V to +0.45V in 0.5M n-PrOH in 1M NaOH.

In the CVs for PANI/Au<sub>N</sub>Pd<sub>1</sub>, there are two oxidation peaks in the forward scan. The oxidation peak around -0.12V is much larger than the peak around +0.25V. These CVs still retain some of the characteristics of the PANI/Au<sub>N</sub> clusters such as the peak positions and peak potentials. In the CVs for PANI/Au<sub>1</sub>Pd<sub>2</sub>, there is one large oxidation peaks in the forward scan with a shoulder that indicates the presence of a smaller second peak. The other CVs for PANI/Au<sub>N</sub>Pd<sub>2</sub> where N = 2-4 display only a single peak around -0.05V.

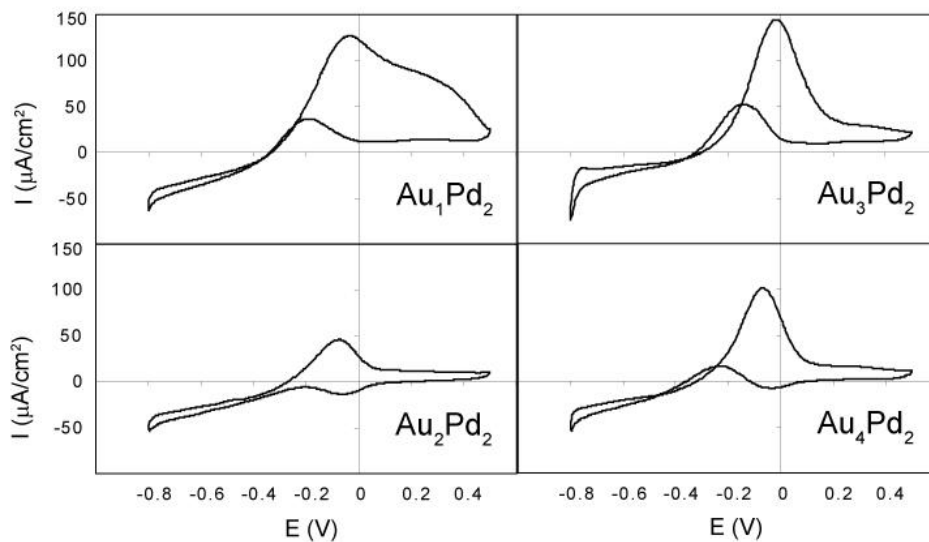


**Figure 6.12.** CVs of PANI/Au<sub>N</sub>Pd<sub>2</sub> for N=1-4 from -0.8V to +0.45V in 0.5M n-PrOH in 1M NaOH.

The peak currents for the oxidation of n-PrOH around -0.04V for Au<sub>N</sub>Pd<sub>1</sub> (Figure 6.13 top) and Au<sub>N</sub>Pd<sub>2</sub> (Figure 6.13 bottom) is plotted against the number of Au atoms present in the bimetallic cluster. The pattern of these peak currents follows the predicted HOMO-LUMO gap energies for Au<sub>N</sub>Pd<sub>1</sub><sup>107</sup> and Au<sub>N</sub>Pd<sub>2</sub><sup>108</sup> until N = 4 is reached.

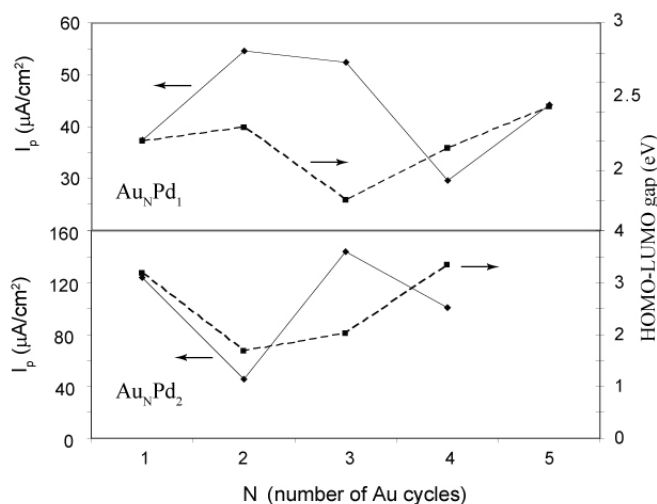


**Figure 6.13.** Peak currents (solid lines) of n-PrOH oxidation (at approximately -0.04V) versus the number of inserted Au atoms in Au<sub>N</sub>Pd<sub>1</sub> (top) and for Au<sub>N</sub>Pd<sub>2</sub> (bottom). The concentration of n-PrOH was 0.5M in 1M NaOH. The dashed line represents calculated variation of the HOMO-LUMO gap energy<sup>104, 105</sup>

The agreement between the observed electrochemical catalytic activity of clusters and predicted HOMO-LUMO gap energies is only a qualitative test. In single metal atomic clusters, the same type of atom occupies all the sites within a particular structure. However, the most available catalytically active surface site in a mixed cluster may depend on the deposition sequence since the clusters are formed from the “bottom up”. The location of the Pd atoms in the structure of the cluster may depend on the sequence order that it is deposited. In other words, the catalytic activity may depend on either having an Au or Pd atom occupying the most accessible site in the structure. Further experiments where the Pd is deposited in a different sequence will need to be performed in order to answer this important question.

For comparison, the electrooxidation of n-PrOH by Au<sub>3</sub>, Pd<sub>3</sub>, Au<sub>1</sub>Pd<sub>2</sub>, and Au<sub>2</sub>Pd<sub>1</sub> is shown in Figure 6.14.

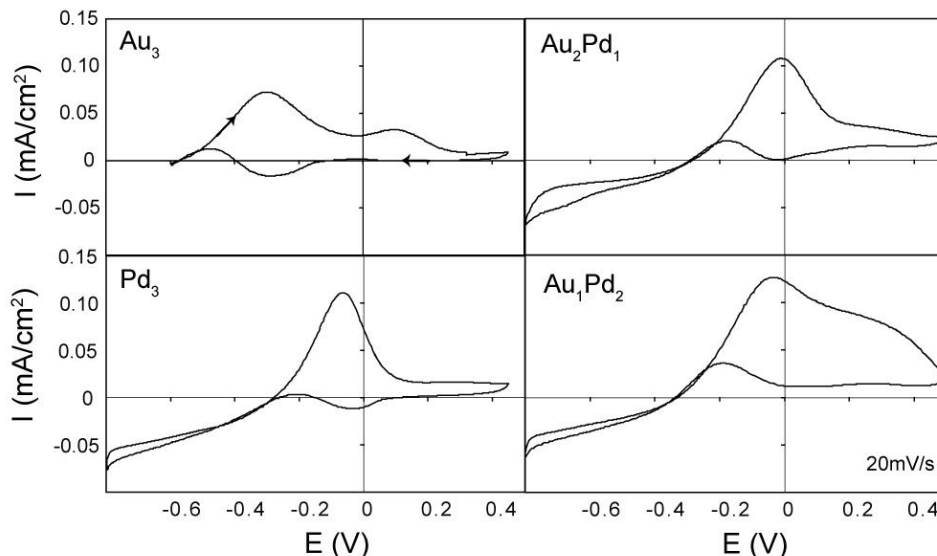


**Figure 6.14.** Comparison of CVs for the oxidation of 0.5M n-PrOH in 1M NaOH for atomic clusters consisting of a total of 3 metal atoms.

Note that all of these atomic clusters contain three atoms of metal. In the films Au<sub>1</sub>Pd<sub>2</sub> and Au<sub>2</sub>Pd<sub>1</sub>, the single atom was deposited last. As shown, the pure Au<sub>3</sub> cluster has two oxidation peaks in the forward scan, but Pd<sub>3</sub> has only one. Now, when we substitute a single atom of a pure metal cluster with an atom of a different metal, the CV starts to look quite different. It is seen that by substituting one atom in Pd<sub>3</sub> with an atom of Au, the CV for Au<sub>1</sub>Pd<sub>2</sub> now more closely resembles the CV of a pure gold cluster containing the same number of atoms. Also, by substituting one atom in Au<sub>3</sub> with an atom of Pd, the CV for Au<sub>2</sub>Pd<sub>1</sub> now more closely resembles the CV of a pure palladium cluster containing the same number of atoms. Since all the atoms in these clusters are surface atoms, the activity will depend not only on the interactions between the two metals, but also the arrangement of the atoms in the atomic cluster. Again, the catalytic

activity may depend on either having an Au or Pd atom occupying the most accessible site in the structure.

In order to confirm these observations, the metal atoms were deposited in a different sequence for the PANI/Au<sub>2</sub>Pd<sub>1</sub> film (Figure 6.15).

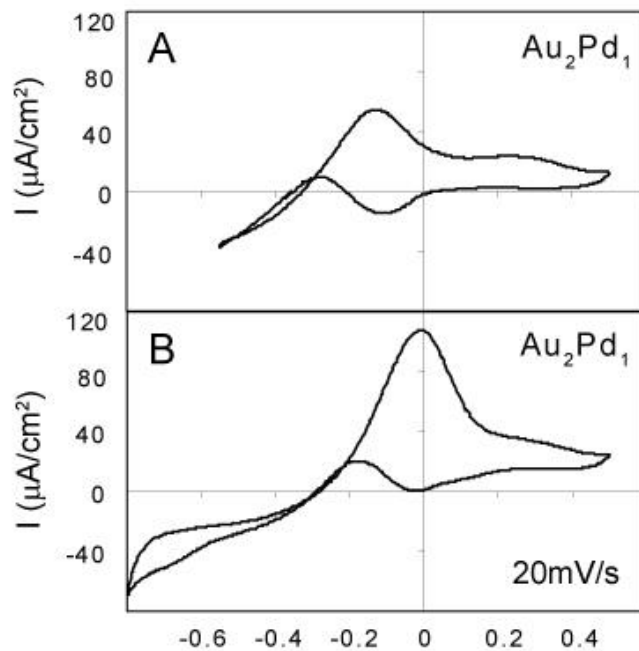


**Figure 6.15.** CVs of Au<sub>2</sub>Pd<sub>1</sub> in 0.5M n-PrOH in 1M NaOH when (A) Pd is deposited first and (B) Au is deposited first.

In Figure 6.15A, the palladium was deposited first. This CV displays two oxidation peaks in the forward scan at potentials similar to the PANI films that contained only atomic gold clusters. This may be an indication that the palladium atom is still in contact with PANI, while the gold atoms are the sites where the oxidation of the alcohol occurs. In Figure 6.15B, the gold was deposited first. Now, the CV has mainly a single oxidation peak in the forward scan that is shifted to a more positive potential similar to PANI films

with atomic palladium clusters. In this case, the oxidation of the alcohol seems to occur mainly on the palladium sites.

There are clear differences in the CVs for the same atomic bimetallic cluster with different deposition sequences. Based on these results, it can be concluded that once the first atom is deposited, it forms a charge transfer complex with the PANI. As more atoms are added, the first deposited atom remains in this charge transfer complex with PANI while the other atoms are added on top of it to form the atomic cluster. Therefore, the catalytic activity will be mostly dictated by the atoms farthest from the PANI film. The catalytic activity will still be influenced by the presence of the atom that was deposited first. The oxidation of n-PrOH occurs on the atoms that are not in direct contact with the PANI film, which are the most accessible to the alcohol. The deposition sequence plays a role in where the atoms are located in the cluster. Further experiments changing the deposition sequence will need to be performed in order to see if the catalytic effects change in larger atomic clusters with more than one atom of each metal.

## CHAPTER 7

### Oxidation of Methanol and Ethanol on PANI/Au<sub>n</sub>Pd<sub>1</sub> Electrodes

#### 7.1 Introduction

The effect of addition of one atom of palladium to n atoms of gold (n=1-5) dispersed in polyaniline electrodes, for the electrooxidation of methanol and ethanol in alkaline solution has been investigated. For comparison, oxidation at pure atomic metal electrodes, Pt/PANI-Au<sub>n=2 to 7</sub> and Pt/PANI-Pd<sub>n=2 to 6</sub>, was performed. It is shown that the one added Pd atom affects the oxidation peak currents and makes a significant difference in selectivity. Similar to the previous studies, the electrocatalytic activity has been correlated with the theoretically predicted HOMO-LUMO gap energies for the atomic metal alloys.

#### 7.2 Experimental

All electrochemical experiments were performed using a standard three-electrode cell and CHI 660 potentiostat (CH Instrument, Inc). The preparation of atomic clusters of gold, Au<sub>n</sub> (n = 2-7), and palladium, Pd (n = 2-6) in polyaniline (PANI), and the method for assembling of bimetallic atomic clusters, Au<sub>n</sub>Pd<sub>1</sub> in PANI was described previously. The counter electrode was a platinum foil. The reference electrode was Ag/AgCl in 1M KCl//1M KNO<sub>3</sub>. All potentials reported are referred to this electrode (E= 236 mV vs S.H.E.). Cyclic voltammograms were initiated from open cell potential and recorded using a scan rate of 50mVs<sup>-1</sup>, unless otherwise stated. The direction in which the CVs

were run is indicated in the figures. The current densities are given per true geometric area of the Pt electrode ( $A = 0.244 \text{ cm}^2$ ). The CVs shown were always at their steady-state.

### 7.3 Catalytic Activity for Oxidation of Methanol, Ethanol, and iso-Propanol

In order to evaluate the effect of adding one atom of Pd to atomic gold electrodes, we first examined the electrochemical oxidation of 0.5M MeOH in 1M KOH at pure atomic metal electrodes, Pt/PANI-Au<sub>n=2 to 7</sub> and Pt/PANI-Pd<sub>n=2 to 6</sub>, (Figure 7.1).

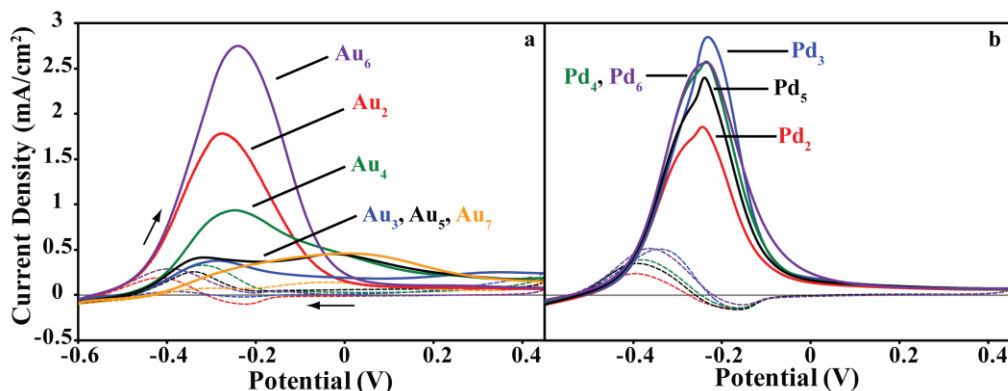


**Figure 7.1.** Cyclic voltammograms recorded in 0.5M MeOH in 1M KOH on (a) Pt/PANI-Au<sub>n=2 to 7</sub> and (b) Pt/PANI-Pd<sub>n=2 to 6</sub>. The reverse scans are shown as dashed lines.

The voltammograms recorded on both the atomic gold and atomic palladium electrodes show similar features. There is a single oxidation peak on the forward scan, at the peak potential ( $E_p$ ) -0.25V corresponding to the oxidation of methanol. For the atomic gold electrodes, it is believed that this oxidation occurs on the platinum substrate, but is affected by the presence of atomic gold in PANI as discussed previously. Oxidation of methanol on the atomic palladium electrodes also takes place at the platinum surface and

is enhanced by the presence of palladium. Since palladium, unlike gold, is active towards the oxidation of methanol, there is a shoulder on this forward oxidation peak, which is attributed to the oxidation of methanol on atomic palladium. In the reverse scans (shown as dashed lines), there is a small reduction peak around -0.2V corresponding to metal oxide reduction followed by oxidation of reaction intermediates and the regeneration of active sites at -0.4V<sup>109,110</sup>.

While the oxidation potentials and the features of the CVs (Figure 7.1a and 7.1b) are similar, the magnitude of their peak current densities reveals differences in behavior of these electrodes. Only the even-numbered atomic gold electrodes (Pt/PANI-Au<sub>n=2, 4, 6</sub>) significantly affect the activity towards the oxidation of methanol on platinum. This variation in activity has been also observed for the oxidation of other aliphatic alcohols and is related to the HOMO-LUMO energy gap of the atomic gold clusters. In comparison, there is very little variation in the peak currents produced by the different numbered atomic palladium clusters. The most active electrode for each metal, Au<sub>6</sub> and Pd<sub>3</sub>, reach approximately the same maximum current density of about 3mA/cm<sup>2</sup>.

In order to determine the activity of the Pt/PANI-Au<sub>n=1 to 5</sub>Pd<sub>1</sub> electrodes, cyclic voltammograms recorded in 0.5M solutions of MeOH, EtOH, and i-PrOH in 1M KOH are compared in Figure 7.2. Although not the primary subject of this study i-PrOH is included in Figure 7.2 because it shows relatively high oxidation activity on purely gold atomic electrodes. Voltammograms recorded in the absence of any alcohol are shown for comparison (Figure 7.2a). It is important to note that the current density scales for each panel are different to better visualize the features of the CVs.

In the forward potential sweep, the CVs recorded in 1M KOH (Figure 7.2a) exhibit a broad wave beginning around  $E_p = -0.1V$  corresponding to the adsorption of  $OH^-$  and its subsequent oxidation to form metal oxides. On the reverse potential scan a broad peak between  $-0.18V$  and  $-0.27V$  indicates the reduction of these metal oxides. Only slight variations in the voltammograms recorded in the background electrolyte are seen when comparing Pt/PANI with and without the bimetallic clusters. These CVs also have similar features to those obtained on the Pt/PANI- $Au_{n=2}$  to  $7$  electrodes in 1M KOH.

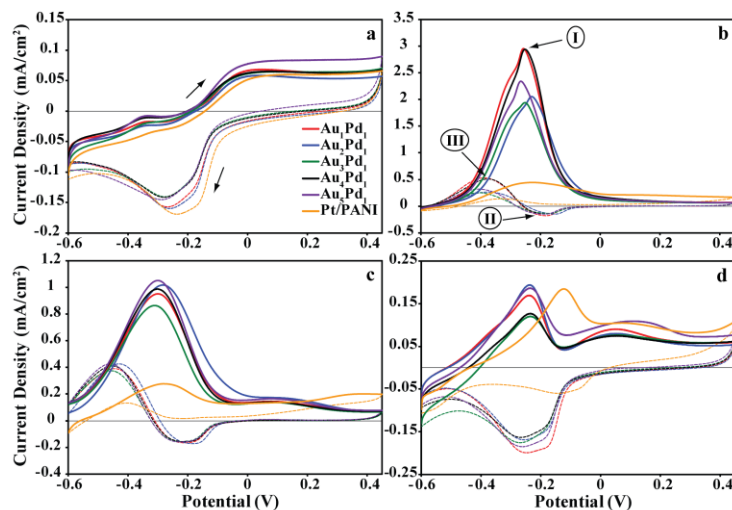


**Figure 7.2.** Voltammograms recorded in (a) 1M KOH with (b) 0.5M MeOH, (c) 0.5M EtOH and (d) 0.5M i-PrOH on Pt/PANI- $Au_{n=1}$  to  $5Pd_1$ . The reverse scans are shown as dashed lines.

However, differences in the activity of these electrodes can be seen when alcohol is present in solution (Figure 7.2b-d). It is important to note that the smallest oxidation current densities for MeOH and EtOH are seen for the Pt/PANI electrode indicating that the introduction of bimetallic clusters into the PANI increases the activity of these electrodes towards the oxidation of MeOH and EtOH.

Cyclic voltammograms recorded on the bimetallic electrodes in the presence of MeOH

and EtOH exhibit some similarities. It is possible to distinguish in them three activity regions. In the positive scan of the potential (Figure 7.2b), an oxidation peak around -0.25V (Region I) is seen resulting from the oxidation of MeOH. The reverse scan shows a peak at -0.2V (Region II) corresponding to the reduction of surface oxides. The oxidation of reaction intermediate species and regeneration of active sites is observed at more negative potentials (Region III). Similar regions are seen for the oxidation of EtOH (Figure 2c). However, the oxidation peak potential ( $E_{ox}$ ) for EtOH is slightly more negative (-0.28V) and the oxidation peak is broader than for MeOH.

The current densities of the oxidation peak ( $i_p$ ) in the forward scan are dependent on the type of alcohol as well as the composition of the electrode. The oxidation of MeOH generates current densities almost two times higher than the oxidation of EtOH for all electrodes. In contrast, for even-numbered of gold clusters without palladium (Pt/PANI-Au<sub>n=2, 4, 6</sub>), EtOH oxidation current densities are higher than those for MeOH as seen in chapter 5. Also, the addition of a single atom of palladium causes the odd-even oscillations in activity for the purely gold clusters to disappear. In all cases the voltammograms of *i*-PrOH show current densities ten times smaller than those for MeOH and are similar to the current densities for the electrode containing no metal clusters. This suggests that these Pt/PANI-Au<sub>n</sub>Pd<sub>1</sub> electrodes are not suitable for the oxidation of *i*-PrOH. This change of activity offers an intriguing opportunity for direct amperometric sensing of EtOH and MeOH in the presence of *i*-PrOH.

Upon addition of one atom of Pd to an atomic gold cluster, both the electronic and geometric configuration of the cluster is changed. The added Pd atom increases the total number of atoms in the cluster which alters the geometry of the cluster. Therefore, in

order to visualize only the electronic effect of the Pd dopant atom on the catalytic activity of the cluster, comparisons must be made between clusters with the same total number of atoms rather than clusters with the same number of gold atoms. This electronic effect can be seen in Figure 7.3 in which the oxidation peak currents for atomic clusters containing the same total number of atoms (i.e.  $Au_n$  and  $Au_{n-1}Pd_1$ ) are compared.

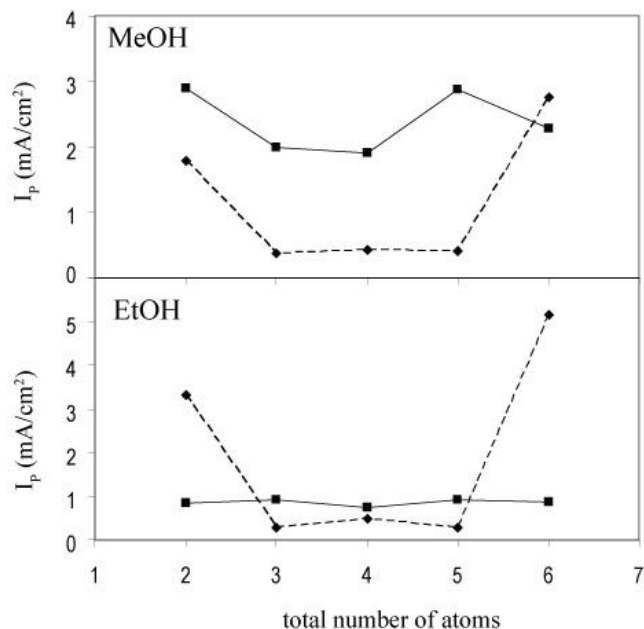


**Figure 7.3.** Oxidation peak currents densities for  $Au_n$  (dashed lines) and  $Au_{n-1}Pd_1$  (solid lines) versus the total number of atoms in the cluster for (a) MeOH and (b) EtOH.

For MeOH, the peak currents for  $Au_{n-1}Pd_1$  are significantly higher than for each of the  $Au_n$  clusters except for  $Au_6$  indicating that the introduction of Pd increases the catalytic activity. The deviation of the  $Au_6$  electrode is due to the high stability of  $Au_6$  as six is a magic number for 2D gold clusters<sup>44</sup>. For EtOH, the oxidation peak currents for  $Au_{n-1}Pd_1$  are slightly higher than the corresponding  $Au_n$  clusters when  $n = 3-5$  but are much lower

when  $n=2$  and  $6$  indicating that the addition of a Pd atom slightly enhances the catalytic activity for  $n = 3-5$  only. Adding Pd completely inactivates the electrode towards oxidation of *i*-PrOH (not shown). This same trend in activation/deactivation of the atomic electrodes is seen when clusters with the same number of gold atoms are compared (i.e.  $Au_n$  and  $Au_nPd_1$ ). In other words, the changes in the catalytic activity are due to changes in the electronic configuration of the gold atomic clusters induced by the dopant palladium atom.

#### 7.4 Comparison to the HOMO-LUMO Gap Energies

Peak current densities for the oxidation peak in the forward scan were compared to the HOMO-LUMO gap energies for neutral bimetallic  $Au_nPd$  clusters calculated by Ai-Jie et al.<sup>107</sup> (Figure 7.4). In general, the current densities recorded in MeOH and EtOH correlate to the calculated HOMO-LUMO gap energies for each  $Au_nPd$  cluster. This result is consistent with previous studies using pure gold clusters. The largest deviation from the expected result was for the oxidation of MeOH at the  $Au_2Pd_1$  electrode and  $Au_5Pd_1$  for both MeOH and EtOH.

The HOMO-LUMO gap energies were calculated for clusters in gas phase. Clearly, our clusters are in a much more complex environment. There are several possible explanations for the deviations from the calculated HOMO-LUMO gap energies. First, PANI is used as a support matrix for these clusters. The substrate can have significant effects on the activities of the clusters. For  $Au_5Pd_1$ , the ground state configuration is planar as seen as an icon in Figure 7.4, however, substrate effects may influence this structure to take on a three dimensional shape which would also affect its activity. In

addition, the orientation of the cluster in the support matrix could affect the peak currents. The activity may depend on whether atoms of Pd, Au, or both are accessible for catalysis and which ones are interacting most with the substrate. Clearly, there are many remaining factors to consider.

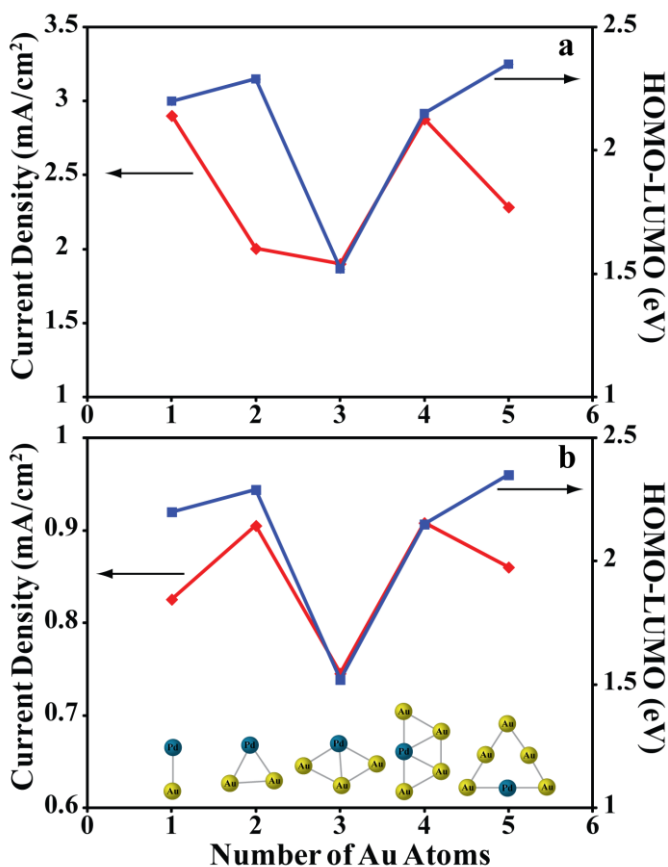


**Figure 7.4.** Current densities of the oxidation peak in the forward scan (shown in red) for (a) 0.5 M MeOH and (b) 0.5M EtOH in 1.0M KOH at Pt/PANI-Au<sub>n</sub>Pd<sub>1</sub> electrode (n =1-5) are compared with the calculated HOMO-LUMO gaps of the ground states of Au<sub>n</sub>Pd<sub>1</sub> clusters for n=1-5 (shown in blue). The ground state geometries are shown as icons.

### 7.5 Scan Rate and Concentration Effects

The effect of scan rate on CVs recorded on Pt/PANIAu<sub>3</sub>Pd<sub>1</sub> and of alcohol concentration on CVs recorded on Pt/PANI-Au<sub>4</sub>Pd<sub>1</sub> is shown in Figures 7.5 and 7.6,

respectively. For both alcohols, the oxidation peak currents are increasing in the forward scan direction with increasing scan rate. The dependence of the oxidation peak current of the alcohols versus the square root of scan rate ( $v^{1/2}$ ) is plotted in the insets of Figure 7.5. For MeOH, the peak current increases linearly with  $v^{1/2}$  up to the scan rate of 10mV/s which may suggest that the oxidation up to that point is diffusion controlled. Above 10mV/s the oxidation appears to revert to surface-confined species. No such dependence is observed for EtOH indicating different oxidation mechanism and a greater role of adsorption. There is virtually no change in the reduction peak potential  $\sim -0.3$  V, even at high scan rate (500mV/s) suggesting a fast electron-transfer process.

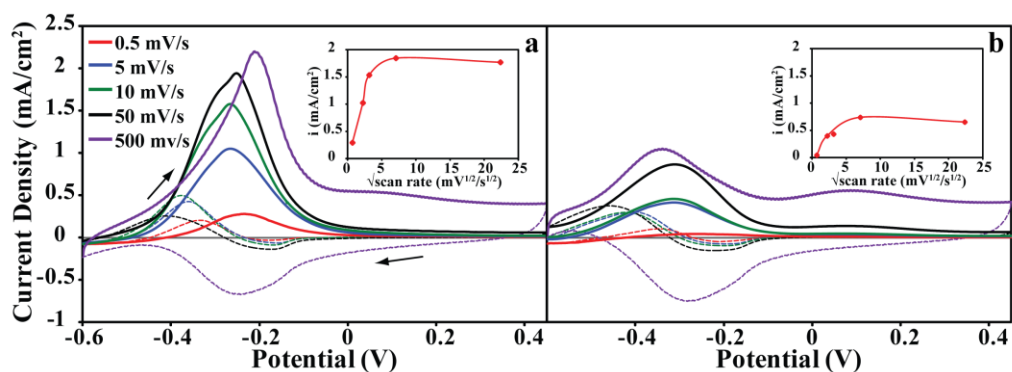


**Figure 7.5.** Scan rate dependence of cyclic voltammograms recorded in (a) 0.5M MeOH and (b) 0.5M EtOH in 1.0M KOH solution on Pt/PANI-Au<sub>3</sub>Pd<sub>1</sub> electrode. The inset shows the current density as a function of the square root of scan rate.

Increasing concentration of the alcohols causes linear increase of  $i_p$  for MeOH, again indicating diffusion control (Figure 7.6a), while adsorption appears to play a more important role in oxidation of EtOH (Figure 7.6b). It can be seen, that increasing alcohol concentrations does not affect the position of peak potentials. This difference in the

behavior of  $i_p$  indicates different mechanisms during oxidation of MeOH and EtOH at Pt/PANI-Au<sub>4</sub>Pd<sub>1</sub> electrode respectively.

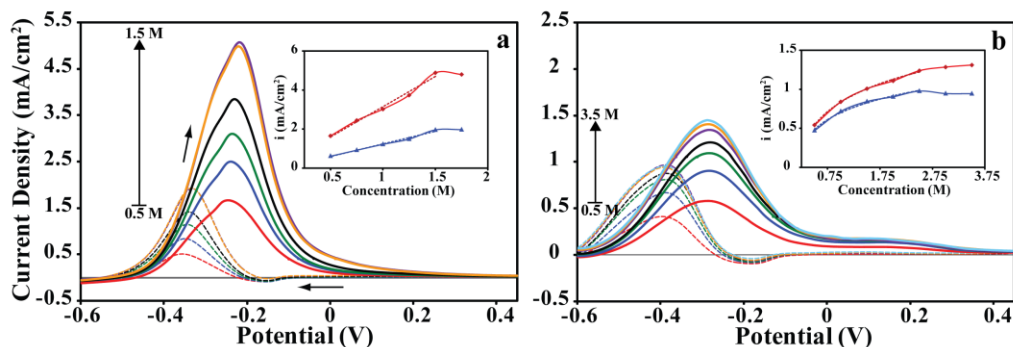


**Figure 7.6.** Concentration dependence of cyclic voltammograms recorded on Pt/PANI-Au<sub>4</sub>Pd<sub>1</sub> in 1.0 M KOH solution with increasing concentrations of (a) MeOH from 0.5M to 1.75M in sequential additions of 0.25M, and of (b) EtOH from 0.5M to 3.5M in sequential additions of 0.5M. The CVs were recorded with a scan rate of 10 mV/s. The insets show the current density of the forward oxidation peaks as a function of the alcohol concentration.

## **CHAPTER 8**

### **Future Work**

#### **8.1 Different Metals**

We have shown that the deposition cycle works for depositing atomic gold clusters in PANI. We have also demonstrated that this same cycle can be used to deposit atomic clusters of a metal other than gold using palladium as an example. An obvious path for future work is to use this cycle to deposit atomic clusters of other metals as well. Other metals that may be used include platinum, iridium, or rhodium. These metals also have affinity for PANI when they are in anionic form with a halide. Silver has also been incorporated into PANI. One important aspect of depositing atomic gold clusters into PANI is the economic impact by using less of this precious metal. Another choice would be to move away from noble or expensive metals and try some cheaper transition metals such as nickel, iron, titanium, or chromium. The cycle would need to have the holding potentials modified for the different metals of interest to avoid spontaneous reduction of the metal to atomic metal while still keeping PANI in its fully oxidized state.

Once the deposition of one of these metals has been achieved, then bimetallic or trimetallic clusters can be deposited. The number of potential catalysts and new materials would be greatly increased by all the different possible combinations of bimetallic or trimetallic atomic clusters.

#### **8.2 Different Deposition Sequences**

As discussed previously, the catalytic activity of the bimetallic  $\text{Au}_2\text{Pd}_1$  clusters depend on their orientation with respect to PANI. In other words, the activity depends on which atoms in the cluster are accessible for the alcohol and which atoms are interacting with the PANI. However, this may get complicated when describing a cluster where there are multiple atoms of each metal. Lowest energy structures for  $\text{Au}_N\text{Pd}_M$  have been calculated and several structures have the same geometry but the location of the atoms is different. Where an atom resides in the cluster orientation may depend on the deposition sequence. To test this experimentally, larger bimetallic clusters should be deposited using several different sequences. In the case of  $\text{Au}_N\text{Pd}_M$  clusters, the Au can be deposited before the Pd. Next, the Pd should be deposited first. Finally, each metal should be deposited in alternating cycles, one or two cycles per metal at a time. Then the catalytic activity can be analyzed to see if it changing. If there is no change, then the orientation is fixed. The deposited atoms will migrate to the lowest energy configuration and the sequence of deposition will not influence it. However, if the activity does change, then the sequence of deposition does influence the configuration of the atoms in the cluster. If this happens, the number of possible combinations of new materials will increase.

### **8.3 Catalytic Activity for Additional Reactions**

Here, we have focused the catalysis aspect of the materials on the oxidation of alcohols. One issue with trying to describe the mechanism by which this occurs is the identification of the intermediates and end products for peak I and peak II was not

performed. Future work should include the identification of these in order to have a more accurate description of the mechanism by which the oxidation occurs.

There are many other reactions that these composite films may be able to catalyze. Gold has been shown to catalyze reactions for: oxidation of carbon monoxide to carbon dioxide, oxidation of alkenes, water gas shift reaction, reduction of nitric oxide by hydrogen, addition of hydrogen chloride to ethyne, and many others<sup>111</sup>. There are many reactions that could be tested with these atomic gold polyaniline composite films that they can not all be named here. Some of these reactions should be explored using these composite materials.

Palladium has been used as a catalyst in coupling reactions such as the Heck reaction between an alkene and an aryl halide and the Suzuki reaction between an aryl halide and a boronic acid. Nickel has also been shown to catalyze coupling reactions of alkenes<sup>112,113</sup>. There are a high number of possible reactions that could benefit from these composite materials.

#### **8.4 Carbon Substrate and Scaling Up**

In order for these materials to have an impact in the scientific industry, the process would have to be scaled up in order to produce compounds on a large scale. A large electrode of considerable size would be necessary for some processes, but a large platinum electrode is not economically feasible due to the cost. Depositing PANI on a large carbon electrode would be much cheaper. Experiments would need to be performed at the bench level using carbon as a substrate to determine if the

catalytic activities will be maintained using a different substrate. This is important since the substrate does influence the catalytic activities of many catalysts.

In the event that a carbon substrate will be insufficient, an alternative method could be considered. In this method, the PANI will be in a powder form contained in a column. At this point, the same atomic metal deposition cycles could be performed. PANI will still be the substrate for metal deposition; however, the PANI itself will not have a substrate. Experiments would be performed on the bench level to confirm that this could work, and then the scale up of this method would be fairly easy.

## APPENDIX A

### POLYANILINE-SUPPORTED ATOMIC GOLD ELECTRODES: COMPARISON WITH MACRO ELECTRODES

#### A.1 Introduction

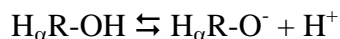
Interest in the electrocatalytic oxidation of alcohols has increased greatly due to their potential application in fuel cells<sup>36,114,115</sup>. This oxidation can be catalyzed by a variety of metals, two of the most active being platinum and gold<sup>32,35,36,116-118</sup>. These metals can either be used in polycrystalline form or as large, polydispersed cluster aggregates containing millions of metal atoms. The aim of this paper is to compare electrochemical behavior of polycrystalline gold electrodes, polycrystalline platinum electrodes, and Pt electrodes coated with polyaniline containing defined atomic Au particles (Pt/PANI/Au<sub>N</sub> with N = 2-7). The electrochemistry of electrodes with N=1 was indistinguishable from that of N=0.

Polyaniline polymerized from an acidic medium have been used as a support matrix for the insertion of metal clusters<sup>23,119</sup>. It is a stable conjugated polymer, which is unique due to its ionic and electronic conductivity<sup>120,121</sup>. Electropolymerization of aniline is done typically in acidic medium and results in the protonated emeraldine (semiquinone) form of PANI. The protonated imine functionality of the PANI has a strong affinity for certain complexed metal anions. In this paper we utilized the strong complexation of AuCl<sub>4</sub><sup>-</sup> for step-wise insertion of Au clusters into the PANI matrix<sup>122</sup>. This redox-driven process can occur spontaneously, just by dipping the platinum coated

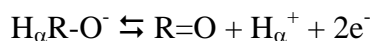
polyaniline (Pt/PANI) electrode into the solution containing  $\text{AuCl}_4^-$ , resulting in polydispersed gold clusters, imbedded in the PANI matrix. In this reaction, PANI in its emeraldine form acts as a reducing agent, which reduces  $\text{AuCl}_4^-$  to metallic gold clusters of various sizes. Only a limited control over the size of the inserted Au particles can be achieved by selection of experimental conditions during this “top down” deposition<sup>26</sup>. On the other hand, in the precisely controlled “bottom-up” deposition process metal is inserted in a step-wise atom-by-atom, defined deposition cycles<sup>84</sup>.

The size control is aided by the stoichiometry of the PANI\* $\text{AuCl}_4^-$  complex formation, while the spontaneous reduction is suppressed by precise and synchronized potential control. The result is a PANI matrix containing  $\text{Au}_N$  clusters with  $N=0$  and 2-7. The electrochemical behavior of the electrodes followed the predicted odd/even pattern of the fluctuation of the HOMO/LUMO gap energy<sup>41,42</sup>.

Electrochemical oxidation of n-propanol (n-PrOH) and of isopropanol (i-PrOH) in 1 M KOH has been used as the probing reactions in order to demonstrate the electrochemical efficiency of various forms of gold. The details of the alcohol oxidation, identification of the oxidation products, the effect of carbonate and the effect of the kind and concentration of hydroxide have not been investigated. All experiments were done in the presence of oxygen, unless stated otherwise. In order to aid visual comparison between different kinds of electrodes the concentration of propanol in 1 M KOH solution was kept constant at 0.5M. Due to the fact that adsorption of organic molecules onto platinum is often irreversible while adsorption onto gold is reversible, the catalytic poisoning effects seen for Pt are not seen for gold<sup>35</sup>. For electrocatalytic oxidation of alcohols on gold, the rate determining step is the cleavage of the C- $\text{H}_\alpha$  bond<sup>36</sup>.



The deprotonation of the alcohol occurs at high pH, and it is dependent on the  $\text{pK}_a$  of the alcohol. Once deprotonated, the reactivity of the alkoxide intermediate,  $\text{H}_\alpha\text{R-O}^-$ , depends on the state of the electrode material being able to abstract the  $\text{H}_\alpha$ . For primary alcohol (e.g. n-PrOH) the alkoxide is more active towards the electrochemical oxidation leading to propionic aldehyde, which can be further oxidized, while for the secondary alcohols (e.g. i-PrOH) the final product is the corresponding ketone (e.g. acetone).



Aldehydes are unstable in alkaline solutions, and in the presence of oxygen decompose to variety of products or react quickly with other acceptors<sup>123</sup>.

The main objective of this work was to contrast the electrochemical behavior of polyaniline supported atomic gold electrodes with that of the bulk Au electrode. Besides the odd/even pattern reported earlier<sup>84</sup>, there are unique aspects of atomic gold electrodes (AGE) that are highlighted by differences in oxidation of n-PrOH and i-PrOH, respectively.

## A.2 Experimental

A standard three-electrode cell and CHI 660 potentiostat (CH Instrument, Inc) were used in all electrochemical experiments. As working electrodes (WE), platinum or gold disk electrodes, both with diameter of 1.2mm ( $A = 1.13 \times 10^{-3} \text{cm}^2$ ) from Bioanalytical Systems (BAS) were used. For preparation of the atomic gold electrodes (AGE) platinum electrodes deposited on quartz crystals ( $A = 0.236 \text{cm}^2$ ) obtained from International Crystals were used. The procedure for the preparation of the defined atomic gold

aggregates in polyaniline films deposited on platinum crystals Pt/PANI/Au<sub>(N= 2 to 7)</sub> was described previously<sup>84</sup>.

The counter electrode (CE) was platinum foil. The reference electrode (REF) was Ag/AgCl in 1M KCl//1M KNO<sub>3</sub>. The double-junction in the reference electrode was used in order to prevent contamination of 1M KOH solution with chloride ion. All potentials reported in this study are referred to this electrode (E= +236 mV versus SHE). The cyclic voltammograms (CVs) were recorded with a scan rate of 50 mV/s, unless stated otherwise. Prior their use, platinum and gold (BAS) electrodes were polished with Buehler micropolish II Al<sub>2</sub>O<sub>3</sub> 0.05 microns and sonicated in water for 6 minutes. If mechanical polishing was not adequate, the electrodes were polished electrochemically in 1M H<sub>2</sub>SO<sub>4</sub> by taking 10 CVs with a scan rate of 1 V/s followed by taking 6 CVs with a scan rate of 0.05 V/s. The CVs were always initiated from open cell potential and recorded within the potential range from -0.7 V to 0.55 V for the BAS electrodes and -0.6 V to 0.45 V for the Pt electrode deposited on quartz crystal. The following compounds, all ACS grade, were used during experimentation: HBF<sub>4</sub> (48%) from Alfa Aesar, aniline (99.5%) and n-propanol from Sigma Aldrich, KOH from EMD, isopropanol from J.T. Baker.

### A.3 Results

The polyaniline matrix is a necessary component of the AGE electrodes. In 1 M KOH solution Pt electrode coated with PANI has its own electrochemical background signature that resembles the CV of the Pt-bulk electrode (Figure A.1). In that figure are shown also representative examples of CVs corresponding to gold oxide formation and reduction for

even number of gold (PANI/Au<sub>4</sub>) and odd number of gold (PANI/Au<sub>5</sub>) in PANI. The reduction of gold oxide in PANI is taking place in the range from -180 to -260 mV. Peak potentials corresponding to the reduction of gold oxide at AGEs correspond to that of the bulk gold electrode<sup>124</sup>. The hints of step-wise Au oxidation are seen only for the AGEs containing odd-number of Au atoms.

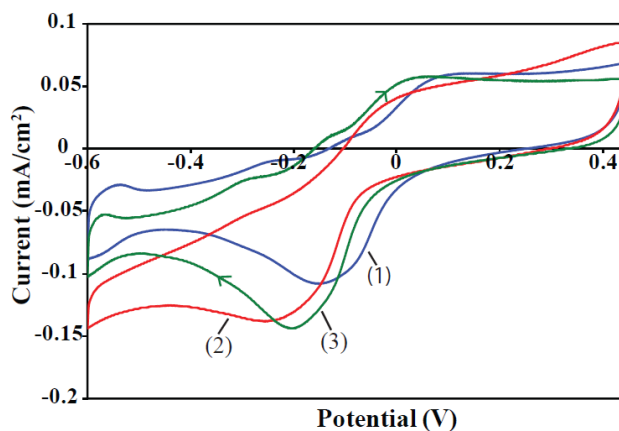


**Figure A.1.** Steady-state cyclic voltammograms for (1) Pt/PANI, (2) Pt/PANI/Au<sub>4</sub> and (3) Pt/PANI/Au<sub>5</sub> .

Oxidation of n-PrOH and i-PrOH in 1M KOH on solid polycrystalline Au electrode is used as the benchmark. Since voltammograms for both alcohols contain the same features we show only the CVs for n-PrOH (Figure A.2). Its oxidation potential peak at +0.240 V belongs to oxidation of chemisorbed alkoxide on the Au surface covered with adsorbed OH<sup>-</sup> ions. Formation of gold oxide at potentials more positive progressively blocks this reaction. The peak oxidation current is increasing with the increasing number of cycles until it reaches a stable state<sup>125</sup>. This feature will be discussed in greater detail later. On the reverse sweep a new oxidation peak at +0.08V appears that is attributed to the removal of the blocking species produced in the forward

scan <sup>63</sup>. Note the progressive increase of both peaks upon cycling, highlighted by the upward pointing arrow.

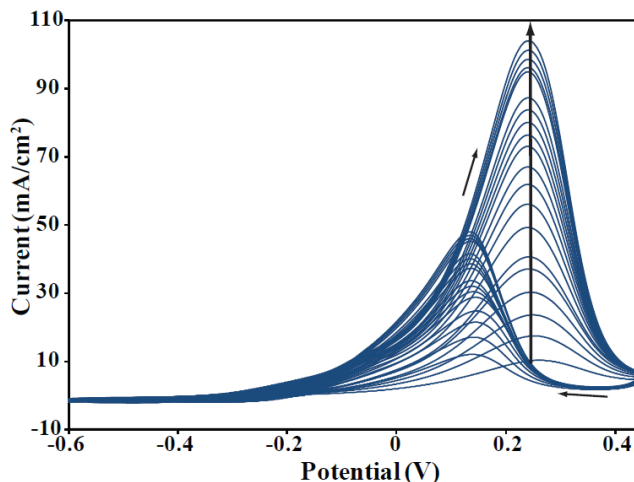


**Figure A.2.** Oxidation of 0.5 M n-PrOH, in 1 M KOH recorded at polycrystalline Au electrode (BAS). Note the progressive increase of the magnitude of the peak currents, indicated by the vertical arrows.

Oxidation of both propanols on AGEs is surveyed in Figure A.3. The first peak (I) located between -0.1V and -0.2V coincides with the oxidation of propanol on Pt electrode coated with polyaniline (Pt/PANI/Au<sub>N=0</sub>), as shown in the inserts to Figure A.3. It is necessary to point out, that while there is only a limited oxidation of propanol on bare Pt electrode, PANI coating makes it possible. When oxidation of n-PrOH is taking place at Pt/PANI/Au<sub>N=0</sub>, oxidation peaks at -0.09V in a forward scan, and at -0.30V on the reverse scan, are seen. In contrast, for i-PrOH only oxidation peak in the forward scan, at -0.13V, is seen. Furthermore, for both alcohols the magnitude of this oxidation peak current at the forward scan remains the same, and it is accompanied by a reduction peak at approx. -0.13V.

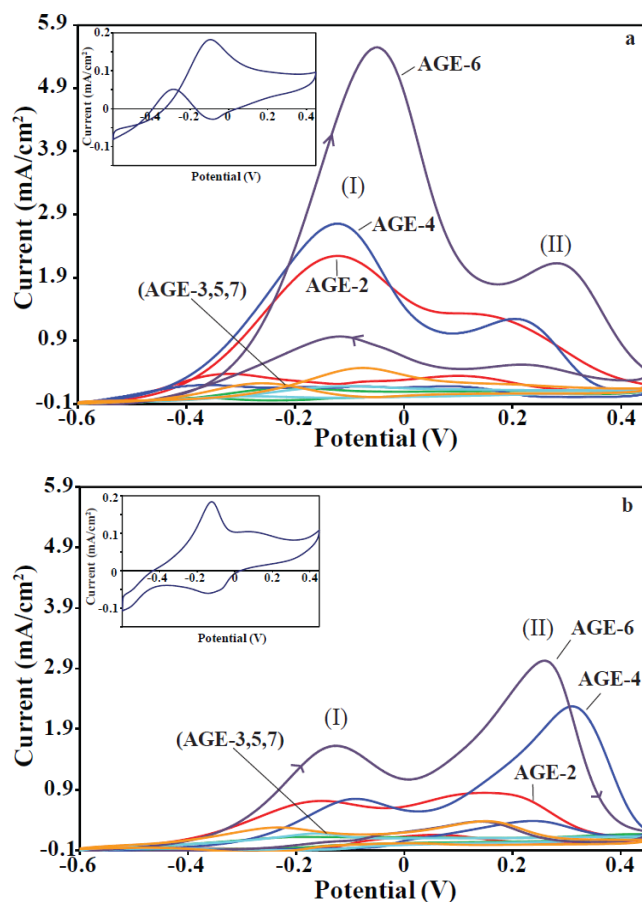


**Figure A.3.** Survey of the steady-state CVs for oxidation of (a) n-PrOH and (b) i-PrOH for Pt/PANI/Au<sub>N</sub> (2 < N < 7) electrodes. The inserts in both panels correspond to N = 0. The inserts are shown at 100x greater magnification in order to more clearly display their features. The numbering of the individual CVs corresponds to the number of inserted Au atoms. Cyclic voltammograms for odd-numbered Au atoms are shown as a (3,5,7) group.

Significant differences between voltammograms recorded for PANI/Au<sub>(N=2 to 7)</sub> in Figure A.3a for oxidation of n-PrOH and Figure A.3b for oxidation of i-PrOH, are evident. The magnitude of the peak (I) current is significantly smaller for i-PrOH when compared to n-PrOH for the same Au<sub>N</sub>. The opposite applies to the peak (II) that is located between 0.2 V and 0.4 V. The magnitude of both peaks somewhat increases in the

presence of oxygen, but it is not completely eliminated by the deaeration of the sample. In other words, while the mediated oxidation by  $\text{OH}^\cdot$  appears to be responsible for peak I, that species is not generated exclusively by the reduction of oxygen. The absence of that peak at solid gold electrode (Figure A.2) is a strong indication that Pt must be present for the peak I (at  $-0.2\text{V}$ ) to appear. The peak II (at  $+0.2\text{V}$ ) is due to the direct oxidation of propanols on Au particles and shows the strong odd/even effect.

In order to obtain more information about the influence of the gold atomic size and its arrangement the results have been summarized and compared to the solid gold electrode. There are several remarkable differences in these voltammograms (Figure A.3); First, there are two oxidation peaks seen on the forward scan and two oxidation peaks on the reverse scan. They are best identified on CV for AGE-6. Second, the position of the oxidation peaks (I) and (II) does depend on the N-number of Au atomic agglomerates in the PANI. The corresponding peaks are clearly separated, by as much as 320 mV for  $\text{Au}_2$ ,  $\text{Au}_4$  and  $\text{Au}_6$ . Third, the dominating "odd/even" activity pattern as reported previously<sup>84</sup> is clearly visible.

Peak current  $i_p$  for oxidation of n-PrOH at Au bulk electrodes has shown linear dependence on the square root of the scan rate,  $v^{1/2}$ , up to  $100 \text{ mVs}^{-1}$ , but at the higher scan rates the  $i_p$  decreased<sup>34</sup>. That behavior has been attributed to the slow, irreversible charge transfer coupled with adsorption. A similar scan rate behavior has been found at AGEs, but with some differences depending on the N-number of gold atoms. The representative plots of  $i_p$  vs  $v^{1/2}$  show linear behavior for the oxidation of n-PrOH at PANI/ $\text{Au}_6$ , with the slope for Peak I being 3.8 times higher than for Peak II. On the other hand the scan rate dependence for oxidation of i-PrOH at PANI/ $\text{Au}_6$  is non-linear for both

peaks, and has approximately the same non-linear trend for the peak I and peak II (Figure A.4). At PANI/Au<sub>5</sub> electrodes (not shown) the peak currents are approximately 20x lower, due to the odd/even effect, but are linear for both alcohols. That could be explained by much lower rate of electron transfer relative to the mass transport and relative to the rate of desorption of the product. The icons representing the calculated highest binding energy (i.e. highest stability) shapes for Au<sub>6</sub> isomers are included<sup>41,42</sup>.

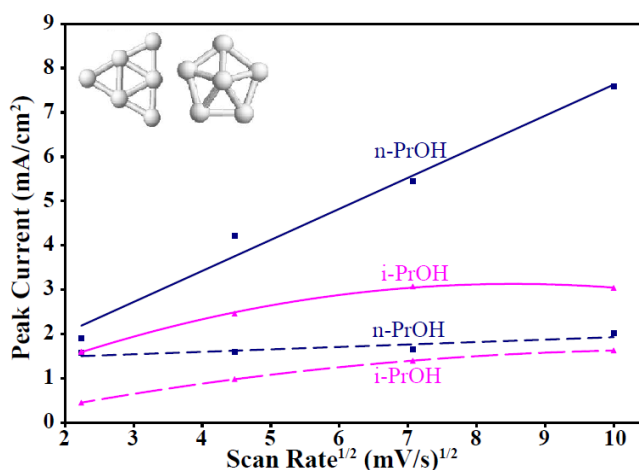


**Figure A.4.** Dependence of peak current on square root of scan rate for Pt/PANI/Au<sub>6</sub> for both alcohols. The range of examined scan rates is 5 to 100 mV s<sup>-1</sup>. The solid lines correspond to peak I, and the dashed lines to peak II. The icons show the calculated highest probability of the shape of the Au<sub>6</sub> clusters.

The change of activity of polycrystalline Au electrode upon oxidation of propanol in 1M KOH is shown in Figure A.5. In that experiment the cycling was interrupted after approximately first 20 cycles (Figure A.5a, point A). After thorough rinsing, the electrode was stored in D.I. water for 10 minutes and the cycling in propanol resumed. Both peaks grew again (Figure A.5b, point B to point C), but both reached a slightly lower steady state. After another 10 min interruption and storage in D.I. water the third set was

recorded (Figure A.5c). The peaks grew again from point D to E, but ended in a lower steady state yet.

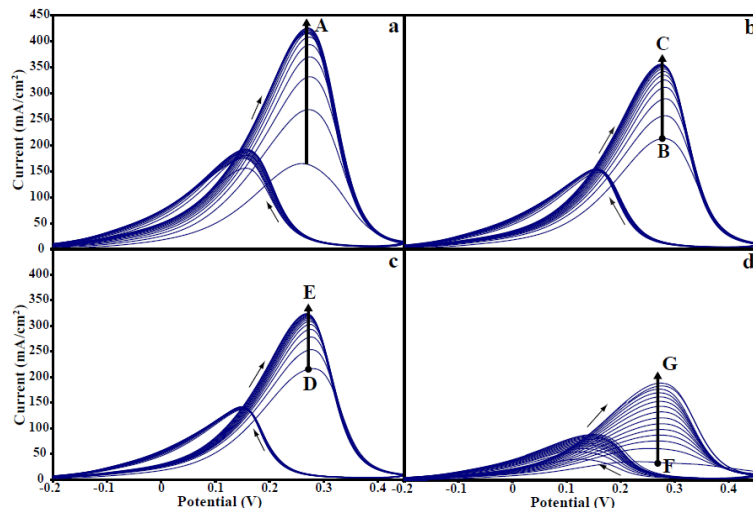


**Figure A.5.** The activation pattern of polycrystalline Au electrode (BAS). The arrows again indicate the changes from scan 1 to 20.

After that the electrode was cycled in 2.5 mM Ru(II)/(III) hexamine in 1M KNO<sub>3</sub>. Cycling of the electrode in this redox couple showed a “normal” cyclic behavior, i.e. steady decrease within the first five cycles until reaching steady state due to formation of depletion layer<sup>126</sup>. Immediately after the Ruhex treatment the same Au electrode resumed the “activation” behavior in oxidation of propanol (Figure A.5d, points F to G). The possible explanation of this behavior is as follows. The oxidation of propanol at Au electrodes in alkaline medium proceeds through the formation of OH<sup>•</sup> radical as an intermediate<sup>34</sup>. It is possible that this species activates the electrode by increasing the number of active sites. That mechanism would be the opposite what has been described in great detail in series of papers, for “deactivation” of Au electrodes with OH<sup>•</sup> generated by the Fenton reagent in mildly acidic medium<sup>127</sup>. In that case the OH<sup>•</sup> radicals

effectively “polished” the Au electrode, removing asperities that apparently serve as the active centers for electron transfer involving radical formation. Likewise, after the “polishing” the redox behavior of Ru(II)/Ru(III) couple was not affected.

The final steady-state scans of CV curves for AGEs (N = 2-7) during propanol oxidation are shown in Figure A.6. The arrows again indicate the increase/decrease of the peak currents. It increases in n-PrOH for both peaks from the 1st to the 20<sup>th</sup> scan for the even-AGEs while it decreases for the odd-AGEs. The exception is the slight increase for both peaks observed for AGE-7 in i-PrOH (not shown). Note also, that the position of the peak again does not change, indicating that the increased value of the peak current reflects only the change in the number of active sites at which the oxidation takes place and not in the change of the electrode kinetics. Thus, the behavior of AGE electrodes seems to follow either the activation or the deactivation path, depending on the odd/even number of gold atoms.

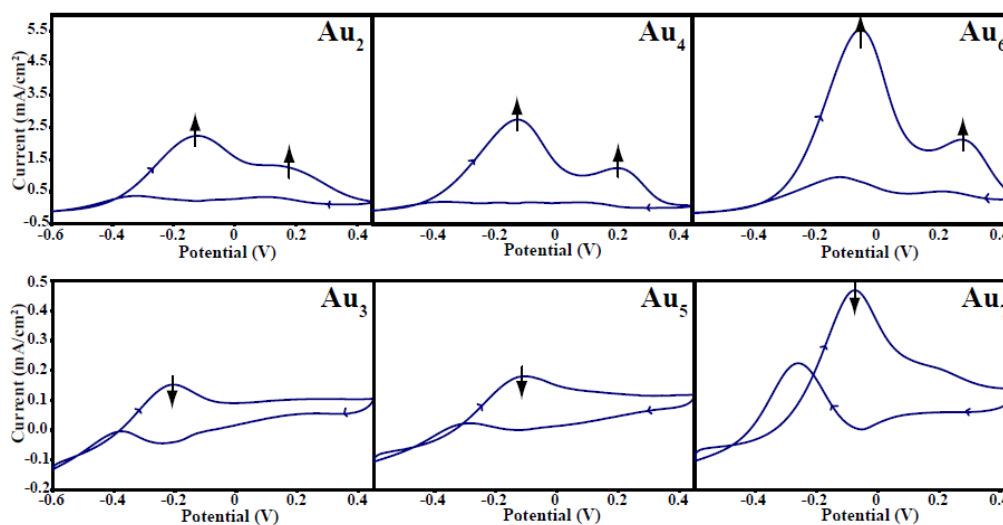


**Figure A.6.** The survey presentation of the activation pattern for the AGEs ( $2 < N < 7$ ) for n-PrOH. Only the final CV's are shown and the arrows again indicate the up/down change. The current scales are greater for the even-AGEs in order to facilitate the visual inspection.

This behavior is illustrated in greater detail on AGE-4 and AGE-5 respectively, which represents the entire even/odd series. The rate of oxidation of both propanols at AGE-4 increases (Figure A.7a,b) while at the AGE-5 it decreases (Figure A.7c,d). There is also a remarkable difference in the behavior of AGE-5 with respect to n-PrOH and i-PrOH.

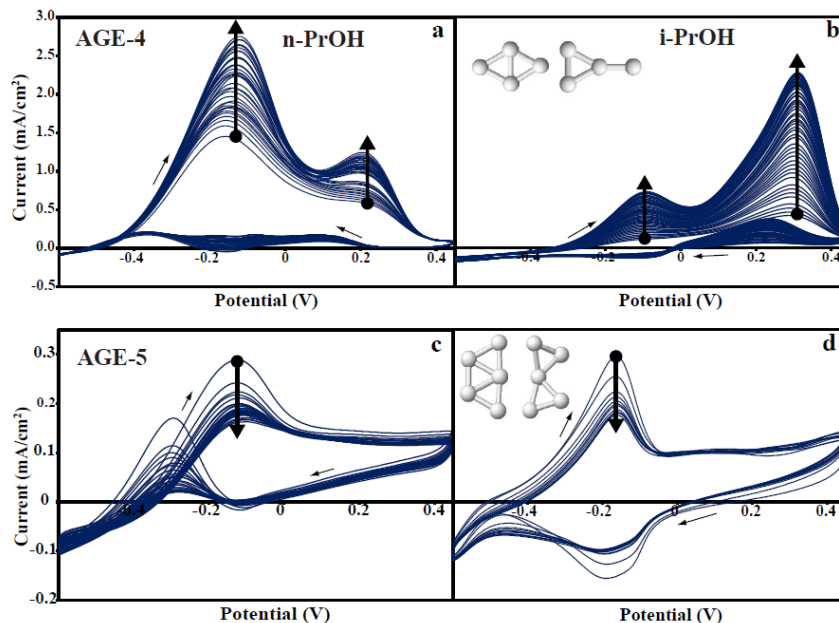


**Figure A.7.** Comparison of the activation pattern for (rows) Pt/PANI/Au<sub>4</sub> and Pt/PANI/Au<sub>5</sub> and for n-PrOH and i-PrOH (columns)

Although the absolute values of the current (for peak at -100 mV) are again approximately 20x higher for AGE-4 than for AGE-5 there is a finite oxidation current at the switching potential (+450 mV) (Figure A.7c,d), indicating that for the odd-AGEs there is only a minimal blockage of the electrode at the end of the positive scan. The icons representing the theoretically calculated shapes of the corresponding atomic clusters are included in the individual panels of Figure A.7. Contrary to the reported deactivation of polycrystalline Au in acidic medium<sup>127</sup> the exposure of the AGEs to the Fenton reagent always increased the peak current of AGEs. At the dimensions involved in AGEs it is hard to argue about "annealing of asperities" being responsible for the "activation" behavior. The observed differences between the odd and even numbered AGEs suggest that the "activation/deactivation" phenomenon is related to the prevailing electronic structure of the active sites.

Polycrystalline gold is usually regarded as an “inert” electrode. Experiments described here and confirmed by others indicate that it is anything but “inert”. The atomic gold electrodes described in here are truly 3-dimensional electrodes in which the Pt substrate, the PANI isolation matrix and the inserted atomic gold all play an important role. When prepared in atomic format the AGEs retain most features of bulk gold electrochemistry, but add some significant differences which are related to the odd/even quantum effects predicted for atomic clusters of metals<sup>41,42</sup>.

There is a catalytic effect for oxidation at both odd and even numbered atomic agglomerates of gold that is predicated on the presence of Pt substrate. It is significantly higher for the even-numbered agglomerates. It indicates that PANI in alkaline medium is non-conducting and porous and that a part of electrochemistry takes place at the Pt surface. It is apparently due to the oxygen reduction and generation of the OH<sup>-</sup> radical. The formed OH<sup>-</sup> is possibly stabilized by PANI and the ensuing oxidation takes place at atomic gold according to its odd/even pattern. Under these conditions it is necessary to compare the current efficiency on the basis of active Au atoms, rather than on the usual scale of the geometric area of the electrode. In order to have a rational comparison of performance of AGE with macroscopic polycrystalline gold electrodes we have arbitrarily chosen 10 micrometers as the convenient minimum thickness of a thin Au electrode prepared by e.g. evaporation, and calculated the number of Au atoms in such an electrode. The estimated amount of Au in AGE of the comparable area and at comparable current efficiency is approximately three orders of magnitude lower than for a polycrystalline gold electrode. Besides the major improvement of economy, AGEs offer

also possibility of enhanced catalytic selectivity due to the shape-related, quantized odd/even effect.

# **APPENDIX B**

## **GEL HYBRID MATERIAL AS THE SENSING GATE OF A CHEMFET**

### **B.1 Introduction**

When gaseous analyte molecules are interacting with the gate material of a Chemically Sensitive Field-effect Transistor (CHEMFET) sensor, they dissolve and transfer partial electronic charge to/from the gate material. Formation of a charge-transfer complex with the sensing layer results in the work function (WF) change of the gate material that is measured as the change of the threshold voltage,  $V_{th}$ <sup>128</sup>.

Organic semiconductors (OS) are ideal as gate materials for this transduction mechanism<sup>82</sup>. They have not only the ability to transduce chemical signal into an electrical one, but also allow control of film morphology, initial work function, conductivity, and solubility properties of the sensing layer. This provides versatility for modification of the sensing matrix that can influence the magnitude and quality of the measured signal.

The aim of this work is to investigate gel-hybrid materials, prepared by blending polyaniline doped with camphorsulphonic acid (PANI-CSA) with room temperature ionic liquid (IL), for their influence on the pathway for gas analyte to the semiconductor/insulator interface of the CHEMFET. The goal of these processed gel-hybrid sensing layers is to shorten the gas sensor response time, to widen the dynamic response range, and to lower the detection limit of the gas or vapor analyte.

Polyaniline film doped with non-volatile camphorsulfonic acid (CSA) in a mole ratio

of 1:2 (CSA/aniline units) has been already used by us for monitoring diagnostic capability of CHEMFET array for filter system<sup>129</sup>. The CHEMFET ammonia gas sensor was responding reversibly and reproducibly to ammonia concentrations in the range from 64 ppm to 2100 ppm, but the response time was in the order of minutes<sup>130</sup>. Based on that observation it has been realized that in order to improve the response time of the CHEMFET, the sensing material must contain solvent that does not evaporate after casting and may even have the ability to dissolve gaseous analytes.

In view of this approach, room temperature ionic liquids (ILs) became of particular interest to us. They are liquid salts at or near room temperature and have attractive properties such as negligible vapor pressure, large liquidus range, high thermal stability, high ionic conductivity, and the ability to solvate compounds of widely varying polarity<sup>131</sup>. They have been already used to make gel-like materials from dispersions of single-wall carbon nanotubes<sup>132</sup>. Those gels resulted in uniform dispersion and strong interactions between the IL and the added material. In this study, 1-butyl-3-methylimidazolium bis(trifluoromethanesulfonyl)amide ([BMIM][Tf<sub>2</sub>N]), tetrahexylammonium bis(trifluoromethanesulfonyl)amide ([THA][Tf<sub>2</sub>N]), and 2-hydroxyethylammonium formate ([HEA][Fm]) have been added to the PANI-CSA casting solution, respectively. The properties of the selected ILs differ from each other, based on the size of the cation, hydrophobicity and solubility of ammonia. The properties of polyaniline gel-hybrid material were characterized as the gate material of CHEMFET and as the sensing layer during exposure to ammonia gas in the range of 15-120 ppm.

## B.2 Experimental

Two stock solutions were used in the preparation of PANI/IL hybrid-gel sensing layer. For the PANI-CSA stock solution, pre-purified polyaniline emeraldine base powder and camphorsulfonic acid, CSA (-) were dissolved in the formic acid, in mole ratio of two CSA molecules per four benzene units of the repeating segments in the PANI chain. The stock solutions of ILs were prepared in formic acid with 0.13, 0.26 and 0.39 wt% of [HEA][Fm], with 0.5, 1.0 and 1.5 wt% of [BMIM][Tf<sub>2</sub>N] and with 0.75, 1.50 and 2.25 wt% of [THA][Tf<sub>2</sub>N]. All IL's were synthesized by using published procedures for [BMIM][Tf<sub>2</sub>N]<sup>133</sup>, [THA][Tf<sub>2</sub>N]<sup>134</sup>, and [HEA][Fm]<sup>135</sup>. Each of the nine stock IL solutions was mixed with the PANI-CSA stock solution in a 1:1 ratio (by volume). The resulting mole fractions,  $\chi$ , of IL in the PANI-CSA casting solutions was calculated to be,  $\chi_{IL} = \chi_{IL} / (\chi_{IL} + \chi_{PANI}) = 0.51, 0.68, \text{ and } 0.76$ , respectively. These solutions were drop cast into the well surrounding the gate contacts of a CHEMFET. The thickness of the sensing layers was measured using a Dektak3ST surface profiler at a speed of 60 $\mu\text{m/s}$  and a stylus weight of 5 mg. For these measurements, each of the mixture was cast into the CHEMFET well four times and was then divided by four to give the final value of the thickness.

The CHEMFET array consists of eight parallel IGFETs with defined wells in the gate area<sup>136</sup>. The GTO3 CHEMFET chip was fabricated at the MIRC at Georgia Institute of Technology. After the chip was mounted and wire bonded to 28-pin dual-in-line ceramic header the gel-hybrid gate material was cast over two gold gate contacts separated by 40  $\mu\text{m}$ .

Before the exposure to the tested gas, for each of the eight CHEMFETs,  $I_D - V_D$  and  $I_D - V_G$  characteristics were recorded using Hewlett Packard 4155A semiconductor

parameter analyzer. From these measurements the threshold voltage,  $V_{th}$ , was determined. The CHEMFET response to test gas was measured in the source-follower configuration.

Before testing the response of the CHEMFETs to ammonia gas, the devices were conditioned in a glass chamber filled with 5 % ammonia gas for 1 hour followed by evacuation at  $10^{-2}$  to  $10^{-3}$  mbar. The testing of the sensor response was done in a flow-through arrangement using gas-dilution system Environics Model S 4000 (Environics). The  $NH_3$  (Airgas, 0.05%), was delivered to the CHEMFET in a controlled, stepwise repeating sequence between 15-120 ppm using air (zero air, Airgas) as the carrier gas at flow rate of  $50 \text{ cm}^3/\text{min}$ . The delivery of ammonia to the CHEMFETs was enhanced by the use of a synthetic jet actuator that was integrated with the CHEMFET to induce small-scale mixing at the surface of the sensor<sup>130</sup>.

### **B.3 Results and Discussion**

The response of the CHEMFET is due solely to the change of the WF of the cast sensing gate material. For the proper CHEMFET operation, it is required that the gate is ohmic, meaning that at least some fraction of the conductivity is electronic. That means that the interface between gold gate contacts and RTILs must be non-polarized<sup>137</sup>. Effect of the WF of the cast material on the transistor characteristics is shown in Figure B.1.

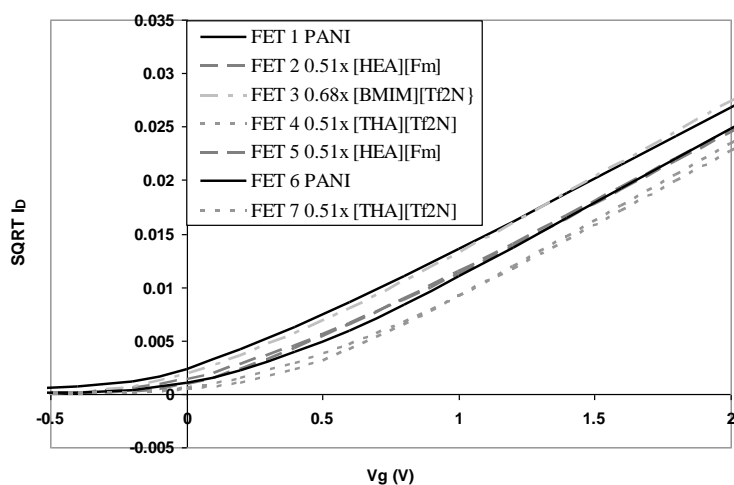


**Figure B.1.** Comparison of  $I_D$ - $V_g$  curves recorded for CHEMFET's with cast PANI-CSA and PANI-CSA/IL gel-hybrid gate material, respectively.

It is seen that there is not a significant difference between the mixed ionic and electronic conductors of PANI-CSA with or without the IL present in the layer. All  $I_D - V_g$  curves have theoretical shape, indicating that the contact between gate metal lead and PANI-CSA is ohmic (i.e. electronic). There are significant changes in threshold voltage  $V_{th}$  of the CHEMFETs. The values of  $V_{th}$  determined from the  $\text{sqrt}(I_D)$ - $V_g$  curves for different amounts of ILs are shown in Table B.1.

**Table B.1.** Changes in  $V_{th}$  of CHEMFETs determined as a function of the added mole fraction of IL,  $\chi$ , relative to the PANI-CSA with no IL in the gate material.

$\chi$	$\Delta V_{th}$ (mV) for different ILs		
	[HEA][Fm]	[BMIM][Tf <sub>2</sub> N]	[THA][Tf <sub>2</sub> N]
0.51	-23.5	-62	-19.6
0.68	-2.6	107.1	-4.2
0.76	-26.6	99.2	-22.9

As expected, the WF of PANI-CSA gate with IL present is affected by the type of the IL: gate materials containing [BMIM][Tf<sub>2</sub>N] show a significant changes of the WF. However, layers cast from PANI-CSA solutions containing [HEA][Fm] or [THA][Tf<sub>2</sub>N] cause rather small, and similar  $\Delta V_{th}$  changes.

In order to explain the differences in the bulk properties of the various gel-hybrid materials, optical absorption spectra were recorded, Figure B.2. It is important to note that all films were cast with the same molar fraction of PANI-CSA in the formic acid solutions and that during the drying step of the drop-cast PANI-CSA film, the formic acid solvent evaporated. The spectrum (a) in Figure B.2 shows two absorption bands specific to emeraldine salt form of PANI: one with maximum around 3.5 eV, corresponding to the  $\pi$ - $\pi^*$  band gap transition, and the other one at 1.5 eV corresponding to the  $\pi_B$ - $\pi_Q$  transition. Some distinct differences are seen when spectra (b) (c) and (d) are compared with the spectrum (a).

**Table B.2.** Ratio of band transitions for different mole fractions ( $\chi$ ) of PANI·CSA/IL.

	Abs <sup>3.5eV</sup> / Abs <sup>1.5eV</sup> of PANI·CSA with IL		
$\chi$ of IL in PANI	[HEA][Fm]	[BMIM][Tf2N]	[THA][Tf2N]
0	0.80	0.80	0.80
0.51	0.73	1.11	0.95
0.68	0.98	1.12	0.87
0.76	0.96	0.79	0.90

The polaron transition at 1.5eV of PANI is shifting to lower energy with [BMIM][Tf2N] and to higher energy with [THA][Tf2N] present in the film matrix, but it does not affect the PANI matrix when [HEA][Fm] was added. The shift in position of the polaron band may signalize changes in the donacity of the OS imparted by the IL. Also with the increased added amount of IL to the PANI·CSA matrix formation of free volume is enhanced. That is essential for a conformational reorganization of the polymeric chains in the gel-hybrid material causing some modest absorbance changes in the region of band gap transitions at 3.5 eV. The ratio of the absorbance of the two bands transitions, 1.5 eV and 3.5 eV, is presented in Table B.2. It is speculated at this point that these changes represent changes in conformational reorganization of the polymer chains.

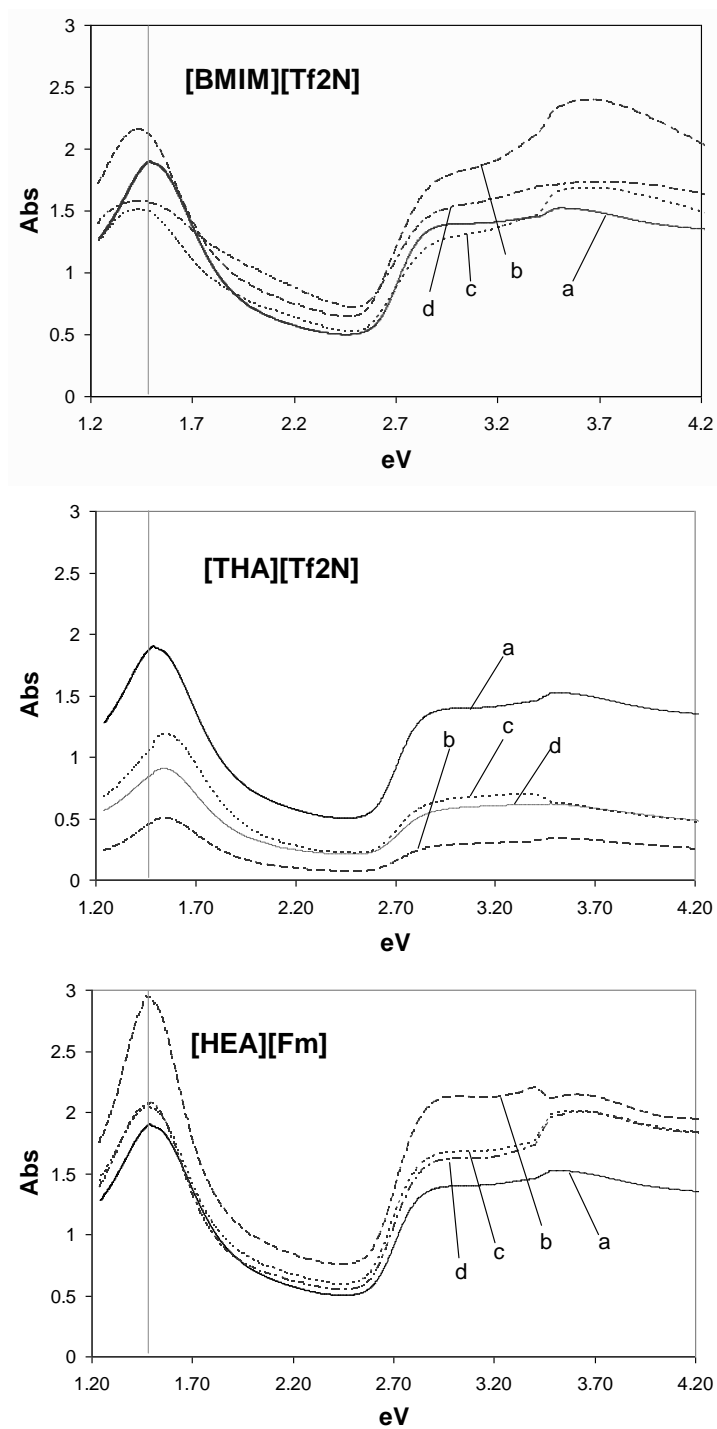


**Figure B.2.** Comparison between electronic properties of PANI-CSA films cast on quartz glass (a) without and with (b)  $0.51\chi$ , (c)  $0.68\chi$  and (d)  $0.76\chi$  of ionic liquid.

Figure B.3 shows an example of the reversible ammonia response of the CHEMFET gate film cast from PANI-CSA with 0.76 mole fraction of [THA][Tf<sub>2</sub>N] in formic acid. For the decreasing NH<sub>3</sub> concentration, the V<sub>g</sub> is increasing. The opposite trend applies for the increasing concentration.

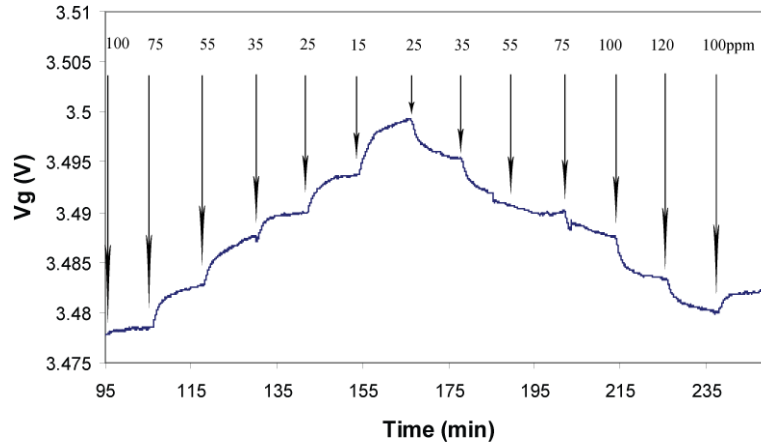


**Figure B.3.** Gate voltage change of CHEMFET with gate layer cast from PANI-CSA with [THA][Tf<sub>2</sub>N] ( $\chi = 0.76$ ) to stepwise changes to ammonia. Dry air was used as the carrier gas.

From the response shown in Figure B.3, the calibration curves for the four different concentrations of ILs with different slopes (sensitivity) were obtained using the following equation<sup>138</sup>.

$$V_g = V_g^o - \frac{2.3kT}{2\delta} \log(P_x + \sum_i P_i)$$

where, V<sub>g</sub> is the gate voltage in the ambient of the inert gas P<sub>i</sub>. Value of V<sub>g</sub><sup>o</sup> is given by its primary doping, and  $\delta$  is a fractional charge donated by the donor gas NH<sub>3</sub> at partial

pressure  $P_x$ . The changes of the gate voltage mirror the Fermi level modulation in the sensing material due to the interactions with the donor/acceptor gas.

As seen in Figure B.4, the sensitivity of the hybrid-gel material depends on the type of IL present in the matrix. The sensitivity to ammonia significantly increased for higher mole fractions of [BMIM][Tf<sub>2</sub>N] in PANI. Only a slight increase in sensitivity was observed when [THA][Tf<sub>2</sub>N] was added to PANI. Almost no difference in sensitivity to ammonia was observed for PANI without IL or with [HEA][Fm].

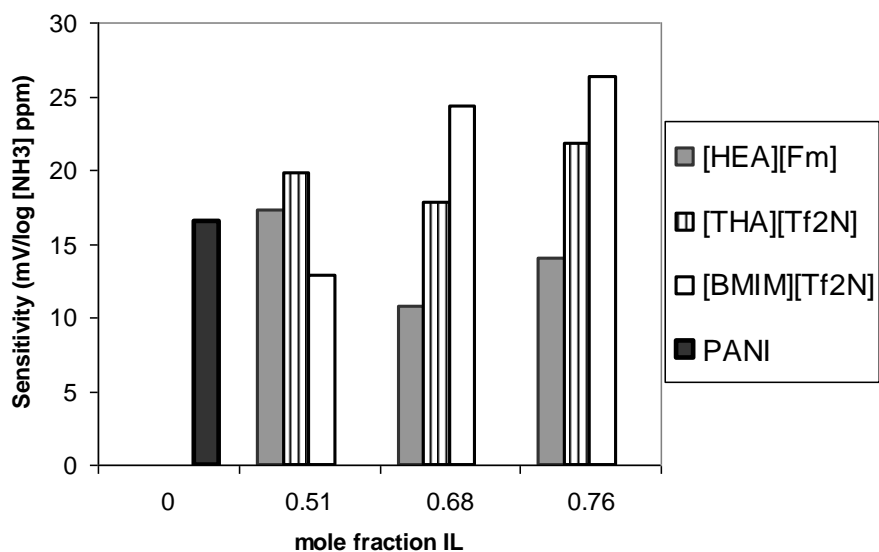


**Figure B.4.** Comparison between averaged sensitivities to ammonia of CHEMFET's as a function of mole fraction of IL in the PANI.CSA matrix.

The changes in the sensitivities indicate that electrons are donated from ammonia to the OS gel hybrid material, with a different value of  $\delta$ .

The response time is expected to decrease with increasing IL content. In Figure B.5, ammonia responses of all hybrid-gel layers are compared for step up (35 ppm to 55ppm) and step down (from 55ppm to 35 ppm) are compared.

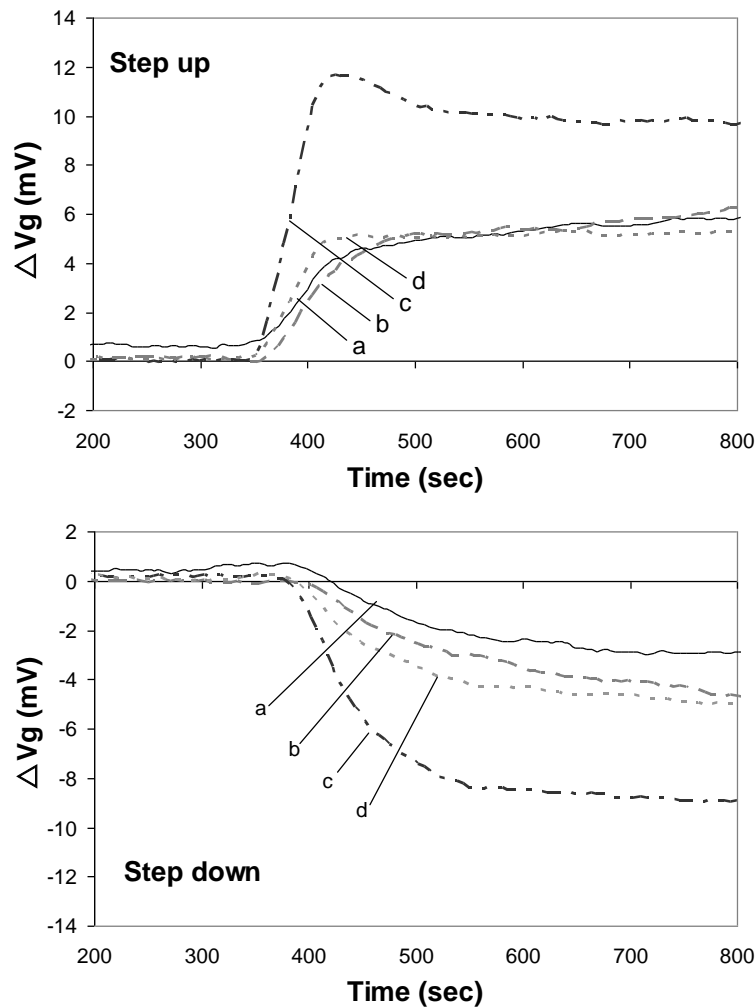


**Figure B.5.** Responses for step up (35 to 55ppm) and step down (55 to 35ppm) in ammonia concentration for PANI films with and without ILs: (a) PANI, (b)  $\chi = 0.51$  for [HEA][Fm], (c)  $\chi = 0.68$  for [BMIM][Tf<sub>2</sub>N] and (d)  $\chi = 0.51$  for [THA][Tf<sub>2</sub>N].

In order to obtain more accurate information about the response times of the layers to ammonia, the response was normalized to the thickness of the cast layers. The results are presented in Table B.3.

**Table B.3.** Film thickness normalized results for 90% response times corresponding to Figure B.5.

Sensing Layer	$\tau_{90\%}/d$ (sec/nm)		
	d (nm)	step up	Step down
PANI only	243	2.47	2.67
[HEA][Fm] $\chi=0.51$	277	2.40	2.23
[BMIM][Tf <sub>2</sub> N] $\chi=0.68$	336	1.19	1.52
[THA][Tf <sub>2</sub> N] $\chi=0.51$	227	1.81	2.51

As shown in Table B.3, appreciable differences were found between the PANI without IL and the PANI with IL present there. The gel-hybrid layer with mole fraction 0.68 of [BMIM][Tf<sub>2</sub>N] responded almost 50% faster than PANI film cast without IL. This significant increase in the response time for that particular IL is given by the fact ammonia is soluble in it<sup>139</sup>. The [THA][Tf<sub>2</sub>N] has the ability to be involved in acid-base interaction<sup>135</sup>.

Gel-hybrid materials made from PANI and room temperature ionic liquid were studied in order to determine if the introduction of IL in the PANI matrix would facilitate response signal to ammonia. The results demonstrate that the sensitivity of the gel-hybrid materials is affected by the solubility of ammonia in IL. The shorter response time results from reduced transport time of the gaseous species through the gel-like PANI

sensing layer, which might also broaden the dynamic range for analyte detection.

## REFERENCES

- [1] Amano, K.; Ishikawa, H.; Kobayashi, A.; Satoh, M.; Hasegawa, E. *Synth. Met.* **1994**, *62*, 229.
- [2] Neoh, K. G.; Kang, E. T.; Khor, S. H.; Tan, K. L. *Polym. Degrad. Stab.* **1990**, *27*, 107.
- [3] Pyo, M. H.; Reynolds, J. R.; Warren, L. F.; Marcy, H. O. *Synth. Met.* **1994**, *68*, 71.
- [4] Khor, S. H.; Neoh, K. G.; Kang, E. T. *J. Appl. Polym. Sci.* **1990**, *40*, 2015.
- [5] Ray, A.; Asturias, G. E.; Kershner, D. L.; Richter, A. F.; Macdiarmid, A. G.; Epstein, A. J. *Synth. Met.* **1989**, *29*, E141.
- [6] Huang, W. S.; Humphrey, B. D.; Macdiarmid, A. G. *Journal of the Chemical Society-Faraday Transactions I* **1986**, *82*, 2385.
- [7] Kang, E. T.; Neoh, K. G.; Tan, K. L. *Surf. Interface Anal.* **1992**, *19*, 33.
- [8] Pekmez, N.; Pekmez, K.; Arca, M.; Yildiz, A. *J. Electroanal. Chem.* **1993**, *353*, 237.
- [9] Cao, Y.; Smith, P.; Heeger, A. J. *Synth. Met.* **1992**, *48*, 91.
- [10] Masters, J. G.; Sun, Y.; Macdiarmid, A. G.; Epstein, A. J. *Synth. Met.* **1991**, *41*, 715.
- [11] Link, S.; El-Sayed, M. A. *J. Phys. Chem. B* **1999**, *103*, 8410.
- [12] Choudhary, T. V.; Goodman, D. W. *Top. Catal.* **2002**, *21*, 25.
- [13] Haruta, M.; Date, M. *Applied Catalysis a-General* **2001**, *222*, 427.
- [14] Frost, J. C. *Nature* **1988**, *334*, 577.

- [15] Haruta, M.; Yamada, N.; Kobayashi, T.; Iijima, S. *J. Catal.* **1989**, *115*, 301.
- [16] Sakurai, H.; Tsubota, S.; Haruta, M. *Applied Catalysis a-General* **1993**, *102*, 125.
- [17] Waters, R. D.; Weimer, J. J.; Smith, J. E. *Catal. Lett.* **1995**, *30*, 181.
- [18] Amaya, T.; Saio, D.; Hirao, T. *Tetrahedron Lett.* **2007**, *48*, 2729.
- [19] Hatchett, D. W.; Wijeratne, R.; Kinyanjui, J. M. *J. Electroanal. Chem.* **2006**, *593*, 203.
- [20] Santhosh, P.; Gopalan, A.; Lee, K. P. *J. Catal.* **2006**, *238*, 177.
- [21] Hatchett, D. W.; Josowicz, M.; Janata, J.; Baer, D. R. *Chem. Mater.* **1999**, *11*, 2989.
- [22] Nagel, Y.; Beck, W. *Z. Anorg. Allg. Chem.* **1985**, *529*, 57.
- [23] Smith, J. A.; Josowicz, M.; Janata, J. *J. Electrochem. Soc.* **2003**, *150*, E384.
- [24] Brust, M.; Walker, M.; Bethell, D.; Schiffrin, D. J.; Whyman, R. *Journal of the Chemical Society-Chemical Communications* **1994**, 801.
- [25] Wilcoxon, J. P.; Provencio, P. P. *J. Phys. Chem. B* **1999**, *103*, 9809.
- [26] Saheb, A.; Smith, J. A.; Josowicz, M.; Janata, J.; Baer, D. R.; Engelhard, M. H. *J. Electroanal. Chem.* **2008**, *621*, 238.
- [27] Hashmi, A. S. K.; Hutchings, G. J. *Angewandte Chemie-International Edition* **2006**, *45*, 7896.
- [28] Meyer, R.; Lemire, C.; Shaikhutdinov, S. K.; Freund, H. *Gold Bulletin* **2004**, *37*, 72.
- [29] Sanchez, A.; Abbet, S.; Heiz, U.; Schneider, W. D.; Hakkinen, H.; Barnett, R. N.; Landman, U. *J. Phys. Chem. A* **1999**, *103*, 9573.

- [30] Assiongbon, K. A.; Roy, D. *Surf. Sci.* **2005**, *594*, 99.
- [31] Borkowska, Z.; Tymosiak-Zielinska, A.; Nowakowski, R. *Electrochim. Acta* **2004**, *49*, 2613.
- [32] De Lima, R. B.; Varela, H. *Gold Bulletin* **2008**, *41*, 15.
- [33] Hernandez, J.; Solla-Gullon, J.; Herrero, E.; Aldaz, A.; Feliu, J. M. *Electrochim. Acta* **2006**, *52*, 1662.
- [34] Ocon, P.; Alonso, C.; Celdran, R.; Gonzalezvelasco, J. *J. Electroanal. Chem.* **1986**, *206*, 179.
- [35] Beltowskabrzezinska, M.; Luczak, T.; Holze, R. *J. Appl. Electrochem.* **1997**, *27*, 999.
- [36] Kwon, Y.; Lai, S. C. S.; Rodriguez, P.; Koper, M. T. M. *J. Am. Chem. Soc.* **2011**, *133*, 6914.
- [37] Iizuka, Y.; Fujiki, H.; Yamauchi, N.; Chijjiwa, T.; Arai, S.; Tsubota, S.; Haruta, M. *Catal. Today* **1997**, *36*, 115.
- [38] Min, B. K.; Friend, C. M. *Chem. Rev.* **2007**, *107*, 2709.
- [39] Lee, S.; Molina, L. M.; Lopez, M. J.; Alonso, J. A.; Hammer, B.; Lee, B.; Seifert, S.; Winans, R. E.; Elam, J. W.; Pellin, M. J.; Vajda, S. *Angewandte Chemie-International Edition* **2009**, *48*, 1467.
- [40] Rodriguez-Vazquez, M. J.; Blanco, M. C.; Lourido, R.; Vazquez-Vazquez, C.; Pastor, E.; Planes, G. A.; Rivas, J.; Lopez-Quintela, M. A. *Langmuir* **2008**, *24*, 12690.
- [41] Fernandez, E. M.; Soler, J. M.; Garzon, I. L.; Balbas, L. C. *Physical Review B* **2004**, *70*, 165403.
- [42] Hakkinen, H.; Landman, U. *Physical Review B* **2000**, *62*, R2287.
- [43] Majumder, C.; Kulshreshtha, S. K. *Physical Review B* **2006**, *73*.

- [44] Janssens, E.; Tanaka, H.; Neukermans, S.; Silverans, R. E.; Lievens, P. *New Journal of Physics* **2003**, *5*.
- [45] Risse, T.; Shaikhutdinov, S.; Nilius, N.; Sterrer, M.; Freund, H. J. *Acc. Chem. Res.* **2008**, *41*, 949.
- [46] Eberhardt, W. *Surf. Sci.* **2002**, *500*, 242.
- [47] Miyamura, H.; Matsubara, R.; Miyazaki, Y.; Kobayashi, S. *Angewandte Chemie-International Edition* **2007**, *46*, 4151.
- [48] Prati, L.; Rossi, M. *J. Catal.* **1998**, *176*, 552.
- [49] Saio, D.; Amaya, T.; Hirao, T. *Adv. Synth. Catal.* **2010**, *352*, 2177.
- [50] Tsunoyama, H.; Sakurai, H.; Negishi, Y.; Tsukuda, T. *J. Am. Chem. Soc.* **2005**, *127*, 9374.
- [51] Nagashree, K. L.; Ahmed, M. F. *Synth. Met.* **2008**, *158*, 610.
- [52] Nagashree, K. L.; Ahmed, M. F. *J. Appl. Electrochem.* **2009**, *39*, 403.
- [53] Palmero, S.; Colina, A.; Munoz, E.; Heras, A.; Ruiz, V.; Lopez-Palacios, J. *Electrochem. Commun.* **2009**, *11*, 122.
- [54] Pandey, R. K.; Lakshminarayanan, V. *Journal of Physical Chemistry C* **2009**, *113*, 21596.
- [55] Hatchett, D. W.; Millick, N. M.; Kinyanjui, J. M.; Pookpanratana, S.; Bar, M.; Hofmann, T.; Luinetti, A.; Heske, C. *Electrochim. Acta* **2011**, *56*, 6060.
- [56] Moghaddam, R. B.; Pickup, P. G. *Electrochim. Acta* **2011**, *56*, 7666.
- [57] Choudary, B. M.; Roy, M.; Roy, S.; Kantam, M. L.; Sreedhar, B.; Kumar, K. V. *Adv. Synth. Catal.* **2006**, *348*, 1734.

- [58] Islam, R. U.; Witcomb, M. J.; Van Der Lingen, E.; Scurrrell, M. S.; Van Otterlo, W.; Mallick, K. *J. Organomet. Chem.* **2011**, *696*, 2206.
- [59] Drelinkiewicz, A.; Hasik, M.; Kloc, M. *Catal. Lett.* **2000**, *64*, 41.
- [60] Drelinkiewicz, A.; Waksmundzka, A.; Makowski, W.; Sobczak, J. W.; Krol, A.; Zieba, A. *Catal. Lett.* **2004**, *94*, 143.
- [61] Liu, H. P.; Ye, J. Q.; Xu, C. W.; Jiang, S. P.; Tong, Y. X. *J. Power Sources* **2008**, *177*, 67.
- [62] Wang, D. Y.; Liu, J. P.; Wu, Z. Y.; Zhang, J. H.; Su, Y. Z.; Liu, Z. L.; Xu, C. W. *International Journal of Electrochemical Science* **2009**, *4*, 1672.
- [63] Ye, J. Q.; Liu, H. P.; Xu, C. W.; Jiang, S. P.; Tong, Y. X. *Electrochem. Commun.* **2007**, *9*, 2760.
- [64] Zanti, G.; Peeters, D. *J. Phys. Chem. A* **2010**, *114*, 10345.
- [65] Dimitratos, N.; Villa, A.; Wang, D.; Porta, F.; Su, D. S.; Prati, L. *J. Catal.* **2006**, *244*, 113.
- [66] Hou, W. B.; Dehm, N. A.; Scott, R. W. *J. Catal.* **2008**, *253*, 22.
- [67] Bianchi, C. L.; Canton, P.; Dimitratos, N.; Porta, F.; Prati, L. *Catal. Today* **2005**, *102*, 203.
- [68] Landon, P.; Collier, P. J.; Carley, A. F.; Chadwick, D.; Papworth, A. J.; Burrows, A.; Kiely, C. J.; Hutchings, G. J. *PCCP* **2003**, *5*, 1917.
- [69] Hillman, A. R.; Mohamoud, M. A. *Electrochim. Acta* **2006**, *51*, 6018.
- [70] Barbero, C.; Miras, M. C.; Haas, O.; Kotz, R. *J. Electrochem. Soc.* **1991**, *138*, 669.
- [71] Orata, D.; Buttry, D. A. *J. Am. Chem. Soc.* **1987**, *109*, 3574.

- [72] Kobayashi, T.; Yoneyama, H.; Tamura, H. *J. Electroanal. Chem.* **1984**, *177*, 293.
- [73] Dinh, H. N.; Ding, J. F.; Xia, S. J.; Birss, V. I. *J. Electroanal. Chem.* **1998**, *459*, 45.
- [74] Lopez-Palacios, J.; Munoz, E.; Heras, M. A.; Colina, A.; Ruiz, V. *Electrochim. Acta* **2006**, *52*, 234.
- [75] Lippe, J.; Holze, R. *J. Electroanal. Chem.* **1992**, *339*, 411.
- [76] Tang, H. Q.; Kitani, A.; Shiotani, M. *Electrochim. Acta* **1996**, *41*, 1561.
- [77] Zhang, A. Q.; Cui, C. Q.; Lee, J. Y. *Synth. Met.* **1995**, *72*, 217.
- [78] Stilwell, D. E.; Park, S. M. *J. Electrochem. Soc.* **1989**, *136*, 688.
- [79] Malinauskas, A.; Holze, R. *J. Appl. Polym. Sci.* **1999**, *73*, 287.
- [80] Kang, E. T.; Neoh, K. G.; Tan, K. L. *Prog. Polym. Sci.* **1998**, *23*, 277.
- [81] Janata, J.; Josowicz, M. *Acc. Chem. Res.* **1998**, *31*, 241.
- [82] Janata, J.; Josowicz, M. *J. Solid State Electrochem.* **2009**, *13*, 41.
- [83] Janata, J. *Chemical Sensors*; Springer, 2009.
- [84] Jonke, A. P.; Josowicz, M.; Janata, J. *J. Electrochem. Soc.* **2012**, *159*, P40.
- [85] Jonke, A. P.; Josowicz, M.; Janata, J. *J. Electrochem. Soc.* **2011**, *158*, E147.
- [86] Mallat, T.; Baiker, A. *Catal. Today* **1994**, *19*, 247.
- [87] Mallat, T.; Baiker, A. *Chem. Rev.* **2004**, *104*, 3037.
- [88] Markiewicz, M. E. P.; Hebert, D. M.; Bergens, S. H. *J. Power Sources* **2006**, *161*, 761.

- [89] Spendelow, J. S.; Wieckowski, A. *PCCP* **2007**, *9*, 2654.
- [90] Lin, H.; Chen, G. L.; Zheng, Z. S.; Zhou, J. Z.; Chen, S. P.; Lin, Z. H. *Acta Physico-Chimica Sinica* **2005**, *21*, 1280.
- [91] Takky, D.; Beden, B.; Leger, J. M.; Lamy, C. *J. Electroanal. Chem.* **1985**, *193*, 159.
- [92] Bronnimann, C.; Bodnar, Z.; Aeschimann, R.; Mallat, T.; Baiker, A. *J. Catal.* **1996**, *161*, 720.
- [93] Jena, N. K.; Chandrakumar, K. R. S.; Ghosh, S. K. *Rsc Advances* **2012**, *2*, 10262.
- [94] Kuang, X. J.; Wang, X. Q.; Liu, G. B. *J. Mol. Model.* **2011**, *17*, 2005.
- [95] Silva, C. G.; Juarez, R.; Marino, T.; Molinari, R.; Garcia, H. *J. Am. Chem. Soc.* **2011**, *133*, 595.
- [96] Chen, S. L.; Schell, M. *Electrochim. Acta* **2000**, *45*, 3069.
- [97] Ficicioglu, F.; Kadirgan, F. *J. Electroanal. Chem.* **1997**, *430*, 179.
- [98] Lai, S. C. S.; Koper, M. T. M. *PCCP* **2009**, *11*, 10446.
- [99] Tripkovic, A. V.; Popovic, K. D.; Momcilovic, J. D.; Drazic, D. M. *J. Electroanal. Chem.* **1998**, *448*, 173.
- [100] Ureta-Zanartu, M. S.; Berrios, C.; Gonzalez, T.; Fernandez, F.; Baez, D.; Salazar, R.; Gutierrez, C. *International Journal of Electrochemical Science* **2012**, *7*, 8905.
- [101] Yu, E. H.; Scott, K.; Reeve, R. W. *J. Electroanal. Chem.* **2003**, *547*, 17.
- [102] Zhang, Y.; Cui, X. J.; Shi, F.; Deng, Y. Q. *Chem. Rev.* **2011**, *112*, 2467.
- [103] Bolzan, A. E. *J. Electroanal. Chem.* **1995**, *380*, 127.

- [104] Denuault, G.; Milhano, C.; Pletcher, D. *PCCP* **2005**, *7*, 3545.
- [105] Nava, P.; Sierka, M.; Ahlrichs, R. *PCCP* **2003**, *5*, 3372.
- [106] Smith, J. A.; Josowicz, M.; Janata, J. *PCCP* **2005**, *7*, 3614.
- [107] Ai-Jie, M.; Xiao-Yu, K.; Gang, C.; Ya-Ru, Z.; Yan-Fang, L.; Peng, L.; Chi, Z. *Mol. Phys.* **2011**, *109*, 1485.
- [108] Guo, J. J.; Yang, J. X.; Die, D. *Physica B-Condensed Matter* **2005**, *367*, 158.
- [109] Tao, B. R.; Zhang, J. A.; Hui, S. C.; Chen, X. J.; Wan, L. J. *Electrochim. Acta* **2010**, *55*, 5019.
- [110] Wang, X. G.; Wang, W. M.; Qi, Z.; Zhao, C. C.; Ji, H.; Zhang, Z. H. *Electrochem. Commun.* **2009**, *11*, 1896.
- [111] Bond, G. C.; Thompson, D. T. *Catalysis Reviews-Science and Engineering* **1999**, *41*, 319.
- [112] Negishi, E.; Takahashi, T.; Baba, S.; Vanhorn, D. E.; Okukado, N. *J. Am. Chem. Soc.* **1987**, *109*, 2393.
- [113] Ng, S. S.; Ho, C. Y.; Schleicher, K. D.; Jamison, T. F. *Pure Appl. Chem.* **2008**, *80*, 929.
- [114] Lamy, C.; Belgsir, E. M.; Leger, J. M. *J. Appl. Electrochem.* **2001**, *31*, 799.
- [115] Sen Gupta, S.; Datta, J. *Journal of Chemical Sciences* **2005**, *117*, 337.
- [116] Cherevko, S.; Kulyk, N.; Chung, C.-H. *Electrochim. Acta* **2012**, *69*, 190.
- [117] Kwon, Y.; Lai, S. C. S.; Rodriguez, P.; Koper, M. T. M. *J. Am. Chem. Soc.*, *133*, 6914.

- [118] Matsuoka, K.; Inaba, M.; Iriyama, Y.; Abe, T.; Ogumi, Z.; Matsuoka, M. *Fuel Cells* **2002**, *2*, 35.
- [119] Hatchett, D. W.; Josowicz, M. *Chem. Rev.* **2008**, *108*, 746.
- [120] Genies, E. M.; Boyle, A.; Lapkowski, M.; Tsintavis, C. *Synth. Met.* **1990**, *36*, 139.
- [121] Syed, A. A.; Dinesan, M. K. *Talanta* **1991**, *38*, 815.
- [122] Jonke, A. P.; Josowicz, M.; Janata, J.; Engelhard, M. H. *J. Electrochem. Soc.* **2010**, *157*, P83.
- [123] McMurry, J. *Organic Chemistry*; 6th ed.; Brooks/Cole: Belmont, CA, 2003.
- [124] Desilvestro, J.; Weaver, M. J. *J. Electroanal. Chem.* **1986**, *209*, 377.
- [125] Celdran, R.; Gonzalezvelasco, J. J. *Electrochim. Acta* **1981**, *26*, 525.
- [126] Bard A, F. L. *Electrochemical Methods Fundamentals and Applications*; 2nd ed.; Wiley & Sons, Inc.: New York, 2001.
- [127] Nowicka, A. M.; Hasse, U.; Sievers, G.; Donten, M.; Stojek, Z.; Fletcher, S.; Scholz, F. *Angewandte Chemie-International Edition* **2010**, *49*, 3006.
- [128] Janata, J.; Josowicz, M. *Nature Materials* **2003**, *2*, 19.
- [129] Sasaki, I.; Josowicz, M.; Janata, J.; Glezer, A. *Analyst* **2006**, *131*, 751.
- [130] Sasaki, I.; Janata, J.; Glezer, A. *IEEE Sens. J.* **2006**, *6*, 1728.
- [131] Wasserscheid, P.; Keim, W. *Angewandte Chemie-International Edition* **2000**, *39*, 3772.
- [132] Fukushima, T.; Kosaka, A.; Ishimura, Y.; Yamamoto, T.; Takigawa, T.; Ishii, N.; Aida, T. *Science* **2003**, *300*, 2072.

- [133] Huddleston, J. G.; Visser, A. E.; Reichert, W. M.; Willauer, H. D.; Broker, G. A.; Rogers, R. D. *Green Chemistry* **2001**, *3*, 156.
- [134] Su, B.; Zhang, M. Q.; Shao, Y. H.; Girault, H. H. *J. Phys. Chem. B* **2006**, *110*, 21460.
- [135] Bicak, N. *J. Mol. Liq.* **2005**, *116*, 15.
- [136] Chen, H.; L'hereec, F.; Sasaki, I.; Janata, J. *Thin Solid Films* **2003**, *444*, 241.
- [137] Saheb, A.; Josowicz, M.; Janata, J. *Anal. Chem.* **2008**, *80*, 4214.
- [138] Janata, J. *Anal. Chem.* **1991**, *63*, 2546.
- [139] Yokozeki, A.; Shiflett, M. B. *Applied Energy* **2007**, *84*, 1258.

## VITA

### ALEX P. JONKE

Mr. Jonke was born in Bronx, New York. He attended public schools in Oklahoma City, Oklahoma, received a B.A. in Chemistry from Kennesaw State University, Kennesaw, Georgia in 2003 and a M.S. in Chemistry from the Georgia Institute of Technology, Atlanta, Georgia in 2007 before pursuing a doctorate in Chemistry at the Georgia Institute of Technology.

### Publications

Schwartz, I., Jonke, A. P., Josowicz, M., Janata, J., “*Polyaniline Electrodes With Atomic Au-Pd Alloys. Oxidation of Methanol and Ethanol*” *Catal. Lett.* 2013 (Accepted).

Schwartz, I., Jonke, A. P., Josowicz, M., Janata, J., “*Effect of Structured Atomic Gold on Electrooxidation of Alcohols in Alkaline Medium*” *Catal. Lett.* 2013 (Accepted).

Jonke, A. P., Steeb, J., Josowicz, M., Janata, J., “*Atomic Clusters of Pd and Au<sub>N</sub>Pd<sub>M</sub> in Polyaniline*” *Catal. Lett.* 2013, 143, 531-538.

Schwartz, I., Jonke, A. P., Josowicz, M., Janata, J., “*Polyaniline-Supported Atomic Gold Electrodes: Comparison with Macro Electrodes*” *Catal. Lett.* 2012, 142, 1344-1351.

Jonke, A. P., Josowicz, M., Janata, J., “*Odd-Even Pattern Observed in Polyaniline/(Au-0 - Au-8) Composites*” *J. Electrochem. Soc.* 2012, 159, P40-P43.

Jonke, A. P., Josowicz, M., Janata, J., “*Polyaniline Doped with Atomic Gold*” *J. Electrochem. Soc.* 2011, 158, E147-E151.

Jonke, A. P., Josowicz, M., Janata, J., and Engelhard, M., “*Electrochemically Controlled Atom by Atom Deposition of Gold into Polyaniline*” *J. Electrochem. Soc.* 2010, 157, P83-P87.

Mayo, India; Jonke, Alex; Janata, Jiri; Josowicz, Mira, “*Gel Hybrid Material as the Sensing Gate of a CHEMFET*” *ECS Transactions* (2009), 19(6), 149-157.